Data Assimilation and Driver Estimation for Space Weather Models using Ensemble Filters

Alexey V. Morozov

UofM Committee:
Dennis S. Bernstein
Aaron J. Ridley
Pierre T. Kabamba
Ilya V. Kolmanovsky

NCAR Collaborators:
Nancy Collins
Timothy J. Hoar
Jeffrey L. Anderson

March 29, 2013

Overview

1 Summary

2 Problem Statement

3 GITM

4 EAKF

5 Assimilating CHAMP Neutral Density

6 Assimilating GPS Total Electron Content

7 Conclusions and Future Work

1 Summary
- Main Contributions
- Publications

2 Problem Statement

3 GITM

4 EAKF

5 Assimilating CHAMP Neutral Density

6 Assimilating GPS Total Electron Content

7 Conclusions and Future Work

Main Contributions

Contributions relating to data assimilation are:

- **modified** the Data Assimilation Research Testbed (DART) to interface it with the Global Ionosphere-Thermosphere Model (GITM),
- **developed** a novel inflation technique for the Ensemble Adjustment Kalman Filter (EAKF) as applied to GITM for purposes of data assimilation and driver estimation, and
- **introduced** an ability to assimilate Total Electron Content (TEC) measurements into the DART-GITM interface.

Main Contributions

Contributions relating to data assimilation are:

- **modified** the Data Assimilation Research Testbed (DART) to interface it with the Global Ionosphere-Thermosphere Model (GITM),
- **developed** a novel inflation technique for the Ensemble Adjustment Kalman Filter (EAKF) as applied to GITM for purposes of data assimilation and driver estimation, and
- **introduced** an ability to assimilate Total Electron Content (TEC) measurements into the DART-GITM interface.

Contributions relating to adaptive control are:

- **described** the Retrospective Cost Adaptive Control (RCAC) stability margins for plants with uncertain nonminimum-phase zeros,
- **introduced** a convex constraint on the controller pole locations to improve RCAC transient and steady-state performance, and
- **modeled** nonlinear system and described the achievable amplitude and frequency control ranges.

Publications

1. M. S. Fledderjohn, M. S. Holzel, **A. V. Morozov**, J. B. Hoagg, and D. S. Bernstein, "On the Accuracy of Least Squares Algorithms for Estimating Zeros," *Proc. Amer. Contr. Conf.*, Baltimore, MD, June 2010.
2. **A. V. Morozov**, J. B. Hoagg, and D. S. Bernstein, "A Computational Study of the Performance and Robustness Properties of Retrospective Cost Adaptive Control," *AIAA Guid. Nav. Contr. Conf.*, Toronto, August 2010.
3. **A. V. Morozov**, J. B. Hoagg, and D. S. Bernstein, "Retrospective Adaptive Control of a Planar Multilink Arm with Nonminimum-Phase Zeros," *Proc. Conf. Dec. Contr.*, pp. 3706–3711, Atlanta, GA, December 2010.
4. **A. V. Morozov**, A. M. D'Amato, J. B. Hoagg, and D. S. Bernstein, "Retrospective Cost Adaptive Control for Nonminimum-Phase Systems with Uncertain Nonminimum-Phase Zeros Using Convex Optimization," *Proc. Amer. Contr. Conf.*, pp. 1188–2293, San Francisco, CA, June 2011.
5. A. M. D'Amato, E. D. Sumer, K. S. Mitchell, **A. V. Morozov**, J. B. Hoagg, and D. S. Bernstein, "Adaptive Output Feedback Control of the NASA GTM Model with Unknown Nonminimum-Phase Zeros," *AIAA Guid. Nav. Contr. Conf.*, Portland, OR, August 2011.
6. **A. V. Morozov**, A. A. Ali, A. M. D'Amato, A. J. Ridley, S. L. Kukreja, and D. S. Bernstein, "Retrospective-Cost-Based Model Refinement for System Emulation and Subsystem Identification," *Proc. Conf. Dec. Contr.*, pp. 2142–2147, Orlando, FL, December 2011.
7. E. D. Sumer, A. M. D'Amato, **A. V. Morozov**, J. B. Hoagg, and D. S. Bernstein, "Robustness of Retrospective Cost Adaptive Control to Markov-Parameter Uncertainty," *Proc. Conf. Dec. Contr.*, pp. 6085–6090, Orlando, FL, December 2011.
8. M. W. Isaacs, J. B. Hoagg, **A. V. Morozov**, and D. S. Bernstein, "A Numerical Study on Controlling a Nonlinear Multilink Arm Using a Retrospective Cost Model Reference Adaptive Controller," *Proc. Conf. Dec. Contr.*, pp. 8008–8013, Orlando, FL, December 2011.
9. **A. V. Morozov**, A. J. Ridley, D. S. Bernstein, N. Collins, T. J. Hoar, and J. L. Anderson, "Data Assimilation and Driver Estimation for the Global Ionosphere-Thermosphere Model Using the Ensemble Adjustment Kalman Filter", *Journal of Atmospheric and Solar-Terrestrial Physics*, 2013, *Submitted*.
10. **A. V. Morozov**, A. G. Burrell, A. J. Ridley, D. S. Bernstein, "Assimilation of the Total Electron Content Measurements into the Global Ionosphere-Thermosphere Model", *Journal of Atmospheric and Solar-Terrestrial Physics*, 2013, *To be submitted*.

1 Summary

2 Problem Statement
- Big Picture
- Problem Statement

3 GITM

4 EAKF

5 Assimilating CHAMP Neutral Density

6 Assimilating GPS Total Electron Content

7 Conclusions and Future Work

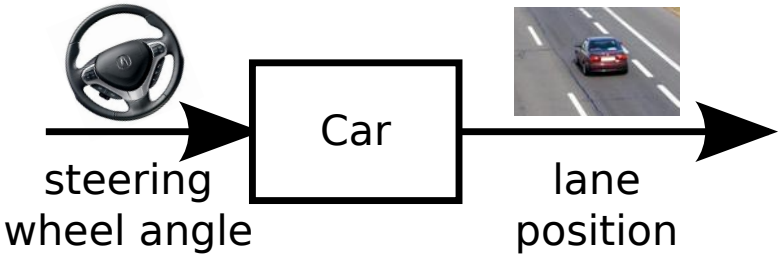
Car
steering
wheel angle
lane
position

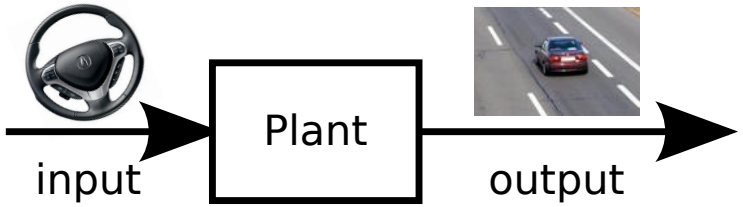
Plant
input
output

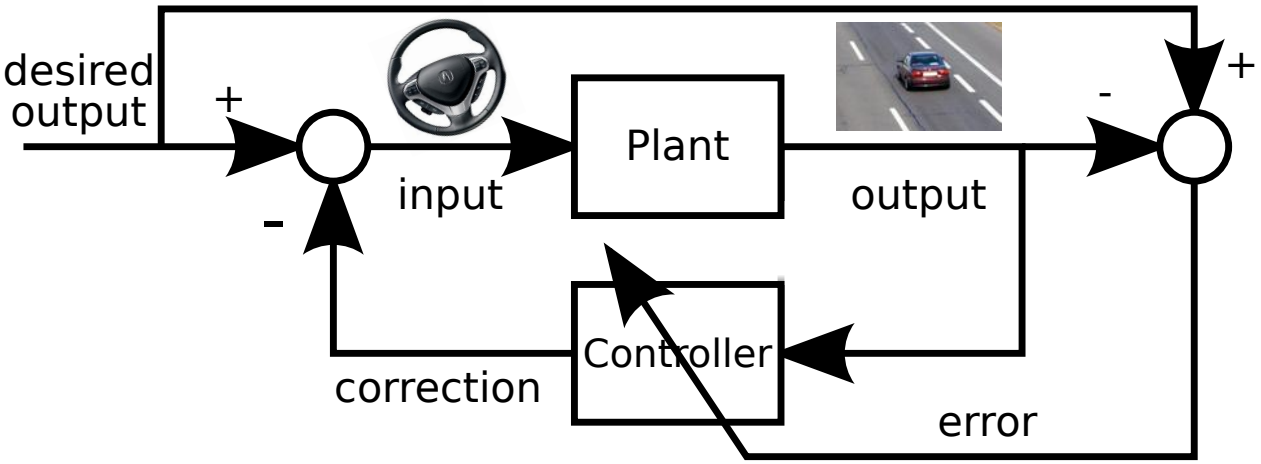
desired
output
+
-
input
Plant
output
-
+
Controller
correction
error

Where does model inversion come in?

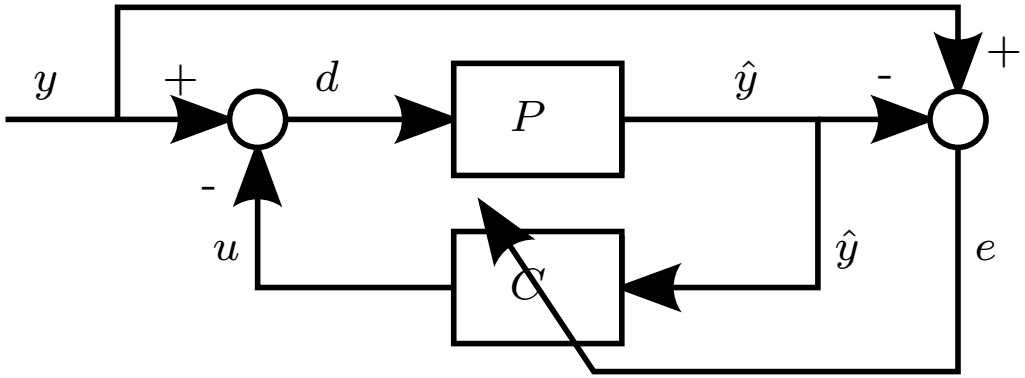

The goal is to make $\hat{y} = y$, that is $\frac{\hat{y}}{y} = 1$ or $e = 0$, that is $\frac{e}{y} = 0$

$$\hat{y} = Pd$$
$$\hat{y} = P(y - C\hat{y})$$
$$\hat{y} = Py - PC\hat{y}$$
$$(1 + PC)\hat{y} = Py$$
$$\frac{\hat{y}}{y} = \frac{P}{1 + PC}$$
$$\frac{P}{1 + PC} \overset{want}{=} 1$$
$$P \overset{w}{=} 1 + PC$$
$$C \overset{w}{=} 1 - P^{-1}$$

$$e = y - \hat{y}$$
$$e = y - \frac{P}{1 + PC} y$$
$$e = \frac{1 + PC - P}{1 + PC} y$$
$$\frac{e}{y} = \frac{1 + PC - P}{1 + PC}$$
$$\frac{1 + PC - P}{1 + PC} \overset{w}{=} 0$$
$$1 + PC - P \overset{w}{=} 0$$
$$C \overset{w}{=} 1 - P^{-1}$$

Example of inversion in frequency domain

Consider a linear plant $P = \frac{1}{z+0.5}$, which can be described in time domain as $\hat{y}_k = -0.5\hat{y}_{k-1} + d_{k-1}$. Suppose the goal is for the plant output $\hat{y}$ to follow desired command y (command following). RCAC converges to controller $C = \frac{0.7104}{z-0.5797}$

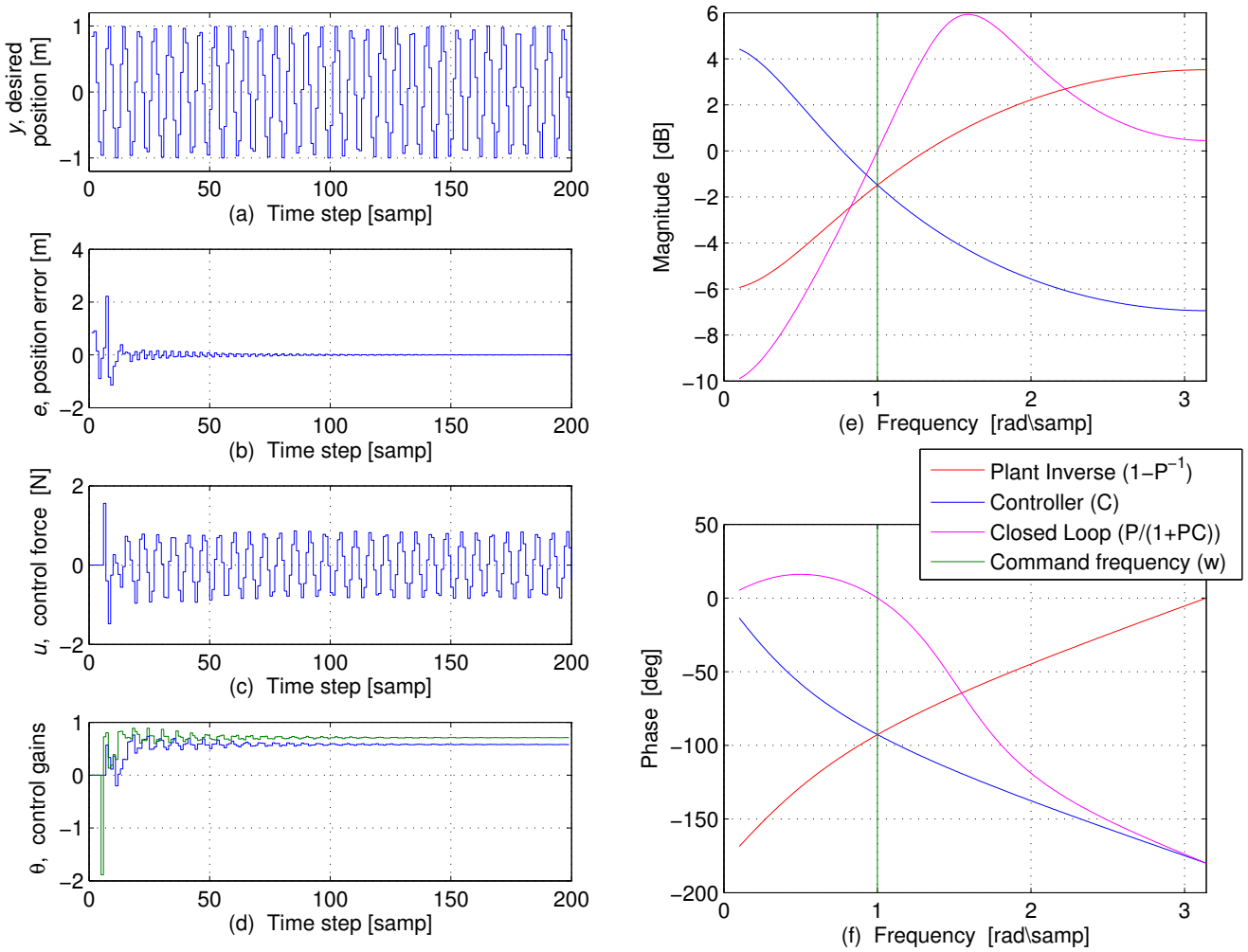

How is data assimilation on GITM similar to driving a car?

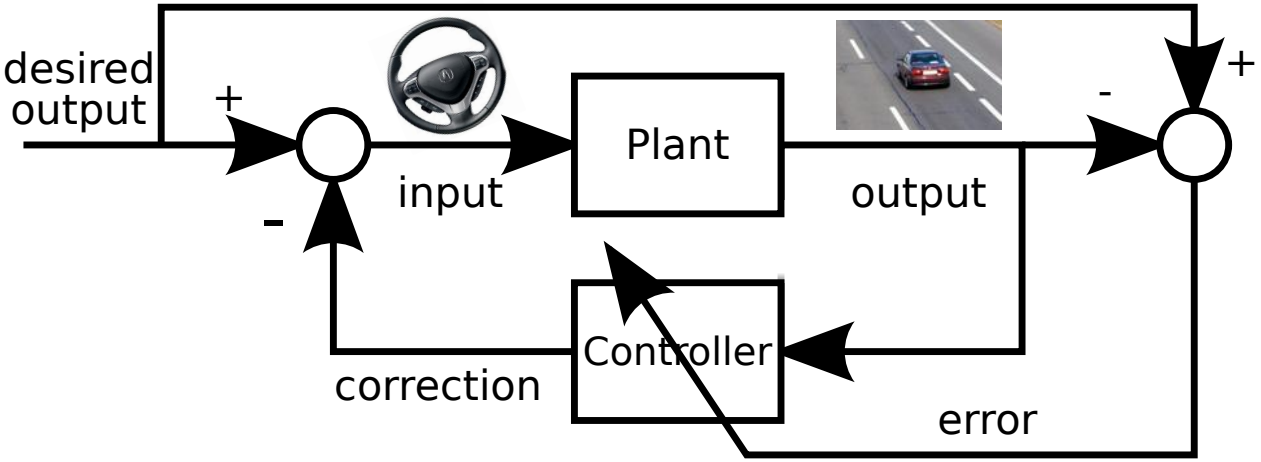

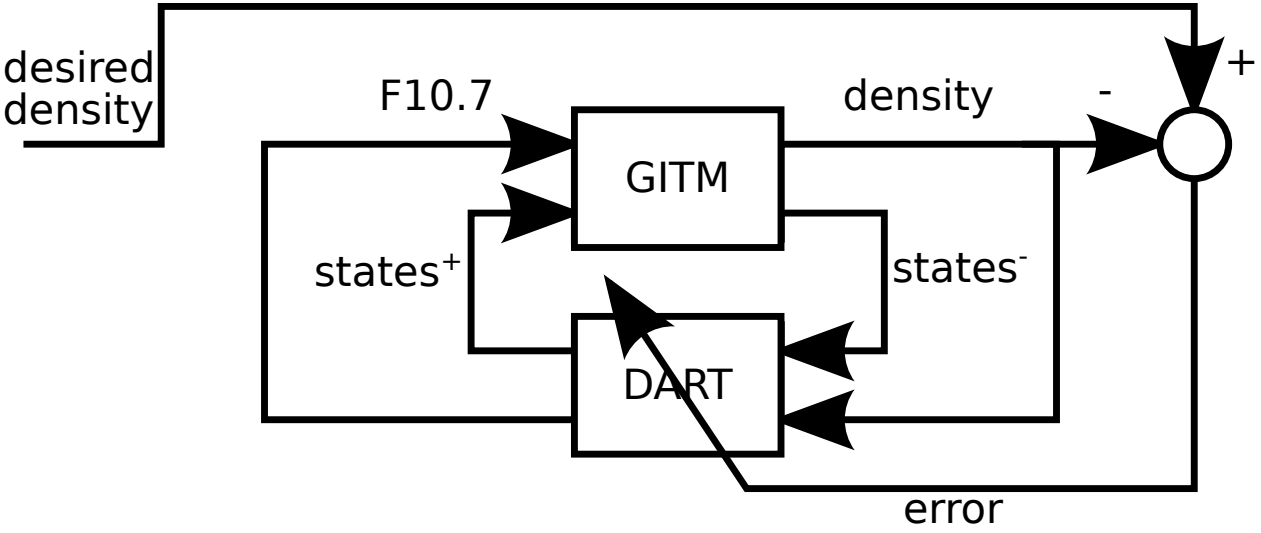

Problem Statement

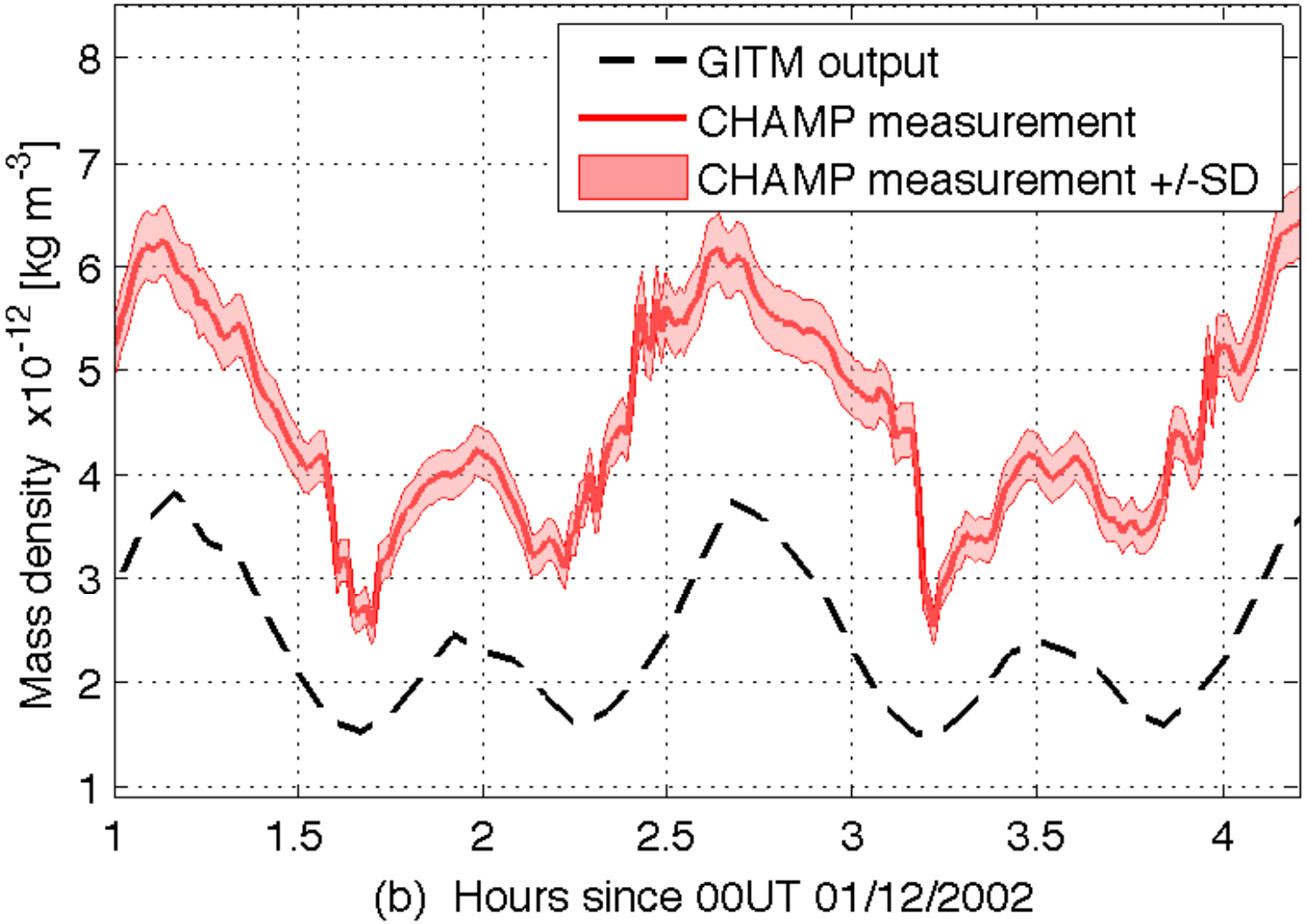

We want to drive GITM output (black) to match the satellite data (red).

1 Summary

2 Problem Statement

3 GITM
- Inputs and Outputs
- Equations
- Implementation

4 EAKF

5 Assimilating CHAMP Neutral Density

6 Assimilating GPS Total Electron Content

7 Conclusions and Future Work

Inputs and Outputs

Inputs					Outputs	
Solar flux index	$F_{10.7}$ or I_∞	$\rightarrow$	GITM	$\rightarrow$	N_s	Neutral number densities
Cooling rates	$L_e(X)$	$\rightarrow$		$\rightarrow$	ρ	Neutral mass density
Heating efficiency	ε	$\rightarrow$		$\rightarrow$	p	Neutral pressure
Thermal conductivity	κ_c	$\rightarrow$		$\rightarrow$	$\mathscr{T}$	Neutral temperature normalized
Earth magnetic field	simplified	$\rightarrow$		$\rightarrow$	$\mathbf{u}$	Neutral velocity
	or APEX			$\rightarrow$	N_j	Ion number densities
Interplanetary	simplified	$\rightarrow$		$\rightarrow$	T_j	Ion temperature normalized
magnetic field	or ACE data			$\rightarrow$	$\mathbf{v}$	Ion velocity
Hemispheric	simplified	$\rightarrow$				
power index	or POES data					
Initialize using	simplified	$\rightarrow$				
	or MSIS/IRI					

Table 21 compiled from [1]

[1] Ridley, A. J., Y. Deng, and G. Toth. "The Global IonosphereThermosphere Model," *Journal of Atmospheric and Solar-Terrestrial Physics* 68, no. 8 (2006)

GITM Vertical Equations

$$\frac{\partial \mathscr{N}_s}{\partial t} + \frac{\partial u_{\mathrm{r},s}}{\partial r} + \frac{2u_{\mathrm{r},s}}{r} + u_{\mathrm{r},s}\frac{\partial \mathscr{N}_s}{\partial r} = \frac{1}{N_s}\mathscr{S}_s, \qquad \text{(continuity)} \qquad (1)$$

$$\frac{\partial u_{\mathrm{r},s}}{\partial t} + u_{\mathrm{r},s}\frac{\partial u_{\mathrm{r},s}}{\partial r} + \frac{u_\theta}{r}\frac{\partial u_{\mathrm{r},s}}{\partial \theta} + \frac{u_\phi}{r\cos(\theta)}\frac{\partial u_{\mathrm{r},s}}{\partial \phi} + \frac{k}{M_s}\frac{\partial T}{\partial r} + \frac{kT}{M_s}\frac{\partial \mathscr{N}_s}{\partial r} =$$

$$g + \mathscr{F}_s + \frac{u_\theta^2 + u_\phi^2}{r} + \cos^2(\theta)\Omega^2 r + 2\cos(\theta)\Omega u_\phi, \qquad \text{(momentum)} \qquad (2)$$

$$\frac{\partial \mathscr{T}}{\partial t} + u_r\frac{\partial \mathscr{T}}{\partial r} + (\gamma - 1)\mathscr{T}\left(\frac{2u_r}{r} + \frac{\partial u_r}{\partial r}\right) = \frac{k}{c_{\mathrm{v}}\rho\bar{m}_{\mathrm{n}}}\mathscr{Q}, \qquad \text{(energy)} \qquad (3)$$

GITM Vertical Equations and source terms

(red - outputs, green - inputs)

$$\frac{\partial \mathscr{N}_s}{\partial t} + \frac{\partial u_{\mathrm{r},s}}{\partial r} + \frac{2u_{\mathrm{r},s}}{r} + u_{\mathrm{r},s}\frac{\partial \mathscr{N}_s}{\partial r} = \frac{1}{N_s}\mathscr{S}_s, \qquad \text{(continuity)} \tag{4}$$

$$\frac{\partial u_{\mathrm{r},s}}{\partial t} + u_{\mathrm{r},s}\frac{\partial u_{\mathrm{r},s}}{\partial r} + \frac{u_\theta}{r}\frac{\partial u_{\mathrm{r},s}}{\partial \theta} + \frac{u_\phi}{r\cos(\theta)}\frac{\partial u_{\mathrm{r},s}}{\partial \phi} + \frac{k}{M_s}\frac{\partial T}{\partial r} + \frac{kT}{M_s}\frac{\partial \mathscr{N}_s}{\partial r} =$$

$$g + \mathscr{F}_s + \frac{u_\theta^2 + u_\phi^2}{r} + \cos^2(\theta)\Omega^2 r + 2\cos(\theta)\Omega u_\phi, \qquad \text{(momentum)} \tag{5}$$

$$\frac{\partial \mathscr{T}}{\partial t} + u_r\frac{\partial \mathscr{T}}{\partial r} + (\gamma - 1)\mathscr{T}\left(\frac{2u_r}{r} + \frac{\partial u_r}{\partial r}\right) = \frac{k}{c_{\mathrm{v}}\rho\bar{m}_{\mathrm{n}}}\mathscr{Q}, \qquad \text{(energy)} \tag{6}$$

$$\mathscr{S}_s = \frac{\partial}{\partial r}\left[N_s K_e\left(\frac{\partial N_s}{\partial r} - \frac{\partial N}{\partial r}\right)\right] + C_s, \tag{7}$$

$$\mathscr{F}_s = \frac{\rho_{\mathrm{i}}}{\rho_s}\nu_{\mathrm{in}}(v_{\mathrm{r}} - u_{\mathrm{r},s}) + \frac{kT}{M_s}\sum_{q\neq s}\frac{N_q}{ND_{qs}}(u_{\mathrm{r},q} - u_{\mathrm{r},s}), \tag{8}$$

$$\mathscr{Q} = Q_{\mathrm{EUV}} + Q_{\mathrm{NO}} + Q_{\mathrm{O}} + \frac{\partial}{\partial r}\left((\kappa_{\mathrm{c}} + \kappa_{\mathrm{eddy}})\frac{\partial T}{\partial r}\right) + N_e\frac{\bar{m}_{\mathrm{i}}\bar{m}_{\mathrm{n}}}{\bar{m}_{\mathrm{i}} + \bar{m}_{\mathrm{n}}}\nu_{\mathrm{in}}(\mathbf{v} - \mathbf{u})^2$$

Implementation

- In the CHAMP simulations, 5° resolution in longitude and latitude is used.
- Variable resolution in altitude (from about $2km$ to about $18km$) is used to span the range between about $100km$ and $660km$.
- The atmosphere is broken up into 32 (8 in longitude, 4 in latitude) blocks to allow for parallel computation.
- A typical EAKF run (20 ensemble members) requires 640 CPUs (cores) and about 8 wall hours per 24 simulated hours on NASA Pleiades supercomputer.

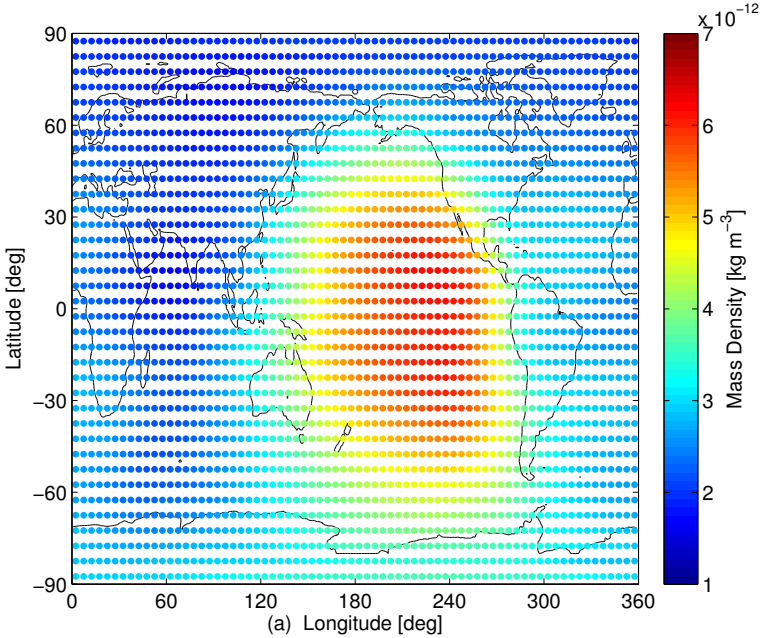

Horizontal resolution.

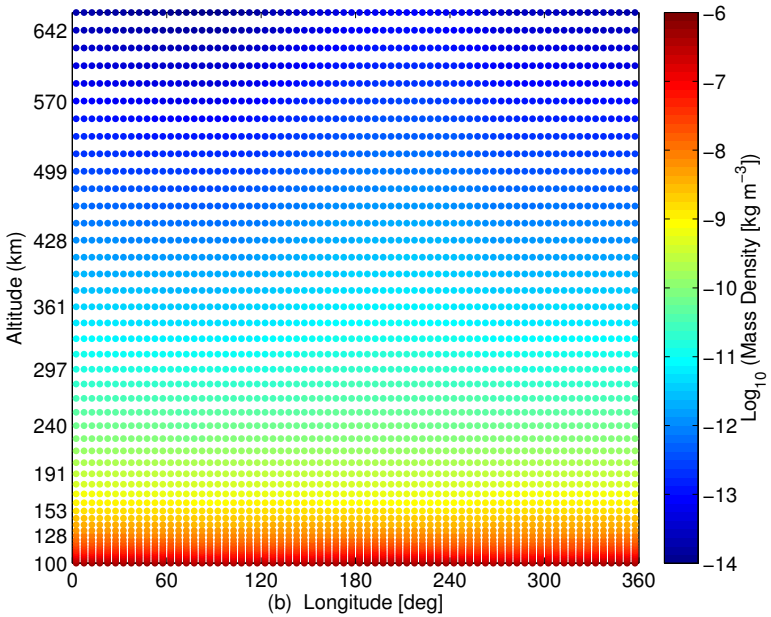

Vertical resolution.

1 Summary

2 Problem Statement

3 GITM

4 EAKF
- Big Picture
- Kalman Filter
- Extended Kalman Filter (EKF)
- Unscented Kalman Filter (UKF)
- Ensemble Kalman Filter (EnKF)
- Ensemble Adjustment Kalman Filter (EAKF)

5 Assimilating CHAMP Neutral Density

6 Assimilating GPS Total Electron Content

Pros and Cons of These Filters

KF $\rightarrow$ EKF $\rightarrow$ UKF $\rightarrow$ EnKF

$\rightarrow$ EAKF

Pros and Cons of These Filters

KF $\rightarrow$ EKF $\rightarrow$ UKF $\rightarrow$ EnKF
$\rightarrow$ EAKF

- KF $\rightarrow$ EKF The advantage of EKF over KF is that it allows the system to be nonlinear.

Pros and Cons of These Filters

KF $\rightarrow$ EKF $\rightarrow$ UKF $\rightarrow$ EnKF
$\rightarrow$ EAKF

- KF $\rightarrow$ EKF The advantage of EKF over KF is that it allows the system to be nonlinear.
- EKF $\rightarrow$ UKF The advantage of UKF over EKF is that it is more accurate in propagating means and covariances through the nonlinear system and does not require linearization.

Pros and Cons of These Filters

KF $\rightarrow$ EKF $\rightarrow$ UKF $\rightarrow$ EnKF
$\rightarrow$ EAKF

- KF $\rightarrow$ EKF The advantage of EKF over KF is that it allows the system to be nonlinear.
- EKF $\rightarrow$ UKF The advantage of UKF over EKF is that it is more accurate in propagating means and covariances through the nonlinear system and does not require linearization.
- UKF $\rightarrow$ EnKF The advantage of EnKF over UKF is that it does not require $2n$ ensemble members (sigma points, particles), and allows the user to pick N, the number of ensemble members. The newest versions of EnKF allow for localization, which improves computational performance even more than just reduction in number of ensemble members.

Pros and Cons of These Filters

KF $\rightarrow$ EKF $\rightarrow$ UKF $\rightarrow$ EnKF
$\rightarrow$ EAKF

- KF $\rightarrow$ EKF The advantage of EKF over KF is that it allows the system to be nonlinear.
- EKF $\rightarrow$ UKF The advantage of UKF over EKF is that it is more accurate in propagating means and covariances through the nonlinear system and does not require linearization.
- UKF $\rightarrow$ EnKF The advantage of EnKF over UKF is that it does not require $2n$ ensemble members (sigma points, particles), and allows the user to pick N, the number of ensemble members. The newest versions of EnKF allow for localization, which improves computational performance even more than just reduction in number of ensemble members.
- UKF $\rightarrow$ EAKF EAKF is similar to EnKF in being an ensemble filter, but utilizes different update equations. Some advantages of EAKF over UKF are addition of localization functionality and decreased computational load.

Kalman Filter

- Consider the linear discrete-time system given by

$$x_k = F_{k-1}x_{k-1} + G_{k-1}u_{k-1} + w_{k-1}, \qquad w_k \sim N(0, Q_k), \tag{10}$$
$$y_k = H_k x_k + v_k, \qquad v_k \sim N(0, R_k), \tag{11}$$

where $x_k \in \mathbb{R}^n, y_k \in \mathbb{R}^m, u_k \in \mathbb{R}^p$, w_k is the process noise, v_k is the measurement noise, and w_k and v_k are uncorrelated (i.e. $E(w_k v_j^T) = 0$).

- If F_k, G_k, H_k, Q_k, R_k, are known, the discrete time Kalman Filter[2] is given by

$$\hat{x}_k^- = F_{k-1}\hat{x}_{k-1}^+ + G_{k-1}u_{k-1}, \qquad \text{(prior estimate)} \tag{12}$$
$$P_k^- = F_{k-1}P_{k-1}^+ F_{k-1}^T + Q_{k-1}, \qquad \text{(prior error covariance)} \tag{13}$$
$$K_k = P_k^- H_k^T (H_k P_k^- H_k^T + R_k)^{-1}, \qquad \text{(estimator gain)} \tag{14}$$
$$P_k^+ = (I - K_k H_k)P_k^-, \qquad \text{(posterior error covariance)} \tag{15}$$
$$\hat{x}_k^+ = \hat{x}_k^- + K_k(y_k - H_k\hat{x}_k^-). \qquad \text{(posterior estimate)} \tag{16}$$

[2] Simon, Dan. Optimal state estimation: Kalman, H infinity, and nonlinear approaches. Wiley-Interscience, 2006.

Kalman Filter and Discrete Algebraic Riccati Equation

- As an aside, we demonstrate that Discrete Algebraic Riccati Equation (DARE) can be derived from the update equations derived so far.
- Substituting (16) into (12), we realize that prior state estimate can be updated directly without computation of the posterior estimate as in

$$\hat{x}_{k+1}^{-} = F_k(I - K_k H_k)\hat{x}_{k-1}^{+} + F_k K_k y_k G_k u_k. \tag{17}$$

- Similarly, by substituting (15) and (14) into (13), it can be shown that prior error covariance matrix can also be updated in one step, as given by

$$P_{k+1}^{-} = F_k(P_k^{-} - \left[P_k^{-} H_k^T (H_k P_k^{-} H_k^T + R_k)^{-1}\right] H_k P_k^{-})F_k^T + Q_k \tag{18}$$

$$= F_k P_k^{-} F_k^T - F_k P_k^{-} H_k^T (H_k P_k^{-} H_k^T + R_k)^{-1} H_k P_k^{-} F_k^T + Q_k, \tag{19}$$

which is the Discrete Algebraic Riccati Equation.

Extended Kalman Filter (EKF)

- Now consider the *non*linear discrete-time system given by

$$x_k = f_{k-1}(x_{k-1}, u_{k-1}, w_{k-1}), \qquad w_k \sim N(0, Q_k), \tag{20}$$
$$y_k = h_k(x_k, v_k), \qquad v_k \sim N(0, R_k), \tag{21}$$

where functions $f_k(\cdot)$ and $h_k(\cdot)$ are known explicitly and hence can be linearized via

$$F_{k-1} = \frac{\partial f_{k-1}}{\partial x}\Big|_{\hat{x}^+_{k-1}}, \qquad L_{k-1} = \frac{\partial f_{k-1}}{\partial w}\Big|_{\hat{x}^+_{k-1}}, \tag{22}$$
$$H_k = \frac{\partial h_k}{\partial x}\Big|_{\hat{x}^-_k}, \qquad M_k = \frac{\partial h_k}{\partial v}\Big|_{\hat{x}^-_k}. \tag{23}$$

- Next, EKF[3] can be updated via

$$\hat{x}^-_k = f_{k-1}(\hat{x}^+_{k-1}, u_{k-1}, 0), \tag{24}$$
$$P^-_k = F_{k-1}P^+_{k-1}F^T_{k-1} + L_{k-1}Q_{k-1}L^T_{k-1}, \tag{25}$$
$$K_k = P^-_k H^T_k (H_k P^-_k H^T_k + M_k R_k M^T_k)^{-1}, \tag{26}$$
$$P^+_k = (I - K_k H_k)P^-_k, \tag{27}$$
$$\hat{x}^+_k = \hat{x}^-_k + K_k \left[y_k - h_k(\hat{x}^-_k, 0)\right]. \tag{28}$$

[3] Simon, Dan. Optimal state estimation: Kalman, H infinity, and nonlinear approaches. Wiley-Interscience, 2006.

Unscented Kalman Filter (UKF)

- Consider the nonlinear discrete-time system with additive noise given by

$$x_k = f_{k-1}(x_{k-1}, u_{k-1}) + w_{k-1}, \tag{29}$$
$$y_k = h_k(x_k) + v_k. \tag{30}$$

- UKF propagates $2n$ realizations (sigma points, $\hat{x}^{(i)}$) of the state's probability density function, as defined and propagated by

$$\hat{x}_{k-1}^{(i)} = \hat{x}_{k-1}^{+} + (-1)^{\lfloor \frac{i-1}{n} \rfloor} \left(\sqrt{nP_{k-1}^{+}}\right)_i^T, \tag{31}$$

$$\hat{x}_k^{(i)} = f_{k-1}(\hat{x}_{k-1}^{(i)}, u_{k-1}), \quad \hat{y}_k^{(i)} = h_k(\hat{x}_k^{(i)}). \tag{32}$$

- Accordingly, UKF can be updated via

$$\hat{x}_k^{-} = \frac{1}{2n}\sum_{i=1}^{2n} \hat{x}_k^{(i)}, \quad \hat{y}_k^{-} = \frac{1}{2n}\sum_{i=1}^{2n} \hat{y}_k^{(i)}, \tag{33}$$

$$P_k^{-} = \sum_{i=1}^{2n}(\hat{x}_k^{(i)} - \hat{x}_k^{-})(\hat{x}_k^{(i)} - \hat{x}_k^{-})^T/(2n) + Q_{k-1}, \tag{34}$$

$$K_k = P_{xy}P_y^{-1}, \quad P_{xy} = \sum_{i=1}^{2n}(\hat{x}_k^{(i)} - \hat{x}_k^{-})(\hat{y}_k^{(i)} - \hat{y}_k^{-})^T/(2n) \tag{35}$$

$$P_k^{+} = P_k^{-} - K_k P_y K_k^T, \quad P_y = \sum_{i=1}^{2n}(\hat{y}_k^{(i)} - \hat{y}_k^{-})(\hat{y}_k^{(i)} - \hat{y}_k^{-})^T/(2n) + R_k \tag{36}$$

$$\hat{x}_k^{+} = \hat{x}_k^{-} + K_k(y_k - \hat{y}_k). \tag{37}$$

Ensemble Kalman Filter (EnKF)

- EnKF generates N vectors of initial conditions ($\hat{x}_1^+$) and feeds these into the model given by (21). Model started from different initial conditions is referred to as different ensemble members.
- Mean states estimate is calculated via $\mu\hat{x}_k^- = \sum_{i=1}^N \frac{\hat{x}_{k,i}^-}{N}$.
- $h_k(\cdot)$ still needs to be known explicitly and its linearization H_k needs to be computed about ensemble mean.
- Accordingly, N EnKF ensemble members can be updated via[4]

$$\hat{x}_{k,i}^- = f_{k-1}(\hat{x}_{k-1,i}^+, u_{k-1}, 0), \tag{38}$$

$$P_k^- = \sum_{i=1}^N (\hat{x}_{k,i}^- - \mu\hat{x}_k^-)(\hat{x}_{k,i}^- - \mu\hat{x}_k^-)^T/(N-1), \tag{39}$$

$$K_k = P_k^- H_k^T (H_k P_k^- H_k^T + M_k R_k M_k^T)^{-1}, \tag{40}$$

$$P_k^+ = (I - K_k H_k) P_k^-, \tag{41}$$

$$\hat{x}_{k,i}^+ = \hat{x}_{k,i}^- + K_k \left[y_k - h_k(\hat{x}_{k,i}^-, 0) \right]. \tag{42}$$

[4] Evensen, Geir. "Sequential data assimilation with a nonlinear quasi-geostrophic model using Monte Carlo methods to forecast error statistics." *J. Geophys. Res.*, - 99 (1994): 10-10.

Ensemble Adjustment Kalman Filter (EAKF)

- First, define joint[5] state-observation vector as

$$z_k = \begin{bmatrix} x_k \\ y_k \end{bmatrix}. \tag{43}$$

- Recall that $x_k \in \mathbb{R}^n, y_k \in \mathbb{R}^m$. We then define $\mathcal{H} \in \mathbb{R}^{m\times(n+m)}$ such that $y_k = \mathcal{H} z_k$, i.e. $\mathcal{H} = [\, 0_{m\times n}\; I_{m\times m} \,]$.
- Accordingly, N EAKF ensembles can be updated via[6]

$$\hat{z}^-_{k,i} = [f_{k-1}(\hat{x}^+_{k-1,i}, u_{k-1}, 0);\; h_k(\hat{x}^+_{k-1,i}, 0)], \tag{44}$$

$$\mathcal{P}^-_k = \sum\nolimits_{i=1}^{N} (\hat{z}^-_{k,i} - \mu\hat{z}^-_k)(\hat{z}^-_{k,i} - \mu\hat{z}^-_k)^T/(N-1), \tag{45}$$

$$\mathcal{A}_k = (\mathcal{F}^T_k)^{-1}\mathcal{G}^T_k(U^T_k)^{-1}B^T_k(\mathcal{G}^T_k)^{-1}\mathcal{F}^T_k, \tag{46}$$

$$\mathcal{P}^+_k = [(\mathcal{P}^-_k)^{-1} + \mathcal{H}^T R^{-1}_k \mathcal{H}]^{-1}, \quad \mu\hat{z}^+_k = \mathcal{P}^+_k[(\mathcal{P}^-_k)^{-1}\mu\hat{z}^-_k + \mathcal{H}^T R^{-1}_k y_k], \tag{47}$$

$$\hat{z}^+_{k,i} = \mathcal{A}^T_k(\hat{z}^-_{k,i} - \mu\hat{z}^-_k) + \mu\hat{z}^+_k. \tag{48}$$

[5] Tarantola, Albert. Inverse problem theory and methods for model parameter estimation. Society for Industrial Mathematics, 2005.

[6] Anderson, Jeffrey L. "An ensemble adjustment Kalman filter for data assimilation." *Monthly Weather Review* 129.12 (2001): 2884-2903.

EAKF: intuition

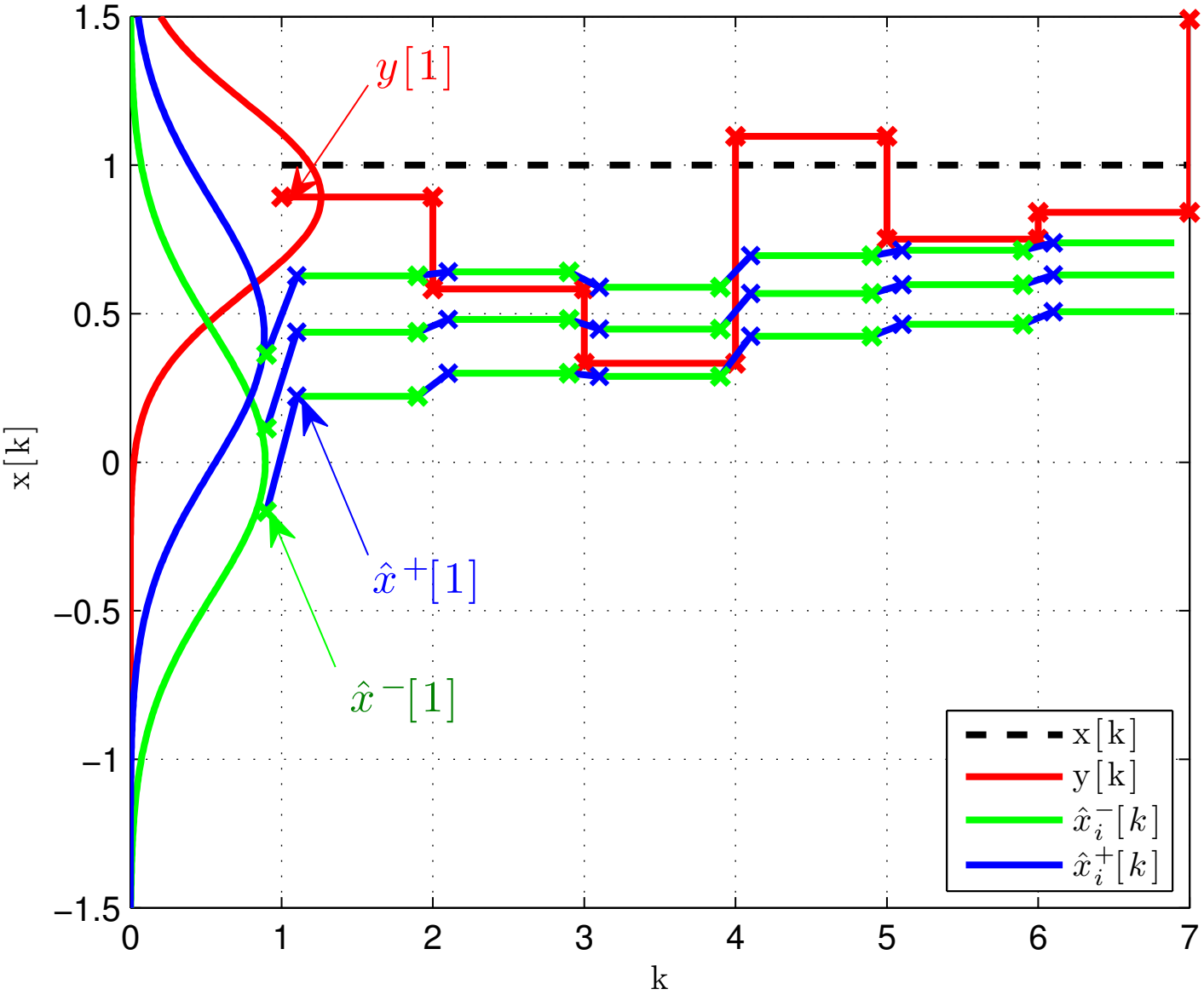

Filter Divergence

- Consider linear system

$$x_k = 0.5x_{k-1} + u_{k-1}, \qquad u_k = 1.0 + \sin(0.5k), \tag{49}$$

$$y_k = x_k + v_k, \qquad v_k \sim N(0, 0.2). \tag{50}$$

- If the driver varies with time but we assume it is constant, ensemble might collapse.

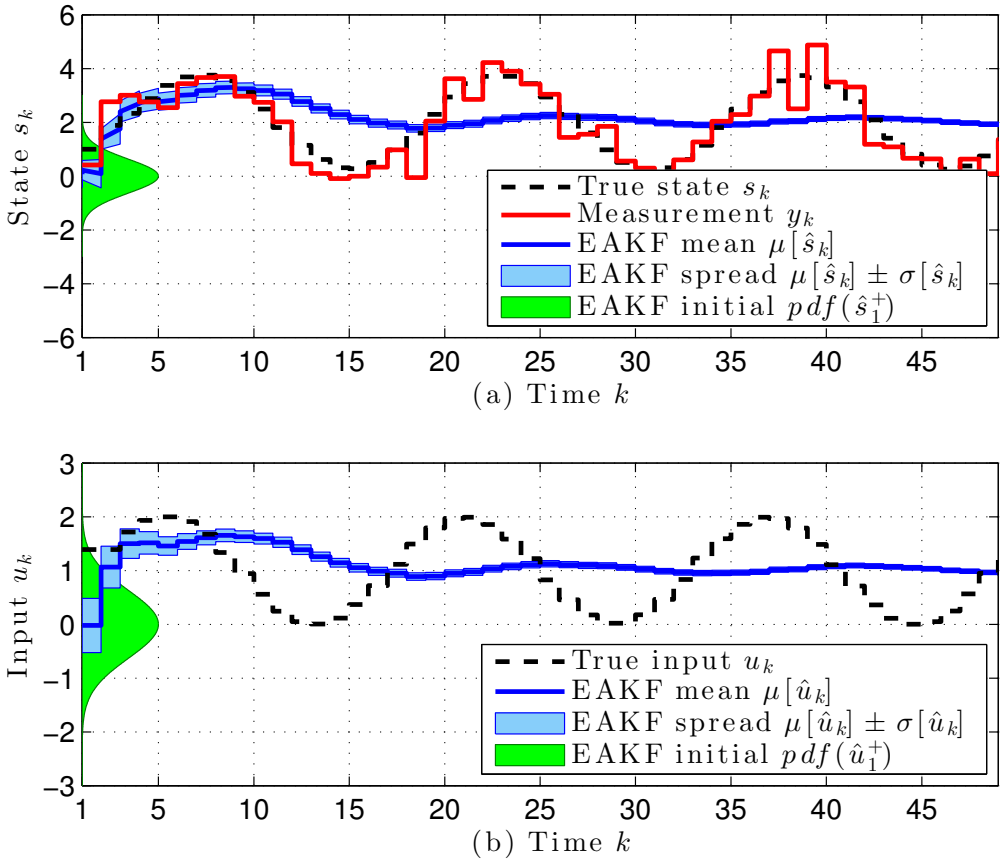

Ensemble Inflation

Ensemble inflation given by

$$\hat{x}_k^- = \sqrt{\lambda}(\hat{x}_k^- - \mu[\hat{x}_k^-]) + \mu[\hat{x}_k^-], \tag{51}$$

with $\lambda = 2.0$ alleviates filter divergence.

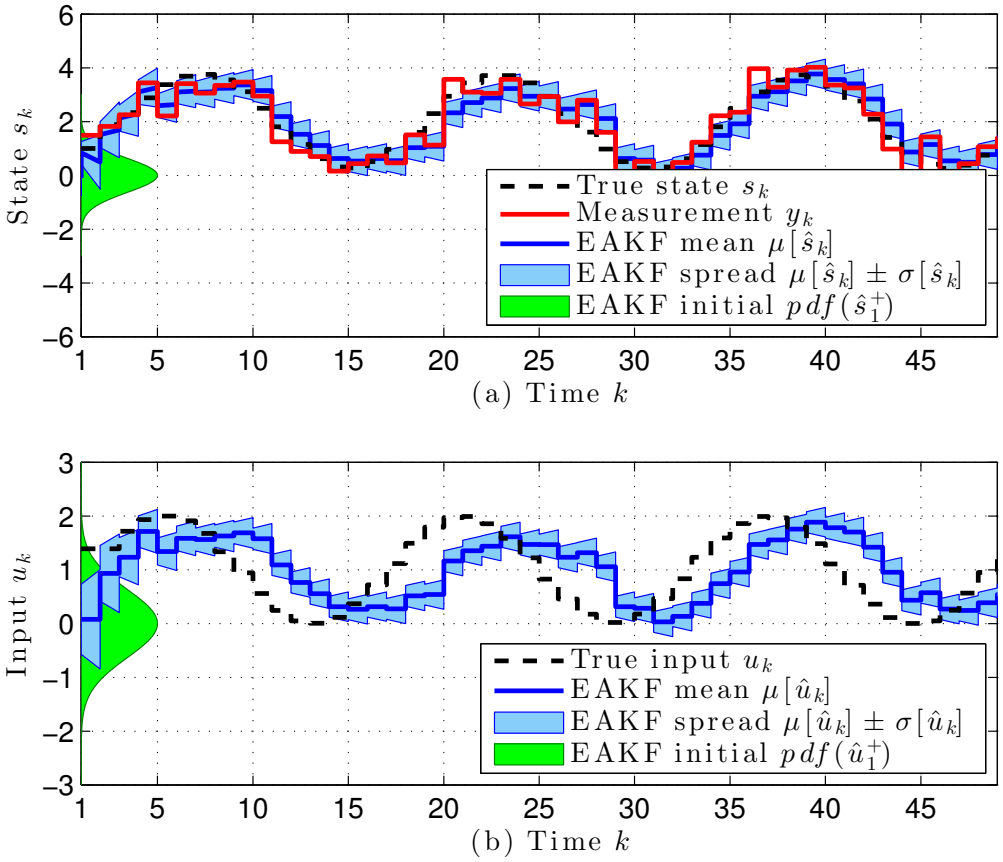

Differential Inflation

Inflating driver by

$$\hat{u}_k^- = \frac{\sqrt{\sigma_i^2}}{\sqrt{\sigma^2[u_k^-]}}(\hat{u}_k^- - \mu[\hat{u}_k^-]) + \mu[\hat{u}_k^-], \tag{52}$$

with $\sigma_i^2 = 0.12$ removes the lag in the driver estimate.

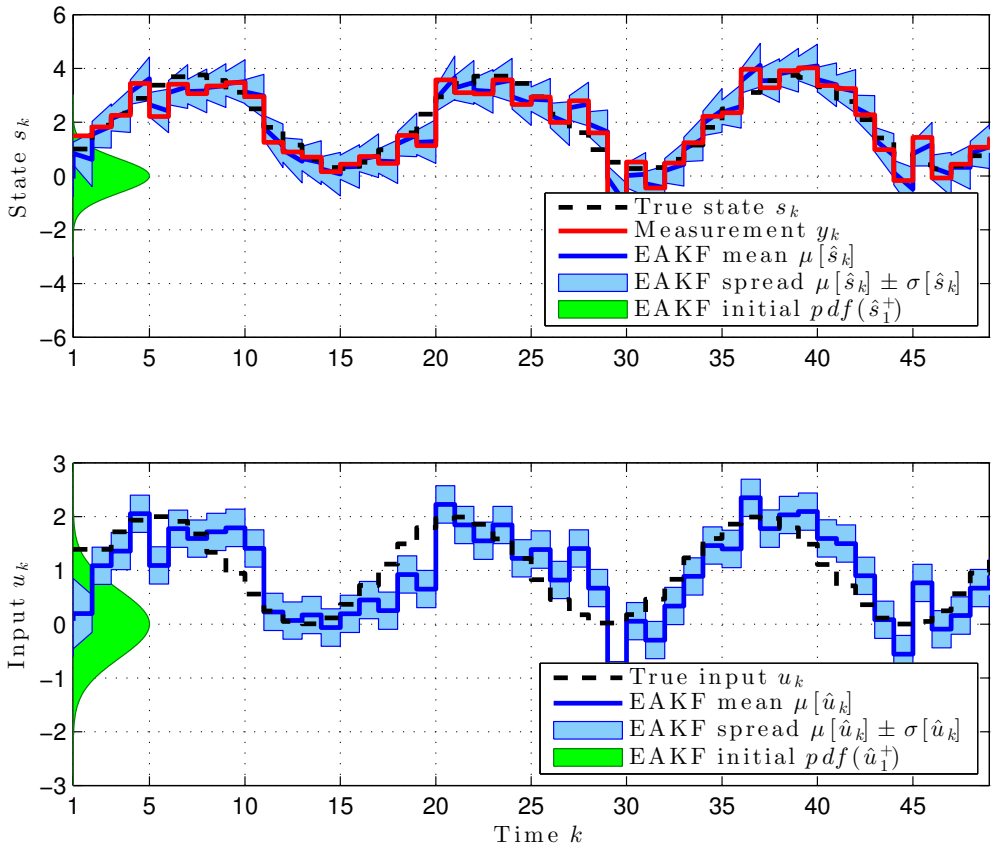

1 Summary

2 Problem Statement

3 GITM

4 EAKF

5 Assimilating CHAMP Neutral Density
- Simulated CHAMP data
- Real CHAMP data

6 Assimilating GPS Total Electron Content

7 Conclusions and Future Work

CHAMP and GRACE orbits

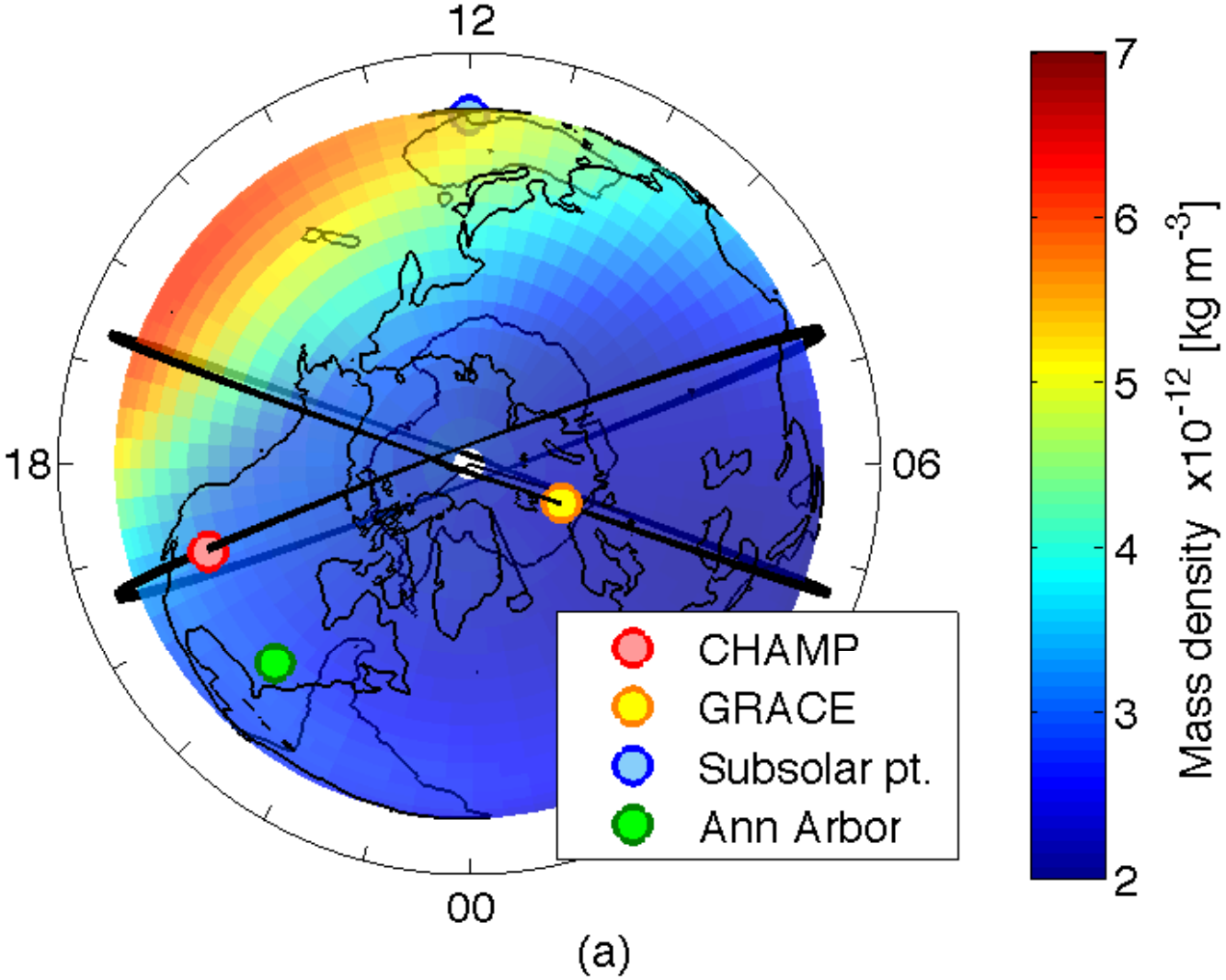

(a)

Sim: Does actual density track the desired density?

- **Measurement source:** ρ from GITM truth simulation ($F_{10.7} = 148$) is interpolated to the CHAMP location
- **Ensemble members:** 20 GITM instances with $F_{10.7} = N(130, 25)$

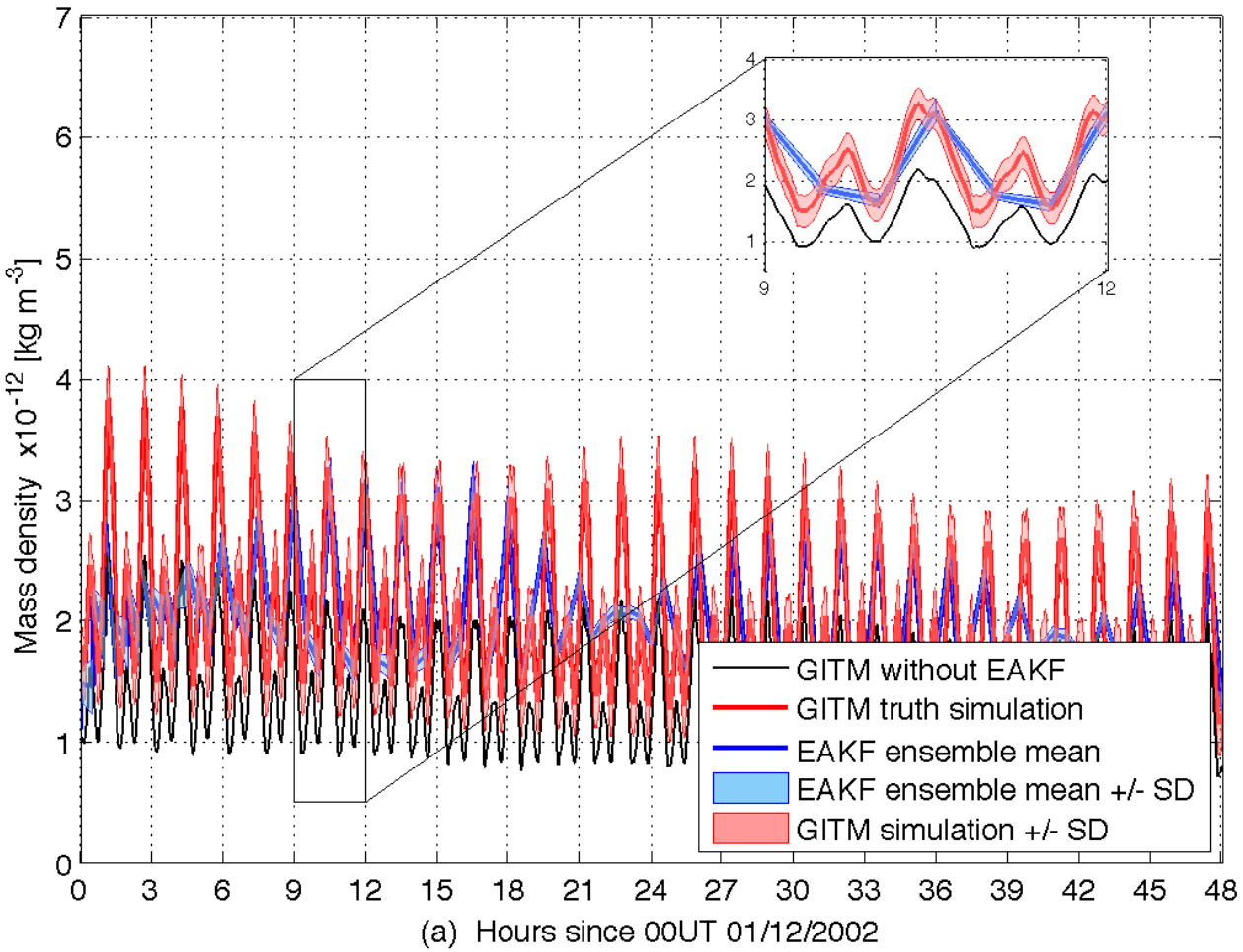

Same plot, but orbit averages

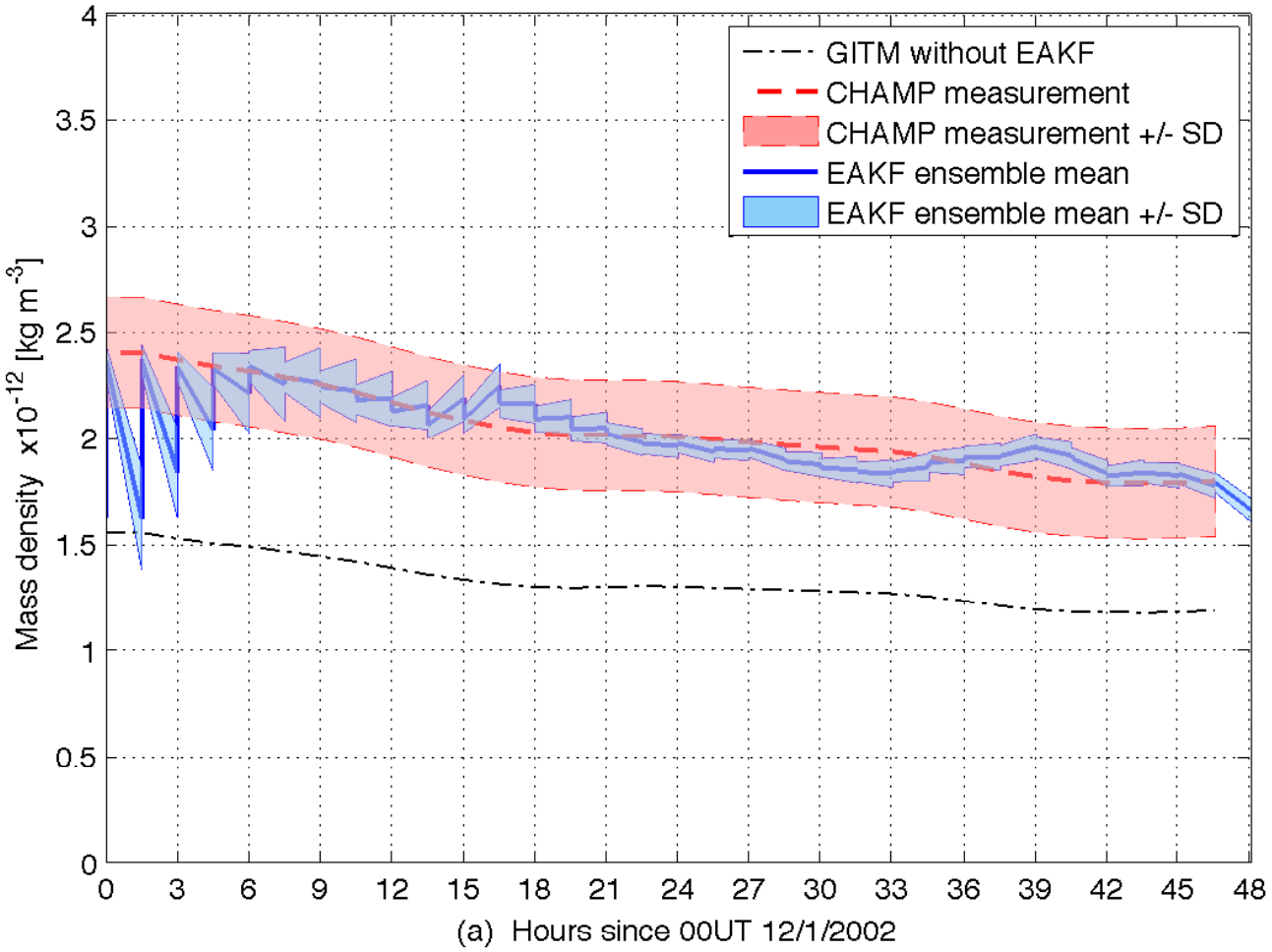

Sim: Does error at the measurement location go to zero?

Define RMS percentage error $\mathrm{RMSPE} \triangleq \frac{\sqrt{\overline{(\rho-\hat{\rho})^2}}}{\sqrt{\overline{\rho^2}}}$

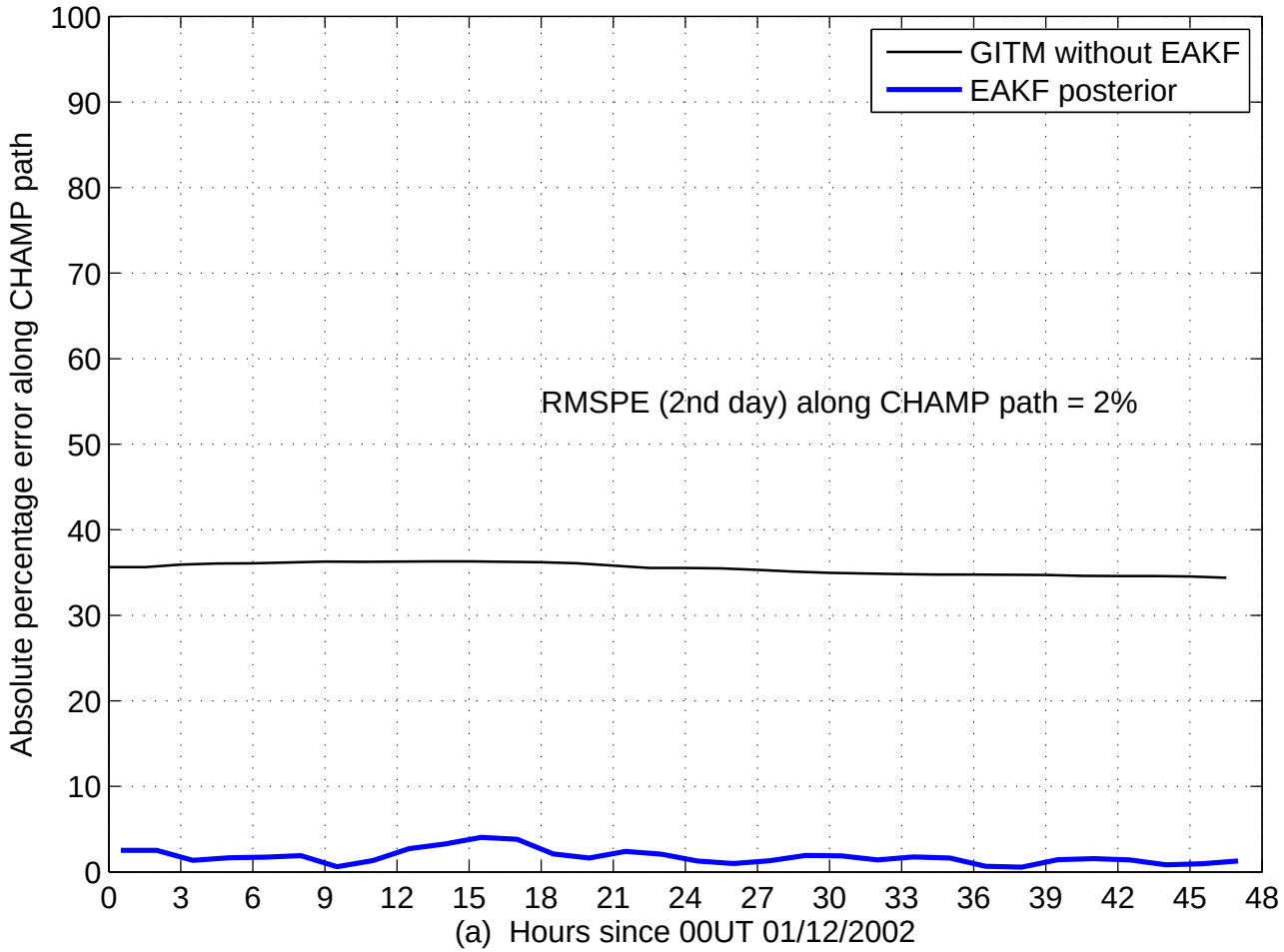

Sim: Does error at the validation location go to zero?

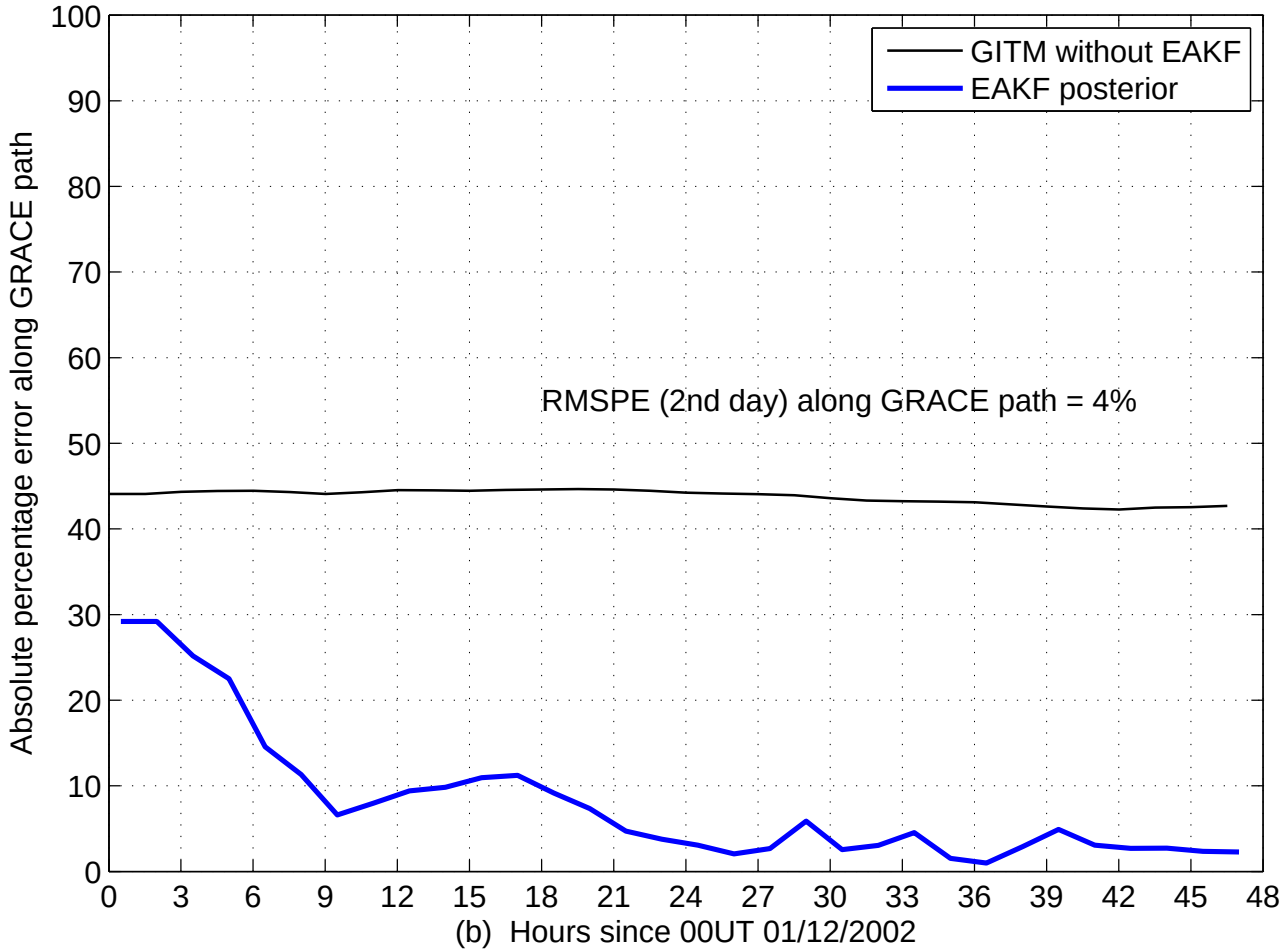

Sim: Does $F_{10.7}$ estimate converge to the true value?

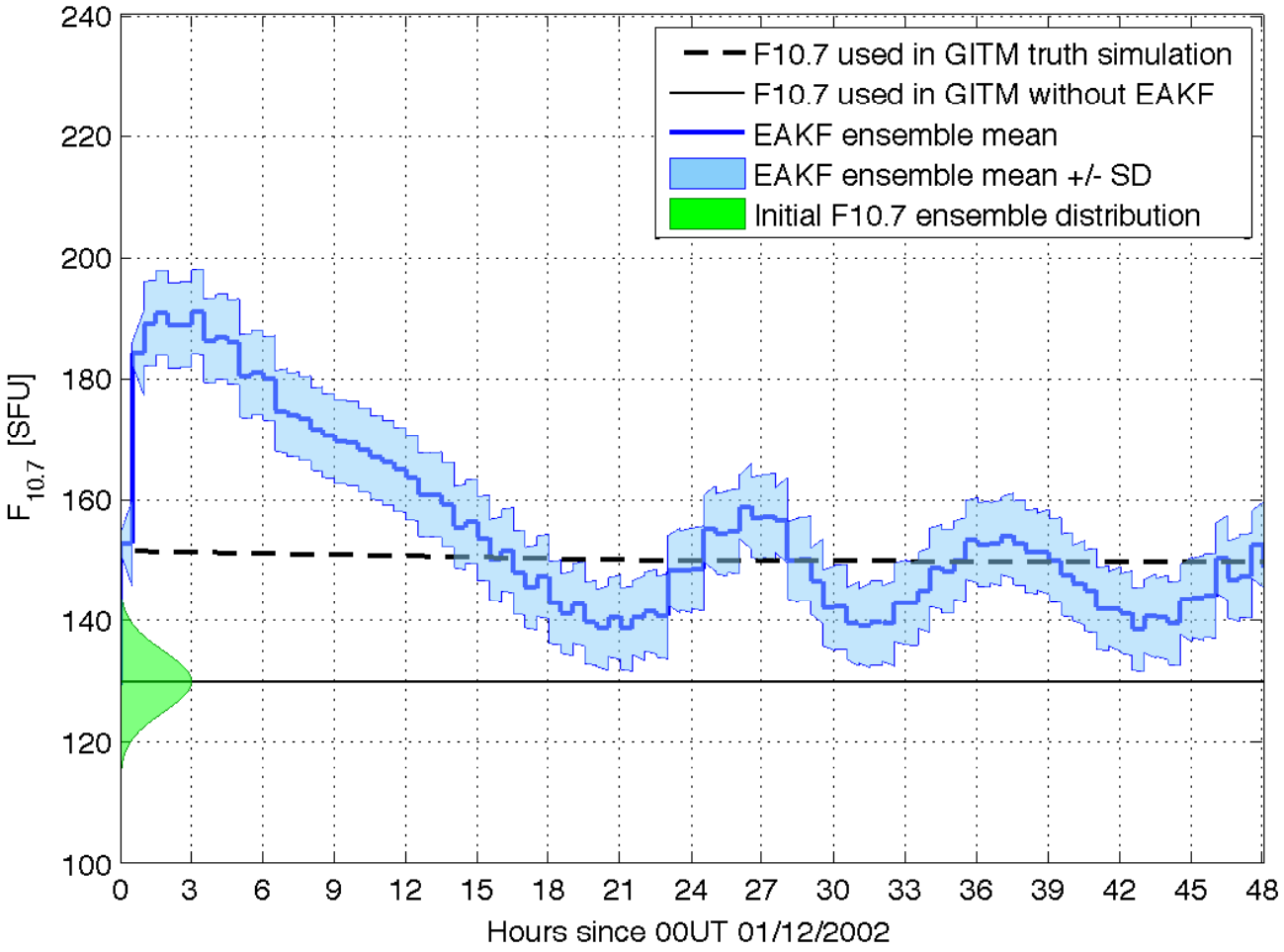

Real: Does actual density track the desired density?

- **Measurement source:** real CHAMP ρ with real CHAMP uncertainty
- **Ensemble members:** 20 GITM instances with $F_{10.7} = N(130, 25)$

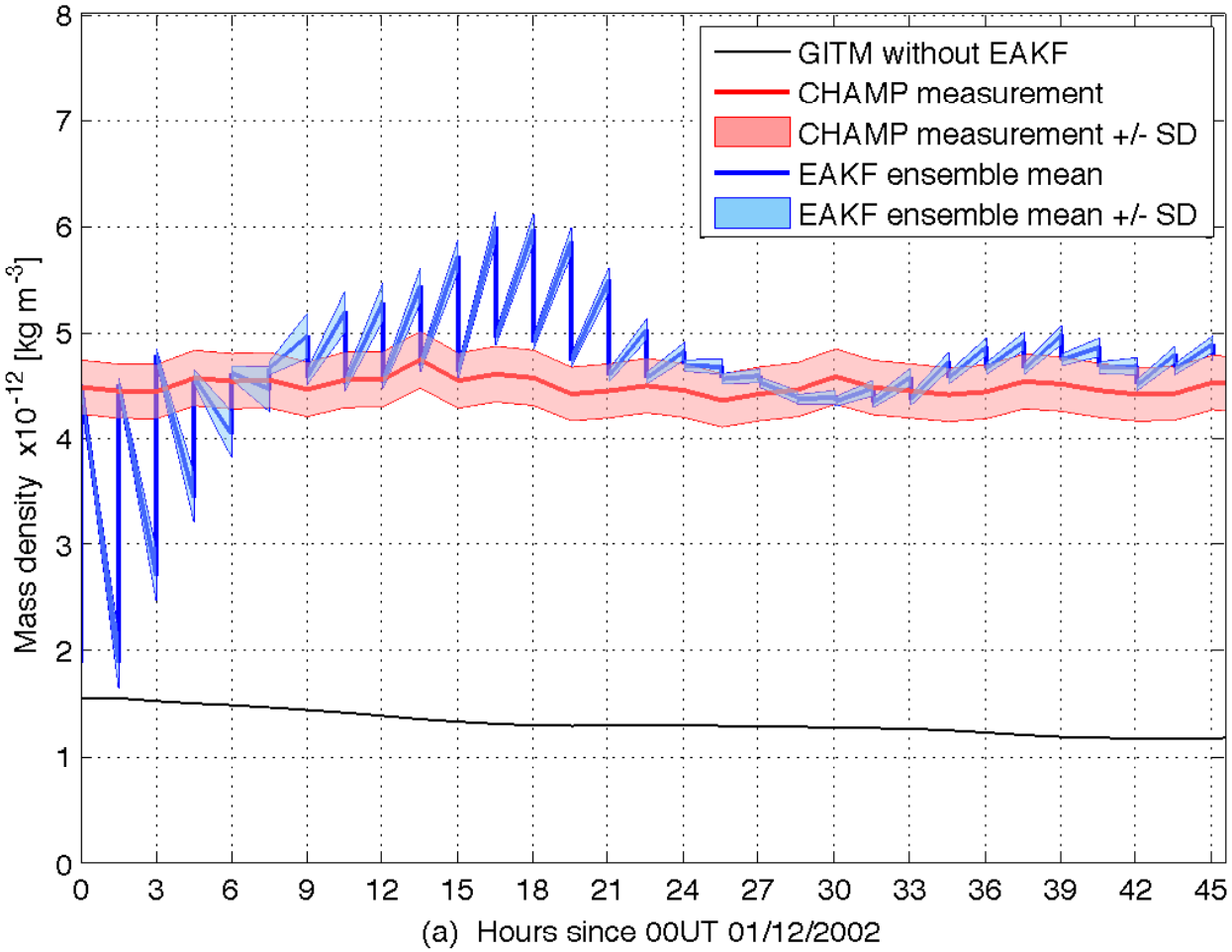

Real: Does error at the measurement location go to zero?

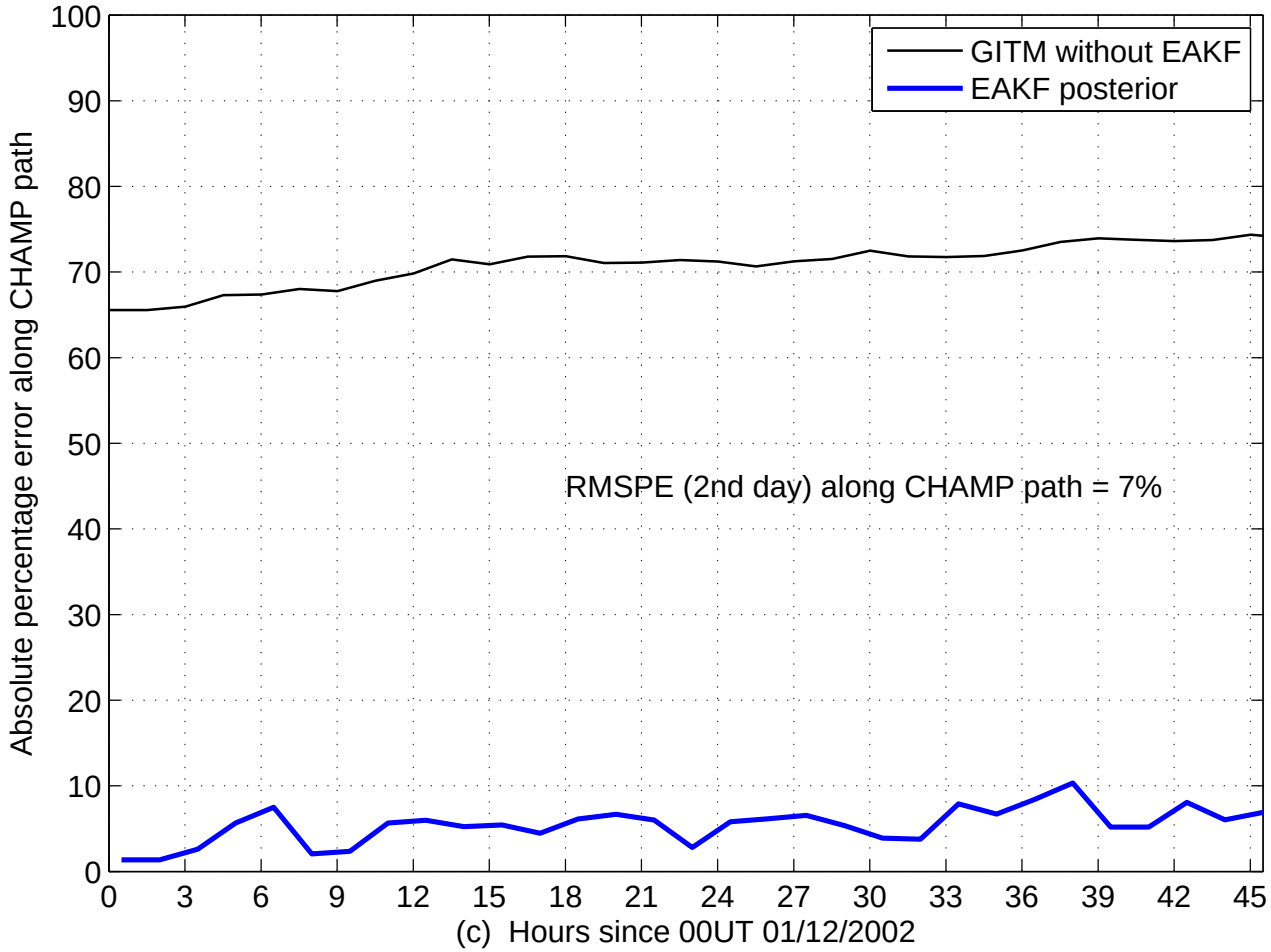

Real: Does error at the validation location go to zero?

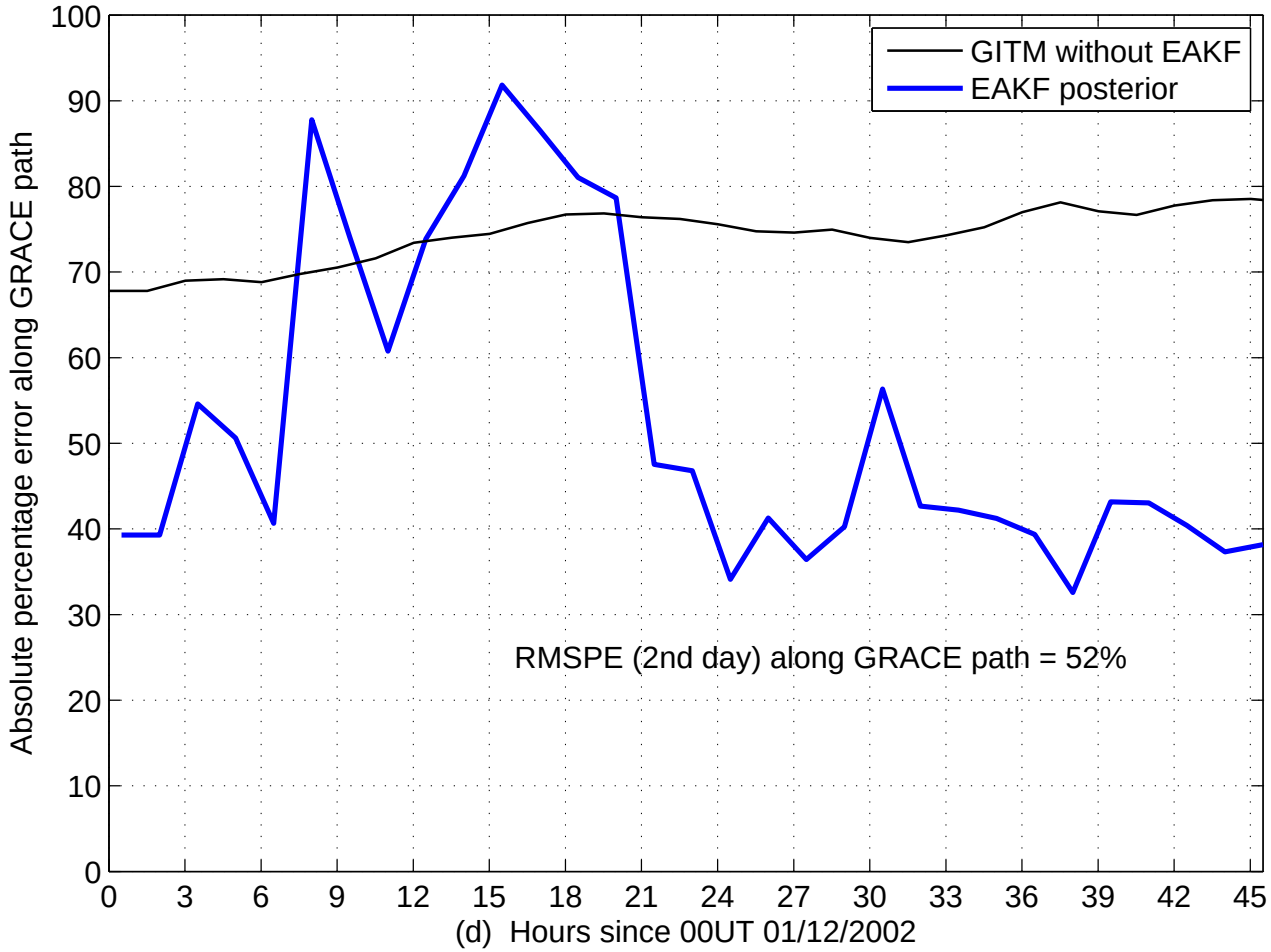

Real: Does $F_{10.7}$ estimate converge to the NOAA value?

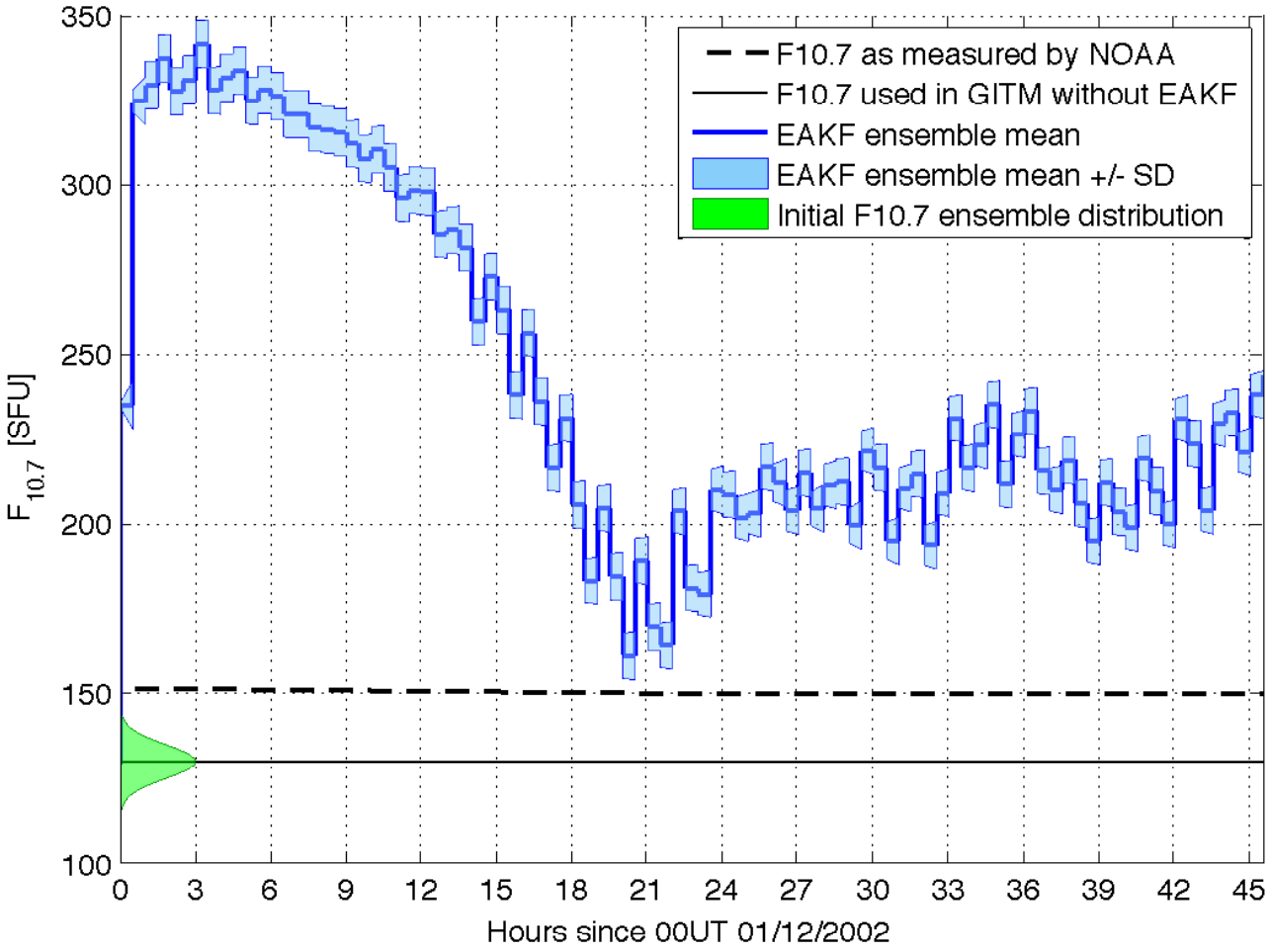

1 Summary

2 Problem Statement

3 GITM

4 EAKF

5 Assimilating CHAMP Neutral Density

6 Assimilating GPS Total Electron Content
- Simulated TEC data
- Real TEC data

7 Conclusions and Future Work

Real TEC data

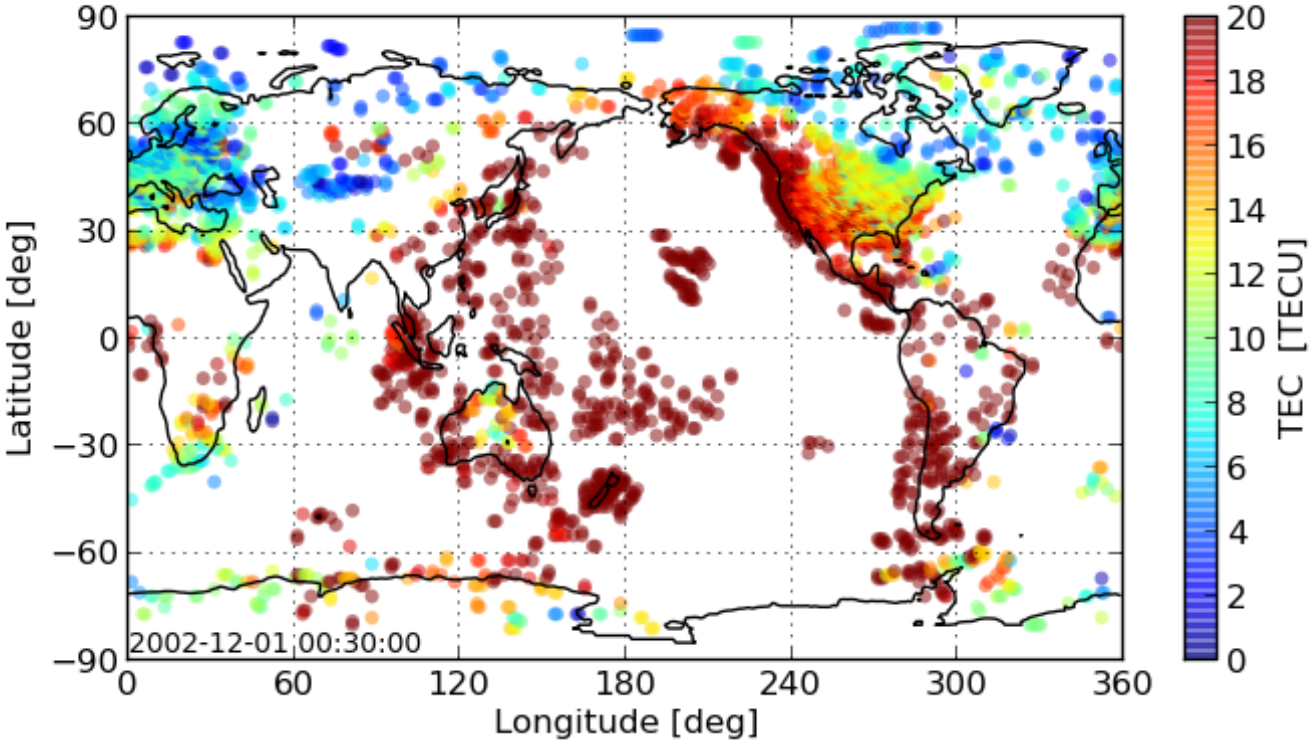

Simulated TEC data

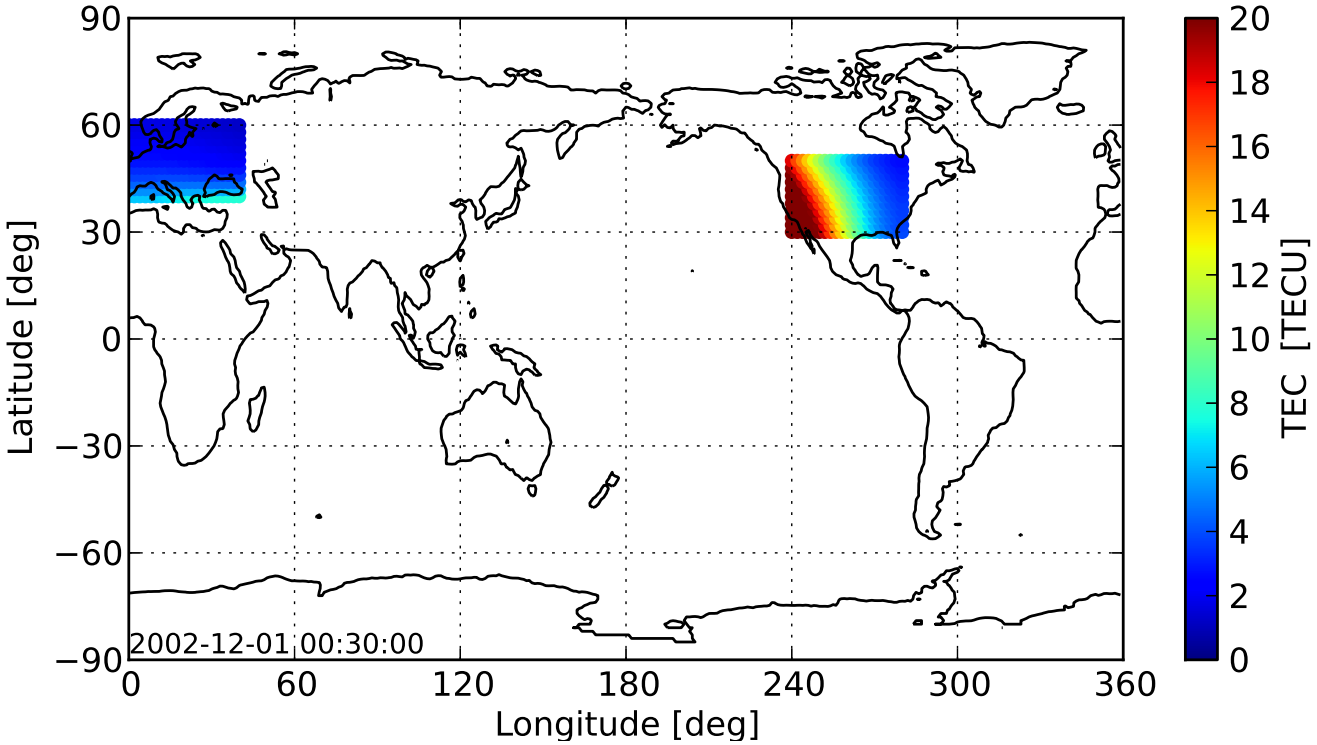

Sim: True and Estimated TEC

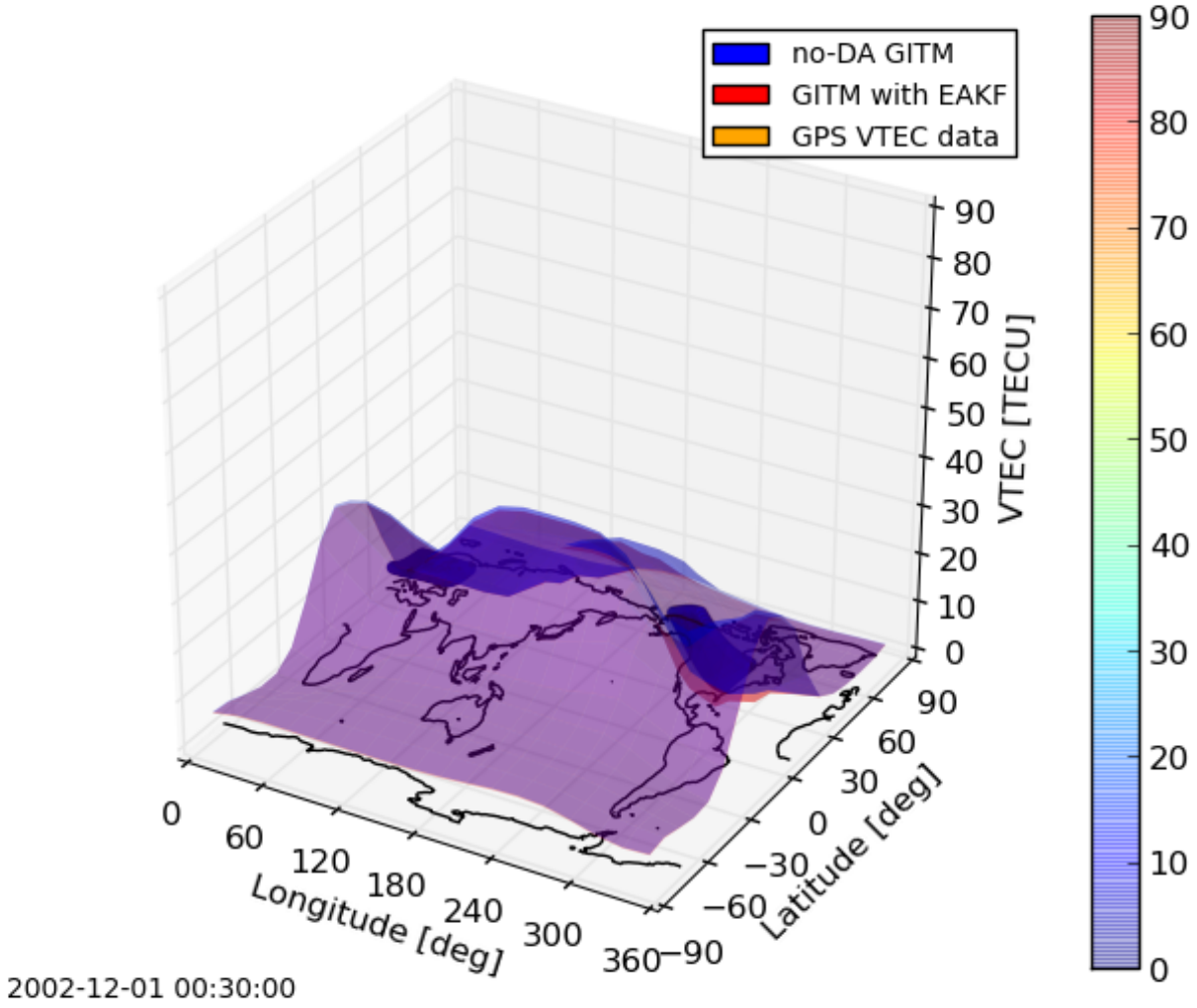

Sim: TEC error

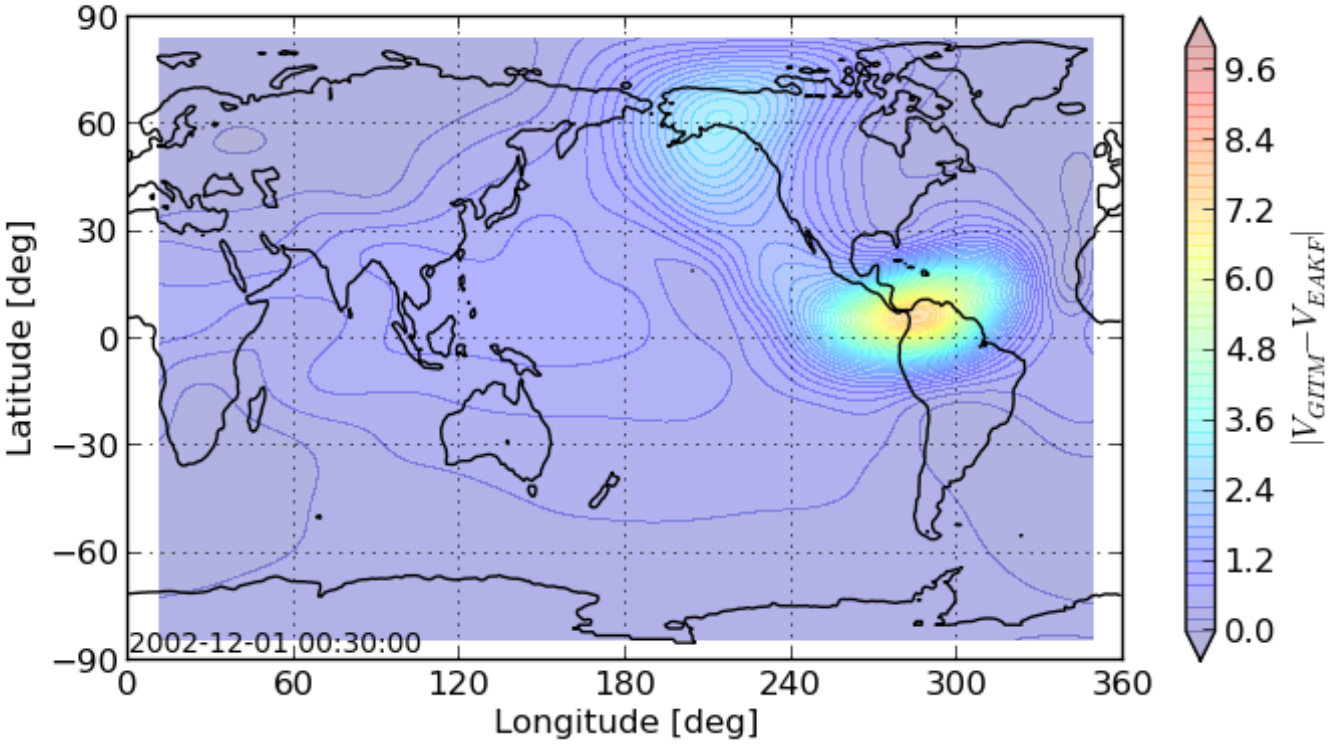

Sim: average error and driver

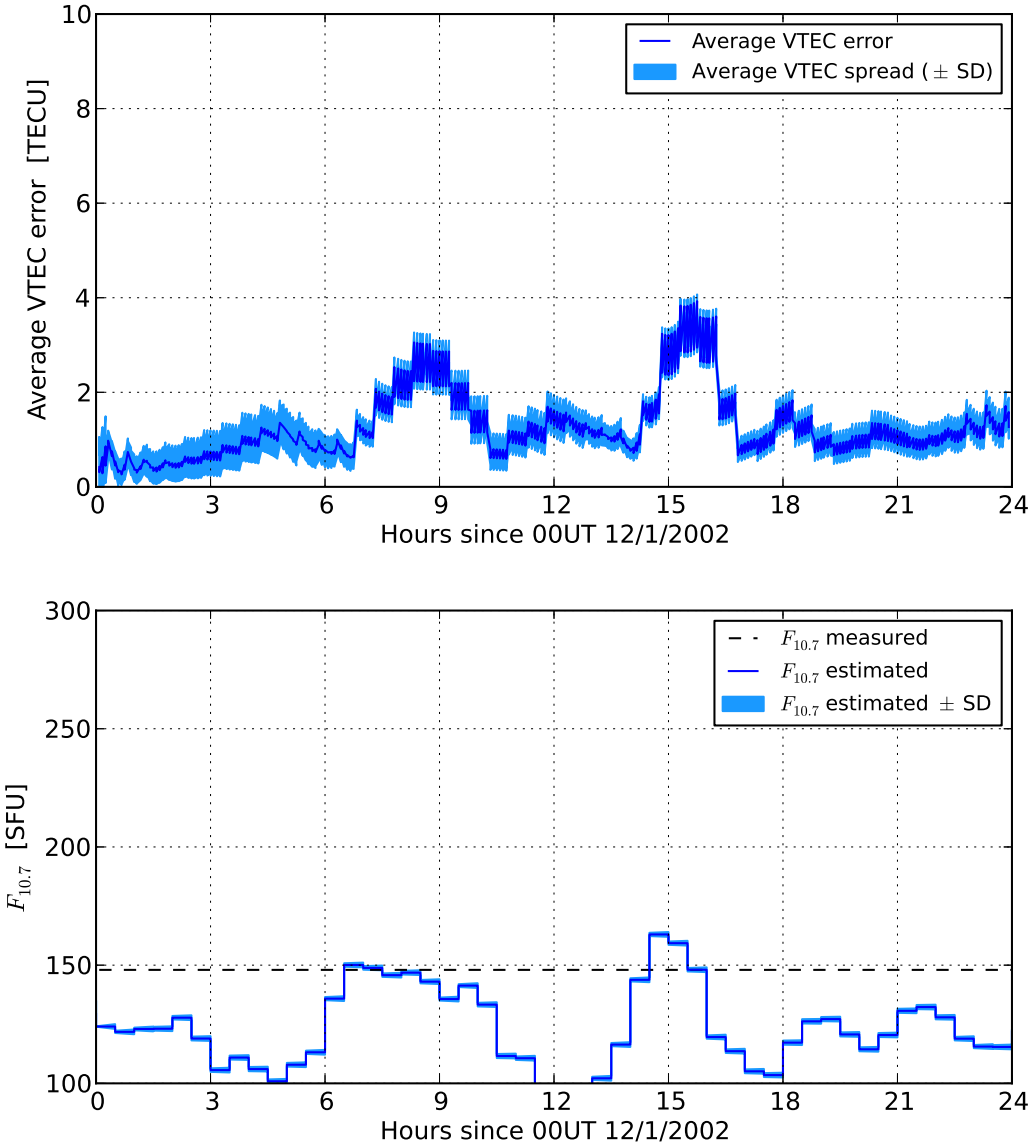

Sim: average error without driver estimation

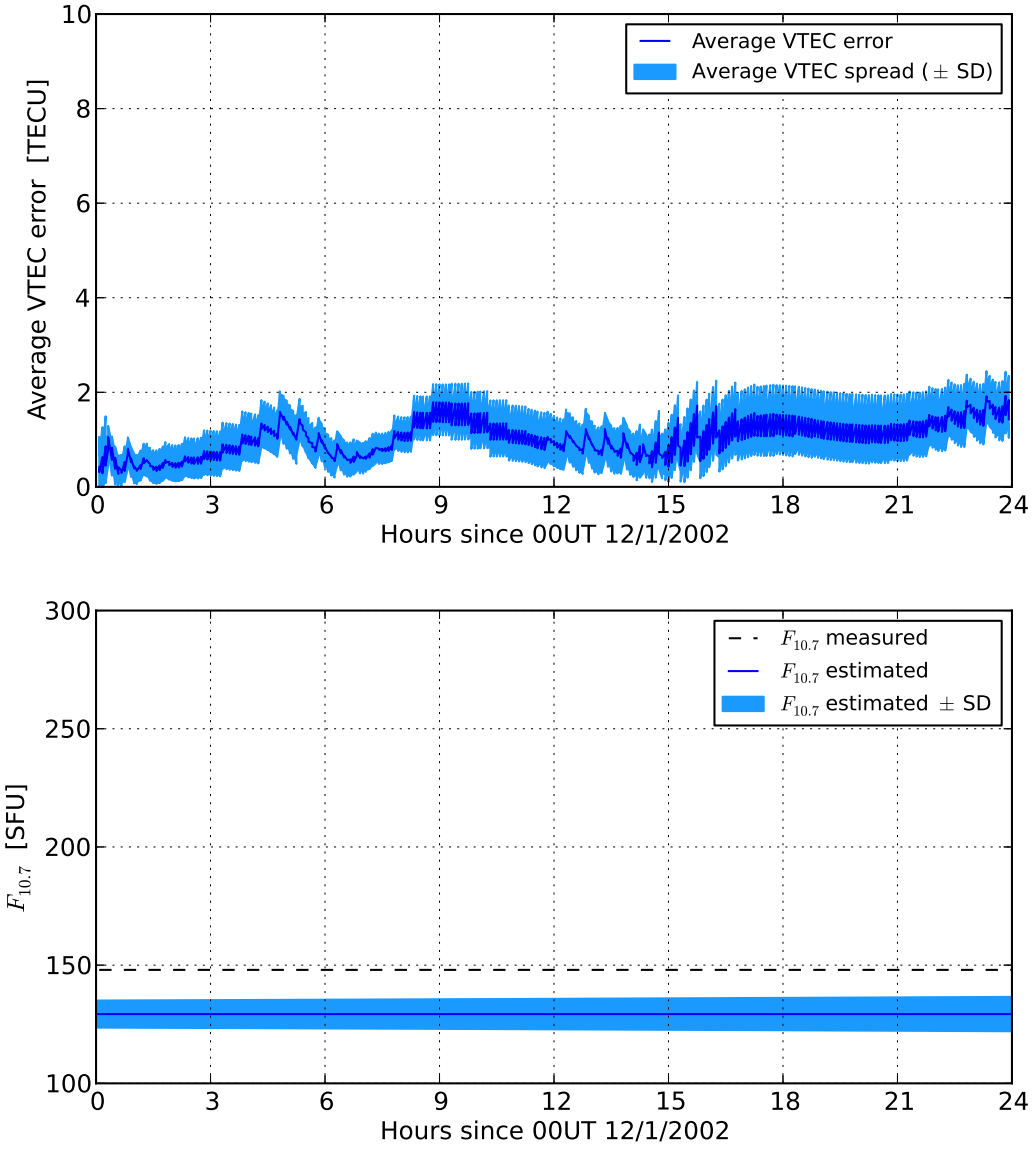

Real: True and Estimated TEC

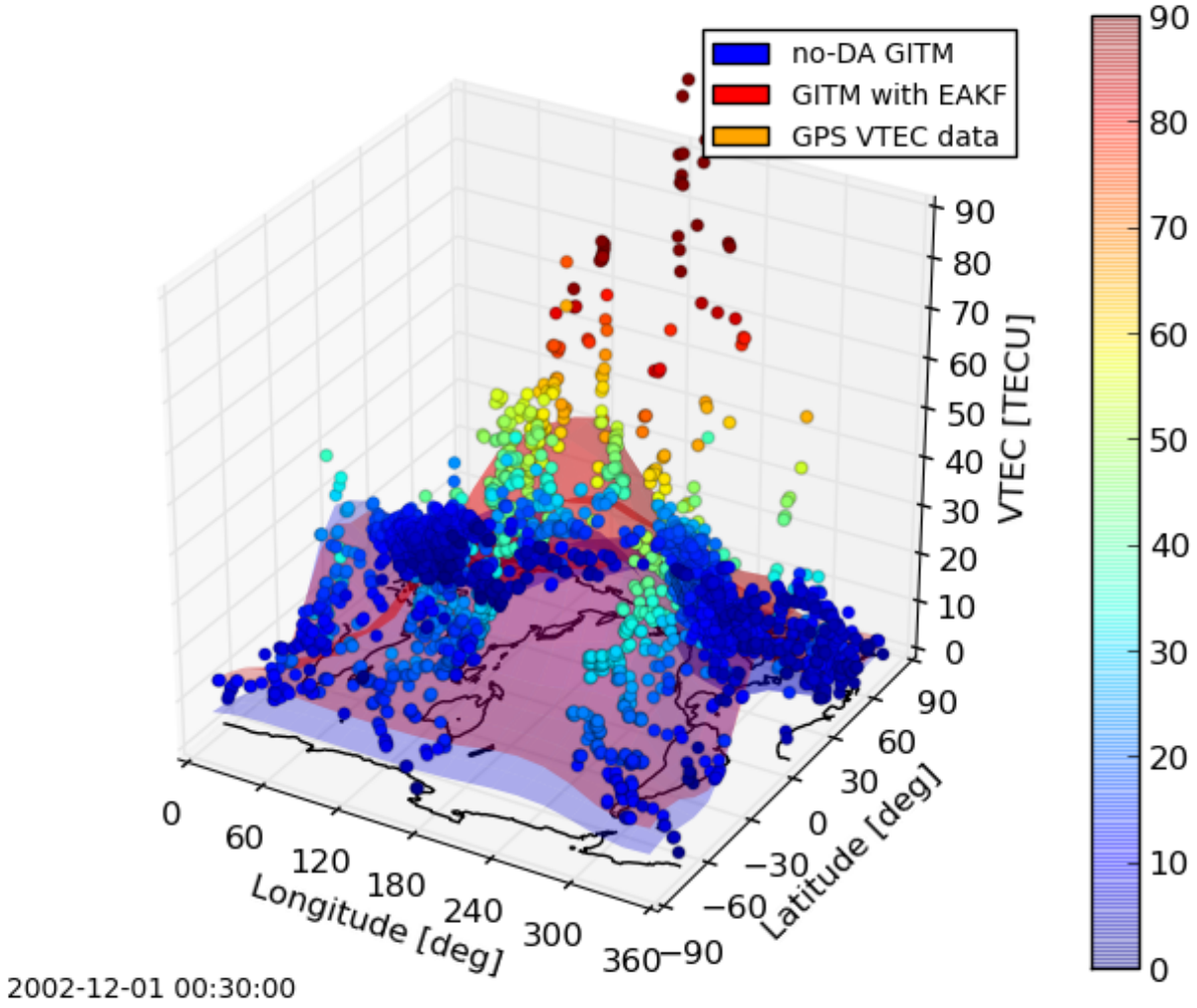

Real: TEC error

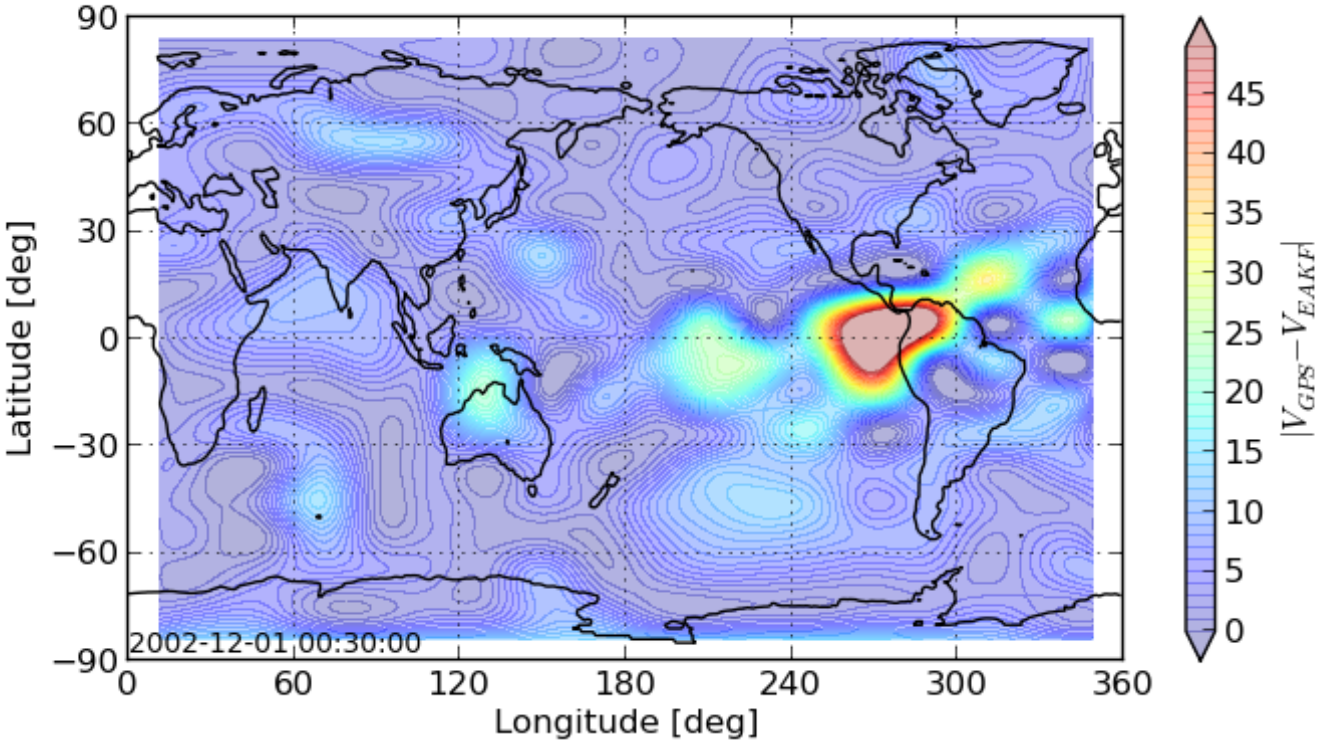

Real: average error and driver

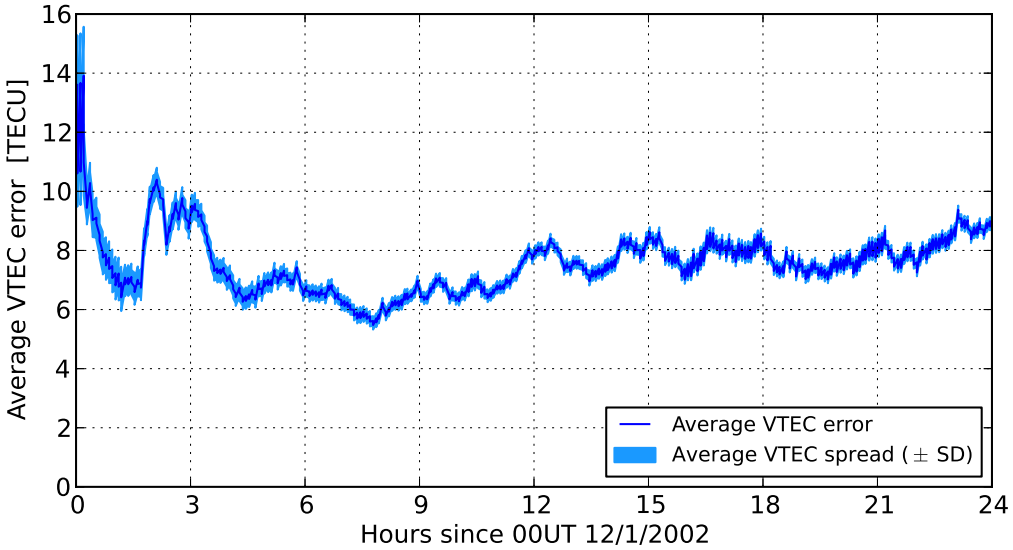

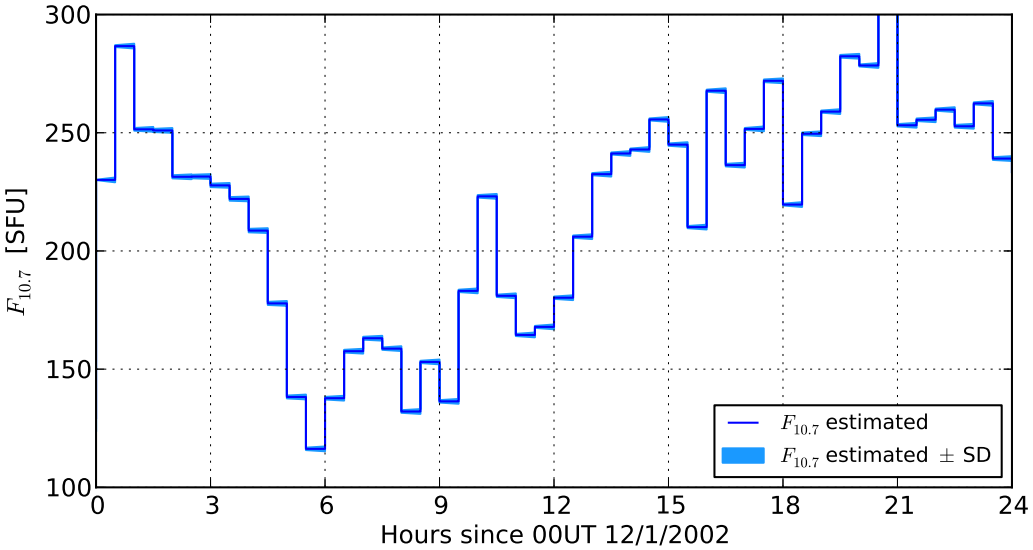

Real: average error without driver estimation

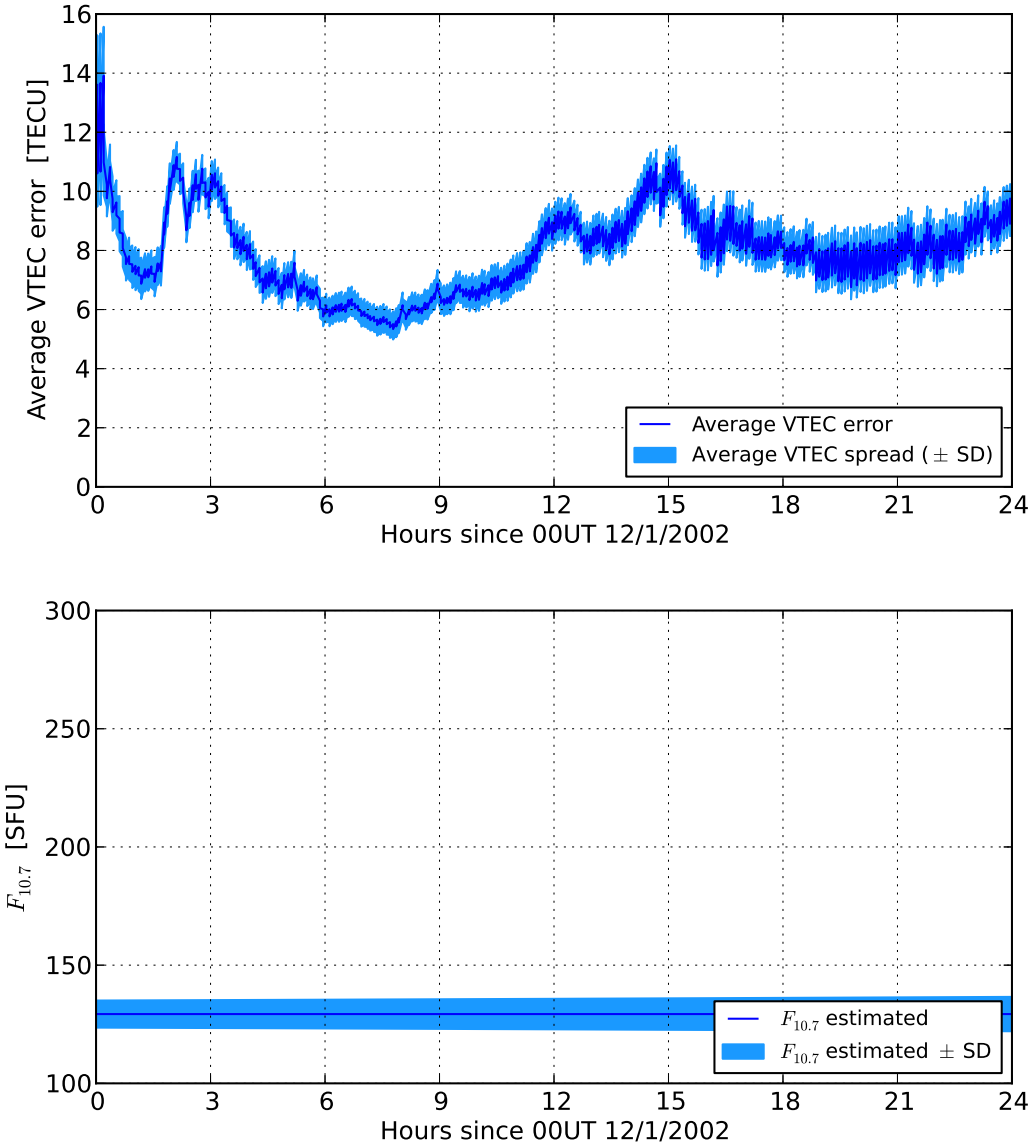

1 Summary

2 Problem Statement

3 GITM

4 EAKF

5 Assimilating CHAMP Neutral Density

6 Assimilating GPS Total Electron Content

7 Conclusions and Future Work

Conclusions

1. **DART-GITM interface:** This dissertation developed the framework for data assimilation of satellite data into a space weather model. In particular, it introduced driver estimation and demonstrated that drivers need to be inflated differently from the model states.
2. **Differential inflation:** The driver estimate was inflated differently from the rest of the variables, that is its spread was set to be constant to allow for continuous updating.
3. **CHAMP density assimilation:** The data assimilation technique was first demonstrated by using sparse thermospheric measurements.
4. **GPS TEC assimilation:** The interface was then modified to handle more global (ionospheric) measurements coming from the GPS satellites. It was found that the driver estimation in this more global case was not needed.

Future Work

1. $F_{10.7}$ **Localization:** $F_{10.7}$ estimate currently affects both the day-side and the night-side. It would be interesting to see the effect of localizing $F_{10.7}$.
2. **Slant TEC:** Only vertical total electron content measurements were considered so far. Implementing slant TEC would allow us to solve a broader class of problems.
3. **Heating efficiency:** Heating efficiency is a stronger driver for TEC, so estimating it using TEC data should be easier than estimating $F_{10.7}$.
4. **Geomagnetic storms:** This study only considered geomagnetic quiet times, so performing data assimilation during geomagnetic storms is subject of future work.

Questions?

RCAC Review

Consider the multi-input, multi-output discrete-time system

$$x(k+1) = Ax(k) + Bu(k) + D_1 w(k), \tag{53}$$
$$y(k) = Cx(k) + Du(k) + D_2 w(k), \tag{54}$$
$$z(k) = E_1 x(k) + E_2 u(k) + E_0 w(k). \tag{55}$$

Our goal is to develop an adaptive controller that generates a control signal u that minimizes the performance z in the presence of the exogenous signal w. For this presentation we consider SISO plants with no direct feedthrough and $z(k) = y(k)$ in command following context (i.e. $E_1 = C$, $E_2 = D = 0$, $E_0 = D_2 \neq 0$, $D_1 = 0$). We define Markov parameters as $H_i \triangleq CA^{i-1}B$ for $i > 0$.

$$z(k) = \sum_{i=1}^{n} -\alpha_i z(k-i) + \sum_{i=d}^{n} \beta_i u(k-i) + \sum_{i=0}^{n} \gamma_i w(k-i), \tag{56}$$

$$u(k) \triangleq \sum_{i=1}^{n_c} M_i(k) u(k-i) + \sum_{i=1}^{n_c} N_i(k) y(k-i), \quad u(k) = \theta(k)\phi(k), \quad \hat{u}(k) = \hat{\theta}(k)\phi(k), \tag{57}$$

$$Z(k) \triangleq \begin{bmatrix} z(k-1) \\ \vdots \\ z(k-p_c) \end{bmatrix}, \quad U(k) \triangleq \begin{bmatrix} u(k-1) \\ \vdots \\ u(k-p_c) \end{bmatrix}, \quad \hat{U}(k) \triangleq \begin{bmatrix} \hat{u}(k-1) \\ \vdots \\ \hat{u}(k-p_c) \end{bmatrix}, \tag{58}$$

$$\bar{B}_{zu} \triangleq [\ 0_d \ \ H_d \times poly(NMPz)\ ], or\ \bar{B}_{zu} = [\ 0_d \ \ H_d \ \ H_{d+1}\ ], \tag{59}$$

$$\hat{Z}(\hat{\theta}(k), k) \triangleq Z(k) - \bar{B}_{zu}\left(U(k) - \hat{U}(k)\right), \tag{60}$$

where green highlighting represents known variables, yellow - measured variables, and red - variables to be found.

RCAC Review continued

We now consider the cost function

$$J(\hat{\theta}, k) \triangleq \hat{Z}^{\mathrm{T}}(\hat{\theta}, k)\hat{Z}(\hat{\theta}, k) + \zeta(k)\mathrm{tr}\left[(\hat{\theta}-\theta)^{\mathrm{T}}(\hat{\theta}-\theta)\right], \tag{61}$$

where the positive scalar $\zeta(k)$ is the learning rate. Substituting (60) into (61), the cost function can be written as the quadratic form

$$J(\hat{\theta}, k) = \left(\mathrm{vec}\ \hat{\theta}\right)^{\mathrm{T}} \mathcal{A}(k)\ \mathrm{vec}\ \hat{\theta} + \mathcal{B}(k)^{\mathrm{T}}\ \mathrm{vec}\ \hat{\theta} + \mathcal{C}(k), \tag{62}$$

where

$$\begin{aligned}
D(k) &\triangleq \sum_{i=1}^{p_{\mathrm{c}}} \phi^{\mathrm{T}}(k-i) \otimes (\bar{B}_{zu}L_i),\\
f(k) &\triangleq Z(k) - \bar{B}_{zu}U(k),\\
\mathcal{A}(k) &\triangleq D^{\mathrm{T}}(k)D(k) + \zeta(k)I_{n_{\mathrm{c}}l_u(l_u+l_y)},\\
\mathcal{B}(k) &\triangleq 2D^{\mathrm{T}}(k)f(k) - 2\zeta(k)\mathrm{vec}\ \theta(k),\\
\mathcal{C}(k) &\triangleq f(k)^{\mathrm{T}}f(k) + \zeta(k)\mathrm{tr}\left[\theta^{\mathrm{T}}(k)\theta(k)\right].
\end{aligned} \tag{63}$$

Since $\mathcal{A}(k)$ is positive definite, $J(\hat{\theta}, k)$ has the strict global minimizer

$$\hat{\theta}(k) = -\tfrac{1}{2}\mathrm{vec}^{-1}(\mathcal{A}(k)^{-1}\mathcal{B}(k)). \tag{64}$$

The controller gain update law is $\theta(k+1) = \hat{\theta}(k)$.

Computational Study of RCAC Robustness

Consider the discrete-time system

$$G(z) = \frac{z - 1.4}{(z - .5)(z - .6)(z - .7)}. \tag{65}$$

With NMP zero location known exactly RCAC achieves transient performance of about 1.6. Transient and steady state performances are defined as

$$z_{tr} = \max_k |z(k)|, \tag{66}$$

$$z_{ss} = \max_{k=900:1000} |z(k)|. \tag{67}$$

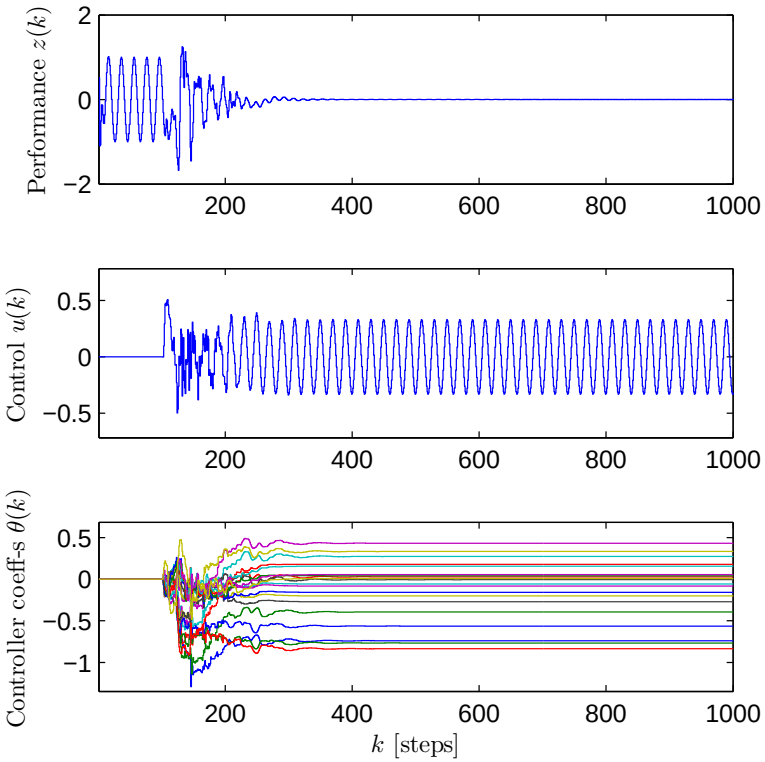

Computational Study of RCAC Robustness continued

When location of the nonminimum phase zero is uncertain, transient performance can become unbounded

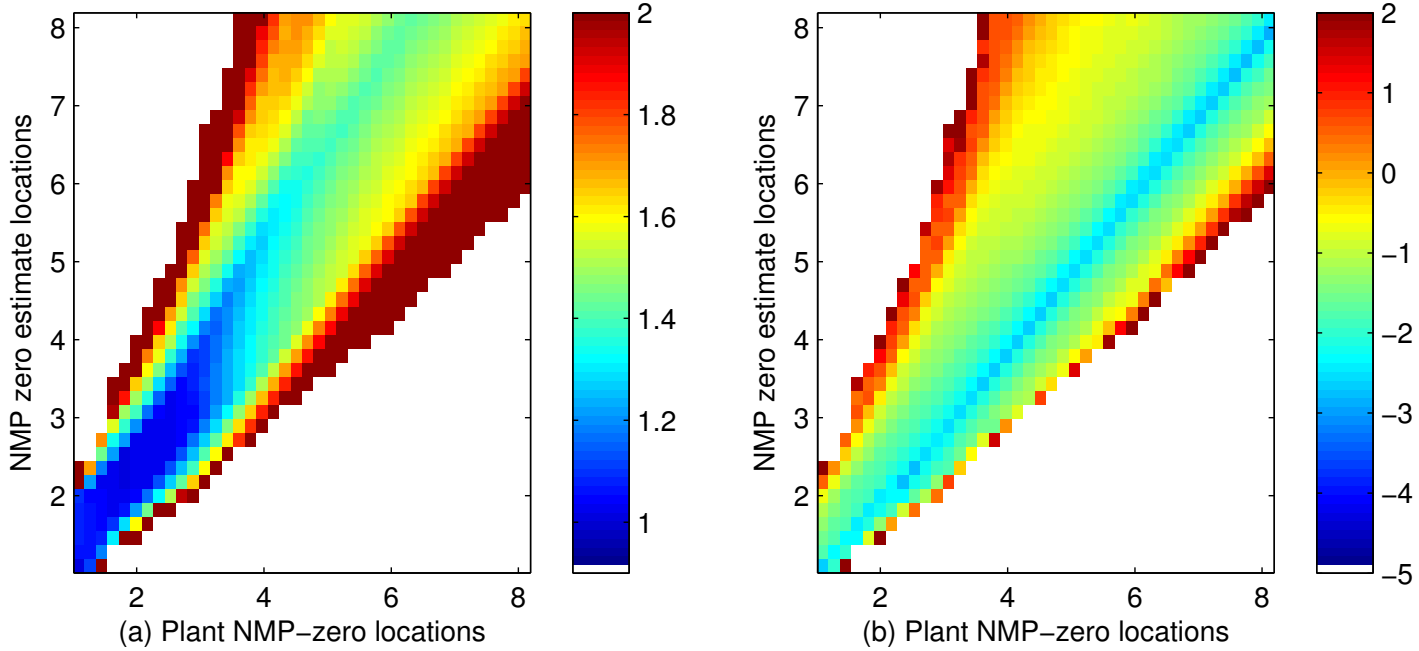

In this plot, the true nonminimum phase zero (x-axis) and zero estimate (y-axis) are varied from 1.1 to 8.1. We conclude that RCAC is more robust to overestimating the location of the nonminimum phase zero than to underestimating it. Additionally, the cases with NMP zeros further out on the real axis result in greater stability margins than those with NMP zeros closer to 1.

Computational Study of RCAC Robustness continued

We now generate 50 stable second order plants with random poles and NMP zero at 2 and test RCAC with NMP zero estimates varying from 1.4 to 10.

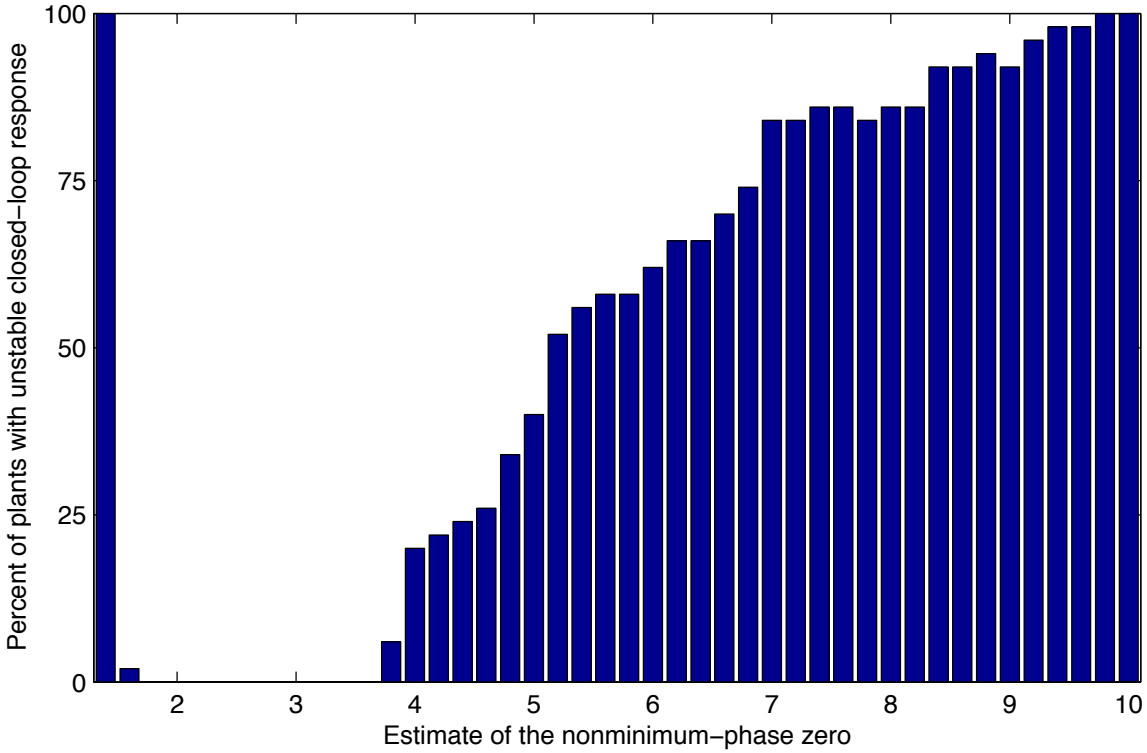

For these 50 random plants, the stability of the closed-loop system is less sensitive to overestimating the location of the NMP zero than it is to underestimating the location of the NMP zero. However, none of the 50 plants have an upward margin in excess of 10, which corresponds to 5 times the true value of the NMP zero.

Computational Study of RCAC Robustness continued

We can extend these findings to plants with higher order and bigger relative degree.

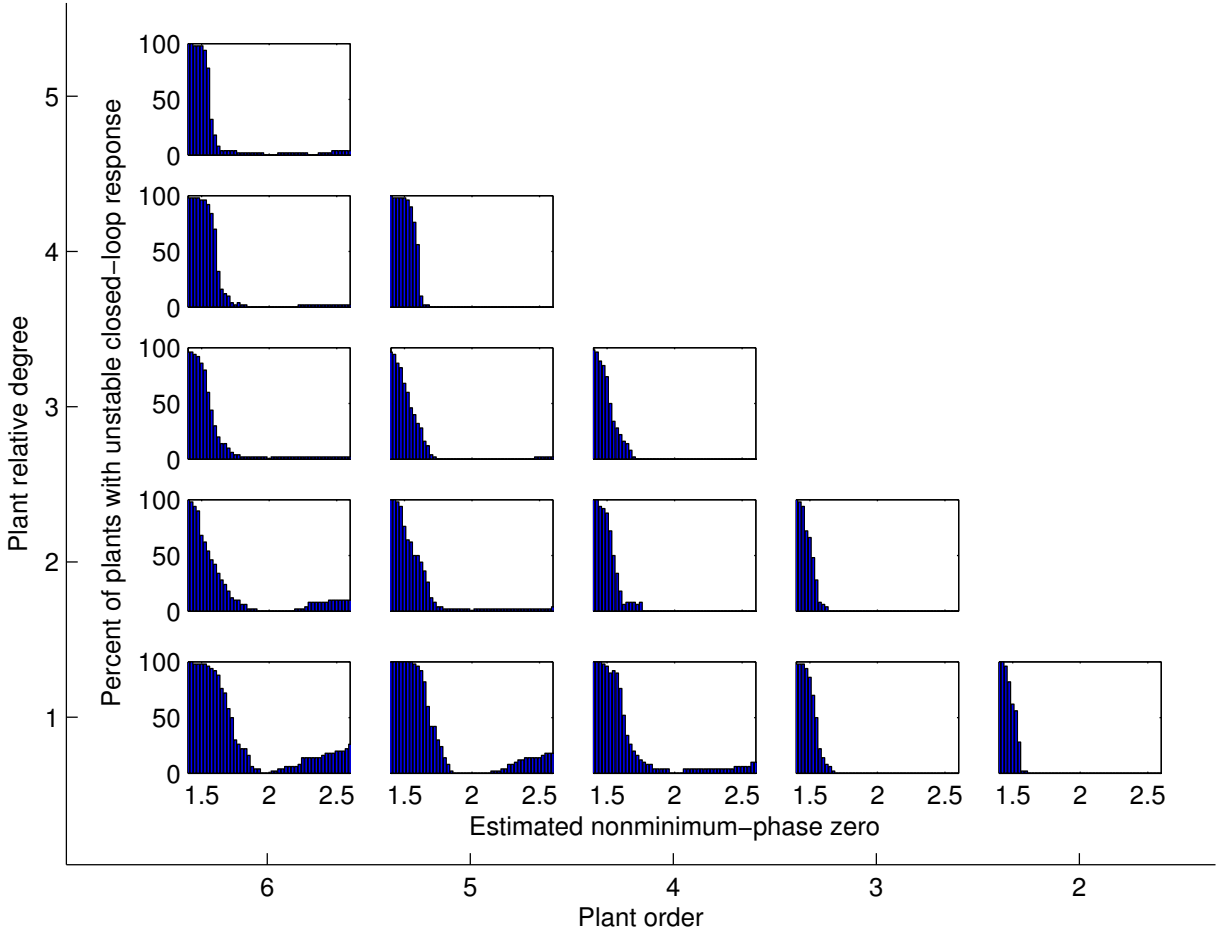

We find that robustness to the estimate of the NMP zero increases in rows from left to right (with decreasing order), and in columns from bottom to top (with increasing relative degree).

Convex Constraint on Pole Locations

The denominator coefficients of the controller (60) are given by

$$\text{den}(\theta(k)) \triangleq [1 \;\; -M_1 \;\; -M_2 \;\; \cdots \;\; -M_{n_c}]. \tag{68}$$

We modify the problem of minimizing (62) by imposing a maximum singular value constraint on the companion-form matrix

$$K \triangleq \begin{bmatrix} M_1 & M_2 & \dots & M_{n_c-1} & M_{n_c} \\ 1 & 0 & \dots & 0 & 0 \\ 0 & 1 & \dots & 0 & 0 \\ \vdots & \vdots & \ddots & \vdots & \vdots \\ 0 & 0 & \dots & 1 & 0 \end{bmatrix}, \tag{69}$$

$$\sigma_{\max}(K) \leq \gamma, \gamma > 1. \tag{70}$$

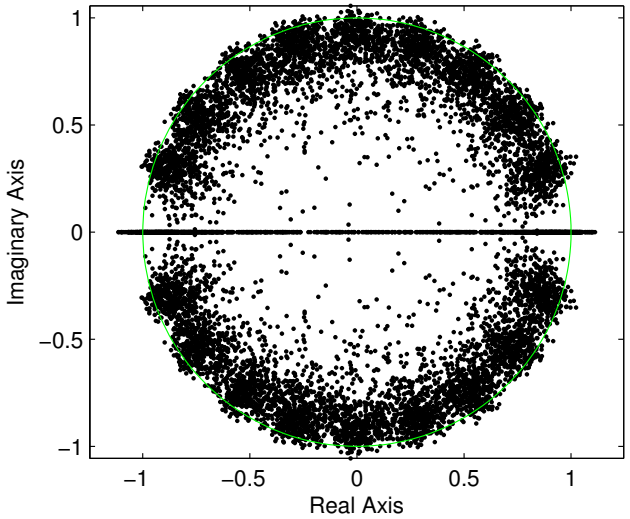

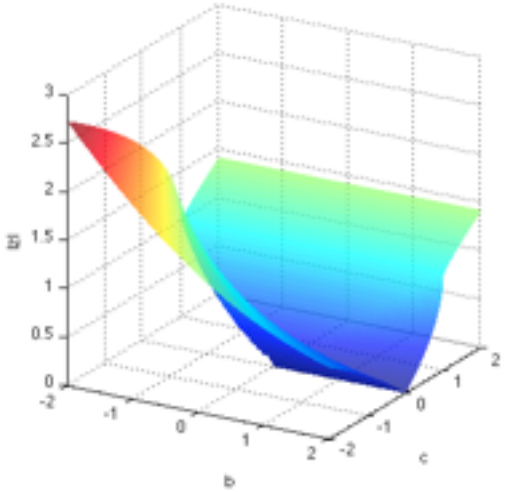

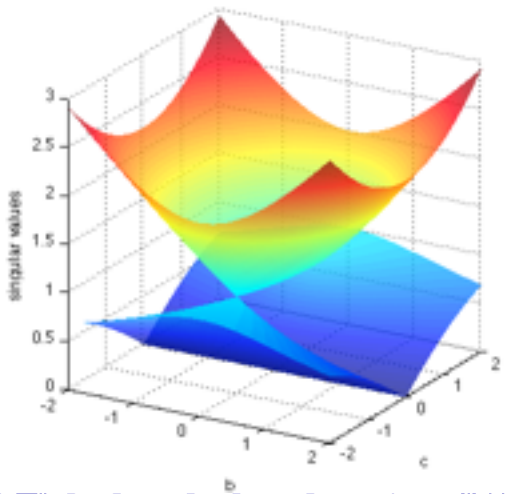

Convex Constraint on Pole Locations continued

Convex constraint improves transient performance

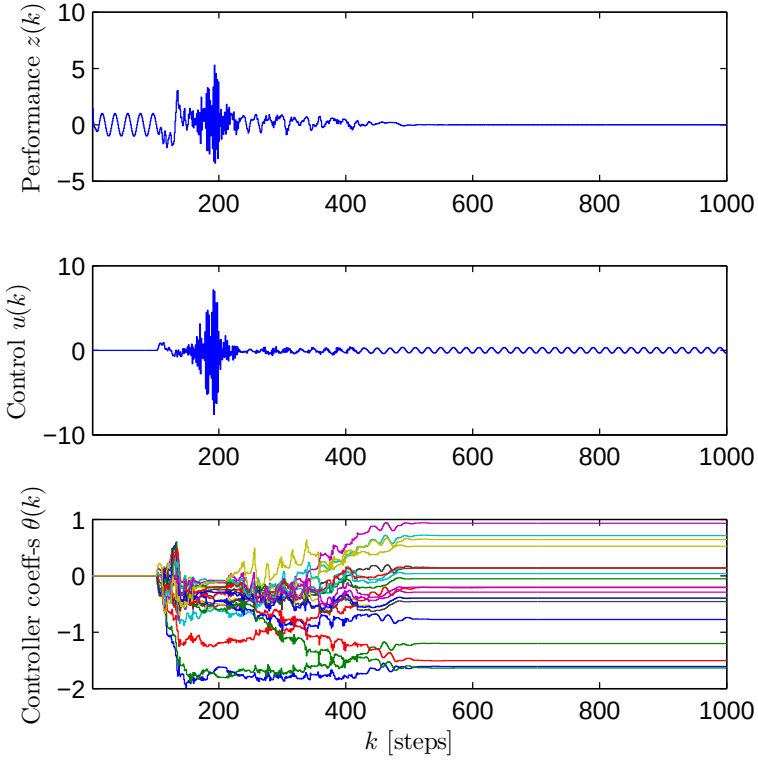

RCAC

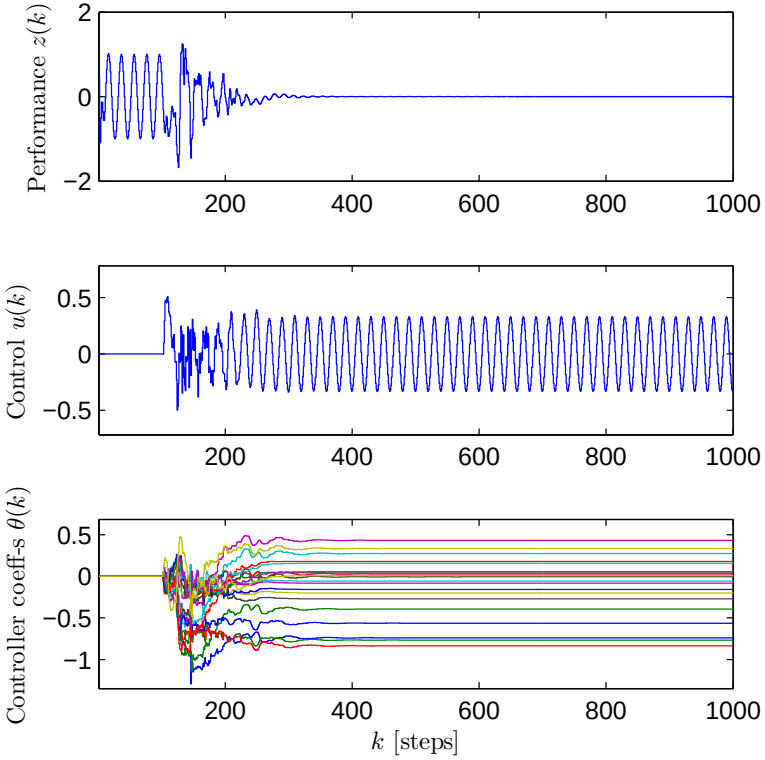

CC-RCAC

Convex Constraint on Pole Locations continued

Evolution of the controller poles is shown as a function of time in terms of color. CC-RCAC poles settle twice as fast.

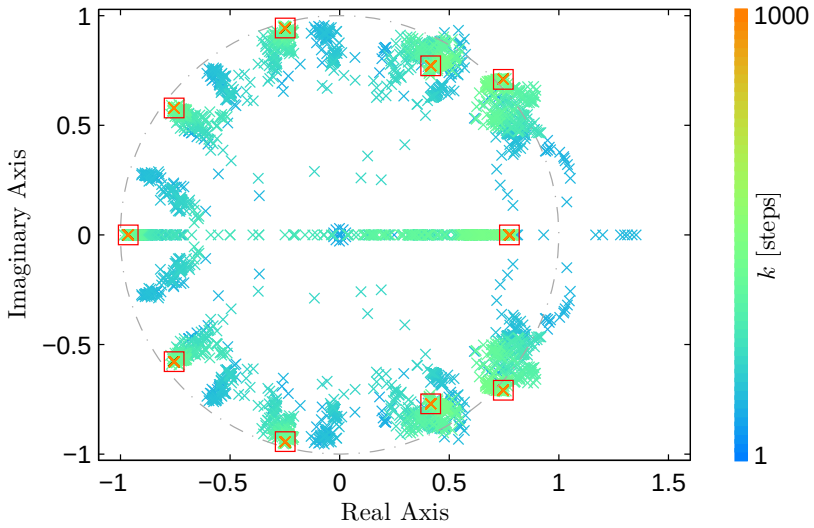

RCAC

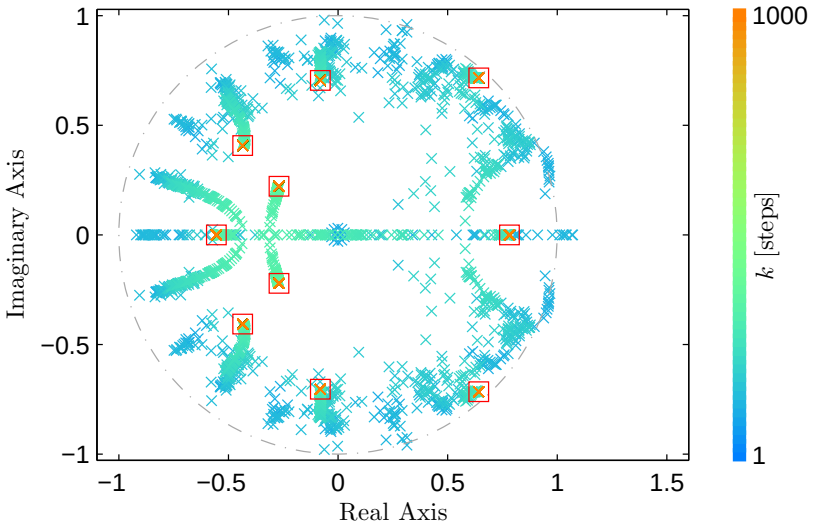

CC-RCAC

Nonlinear Multilink Arm

Consider planar multilink arm

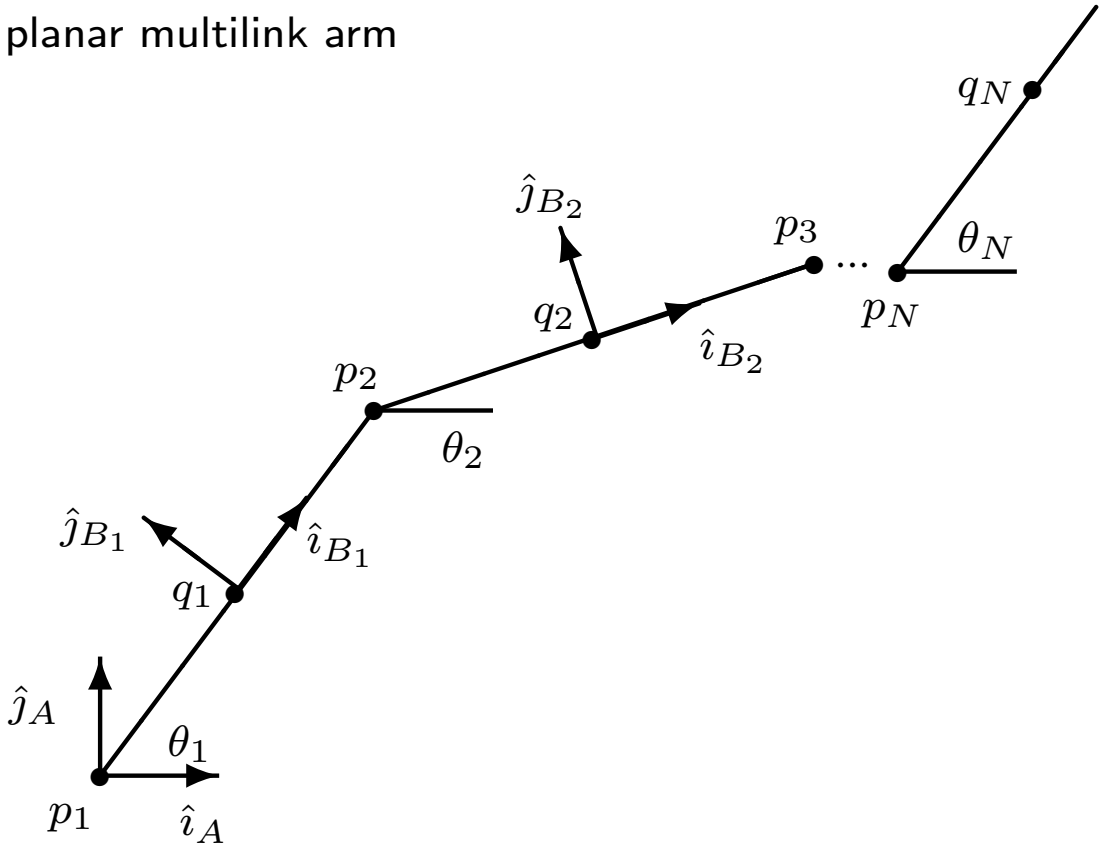

$$\begin{bmatrix} \frac{m_1 l_1^2}{3} + m_2 l_1^2 & \frac{m_2 l_1 l_2}{2}\cos(\theta_1-\theta_2) \\ \frac{m_2 l_1 l_2}{2}\cos(\theta_1-\theta_2) & \frac{m_2 l_2^2}{3} \end{bmatrix} \begin{bmatrix} \ddot{\theta}_1 \\ \ddot{\theta}_2 \end{bmatrix} + \begin{bmatrix} \frac{m_2 l_1 l_2}{2}\sin(\theta_1-\theta_2)\dot{\theta}_2^2 \\ -\frac{m_2 l_1 l_2}{2}\sin(\theta_1-\theta_2)\dot{\theta}_1^2 \end{bmatrix}$$

$$+ \begin{bmatrix} c_1 + c_2 & -c_2 \\ -c_2 & c_2 \end{bmatrix} \begin{bmatrix} \dot{\theta}_1 \\ \dot{\theta}_2 \end{bmatrix} + \begin{bmatrix} k_1 + k_2 & -k_2 \\ -k_2 & k_2 \end{bmatrix} \begin{bmatrix} \theta_1 \\ \theta_2 \end{bmatrix} = \begin{bmatrix} u(t) \\ 0 \end{bmatrix} \tag{71}$$

Nonlinear Multilink Arm continued

Nonlinear system can be controlled for small command magnitudes and frequencies.

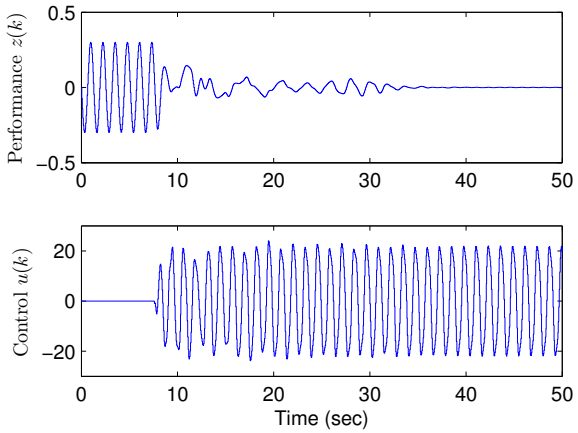

RCAC performance at empirically found maximum command amplitude.

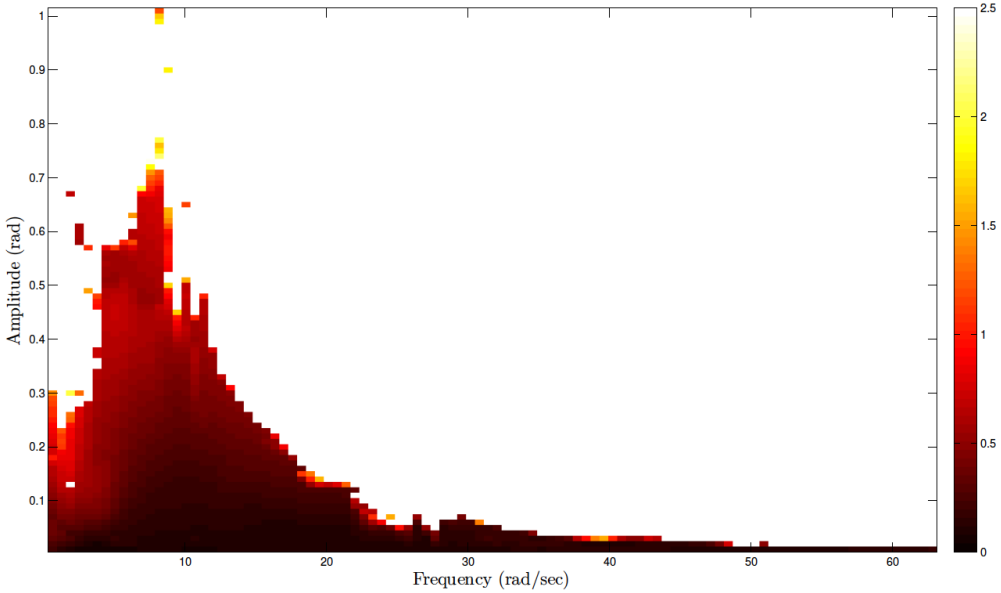

Region plot for RC-MRAC, taken from [1]

[1] M. W. Isaacs, J. B. Hoagg, A. V. Morozov, and D. S. Bernstein, "A Numerical Study on Controlling a Nonlinear Multilink Arm Using a Retrospective Cost Model Reference Adaptive Controller," Proc. Conf. Dec. Contr., pp. 8008–8013, Orlando, FL, December 2011.

Vertical Energy Equation

$$\frac{\partial \mathscr{T}}{\partial t} + u_r \frac{\partial \mathscr{T}}{\partial r} + (\gamma - 1)\mathscr{T}\left(\frac{2u_r}{r} + \frac{\partial u_r}{\partial r}\right) = \frac{k}{c_{\mathrm{v}}\,\rho\,\bar{m}_{\mathrm{n}}}\mathscr{Q}, \tag{72}$$

$$\mathscr{Q} = Q_{\mathrm{EUV}} + Q_{\mathrm{NO}} + Q_{\mathrm{O}} + \frac{\partial}{\partial r}\left((\kappa_{\mathrm{c}} + \kappa_{\mathrm{eddy}})\frac{\partial T}{\partial r}\right) + N_e \frac{\bar{m}_{\mathrm{i}}\bar{m}_{\mathrm{n}}}{\bar{m}_{\mathrm{i}} + \bar{m}_{\mathrm{n}}}\nu_{\mathrm{in}}(\mathbf{v} - \mathbf{u})^2,$$

$$Q_{\mathrm{EUV}} = \sum_s \sum_\lambda \left[N_s(z)\, I_\infty(\lambda)\, e^{-\sec(\chi)\sum_s N_s(z)\sigma_s^a(\lambda)H_s(z)}\right], \tag{73}$$

$$I_\infty(\lambda) = f(\lambda)\left[1 + a(\lambda)\left(\frac{F_{10.7} + \left\langle F_{10.7}\right\rangle_{81d}}{2} + 80\right)\right], \tag{74}$$

where equation (73) is a combination of equation (9.17)[7] and notes from AOSS 495. Equation (74) is an empirical model.[8]

[7] Schunk, R. W., and A. F. Nagy. "Ionospheres: Physics, Plasma Physics, and Chemistry." *Cambridge University Press*, 2004.

[8] Richards, P. G., J. A. Fennelly, and D. G. Torr, "EUVAC: A Solar EUV Flux Model for Aeronomic Calculations", *J. Geophys. Res.*, 99(A5), (1994)

EAKF Implementation notes

First, some notes on matrices that were not defined above.

1. $\mathcal{F}_k$ comes from SVD of $\mathcal{P}_k^- = \mathcal{F}_k D_k \mathcal{F}_k^T$.
2. $\mathcal{G}_k$ is a square root of D_k, as in $\mathcal{G}_k = D_k^{1/2}$.
3. U_k comes from SVD of $\mathcal{G}_k^T \mathcal{F}_k^T \mathcal{H}^T R^{-1} \mathcal{H} \mathcal{F}_k \mathcal{G}_k = U_k J_k U_k^T$.
4. B_k is a square root of $I + J_k$, as in $B_k = (I_{n+m} + J_k)^{-1/2}$.

Second, here are some notes

- The EAKF procedure presented so far is not exactly what is implemented in DART.
- The procedure presented here is the closest EAKF representation to other filters, but does not incorporate localization and is not optimized for parallel implementation.
- The version that is implemented in DART is described in [9] and [10].

[9] Anderson, Jeffrey L. "A local least squares framework for ensemble filtering." Monthly Weather Review 131.4 (2003): 634-642.

[10] Anderson, Jeffrey L., and Nancy Collins. "Scalable implementations of ensemble filter algorithms for data assimilation." Journal of Atmospheric and Oceanic Technology 24.8 (2007): 1452-1463

8 Results

- Simulated measurement above Ann Arbor
- Simulated measurement at Subsolar Point
- Simulated measurement at CHAMP location
- Real measurement from CHAMP
- Real measurement from CHAMP with advanced IMF and HPI models

Simulated measurement above Ann Arbor

- **Measurement source:** GITM truth simulation with an input of $F_{10.7}$ fixed at about 150. ρ at ($82.5°$W, $42.5°$N, 394km) is recorded with associated uncertainty (R) of $2.6 \times 10^{-12} kg/m3$.
- **Ensemble members:** 20 GITM instances prespun for 2 days prior to Dec 01 with $\hat{F}_{10.7}$ values coming from normal distribution $\sim N(130, 25)$. $\hat{F}^{-}_{10.7}$ is inflated using $\mathcal{P}_i = 49$.

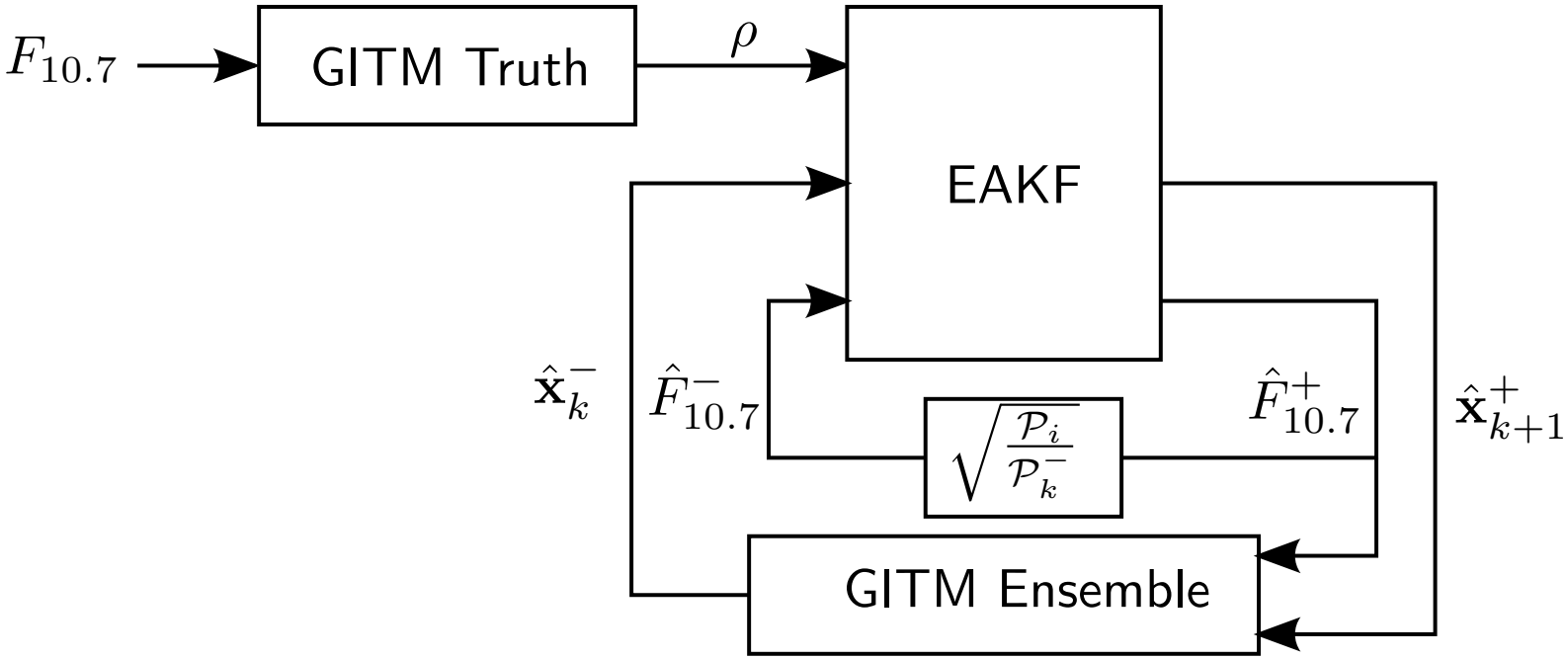

ρ above Ann Arbor

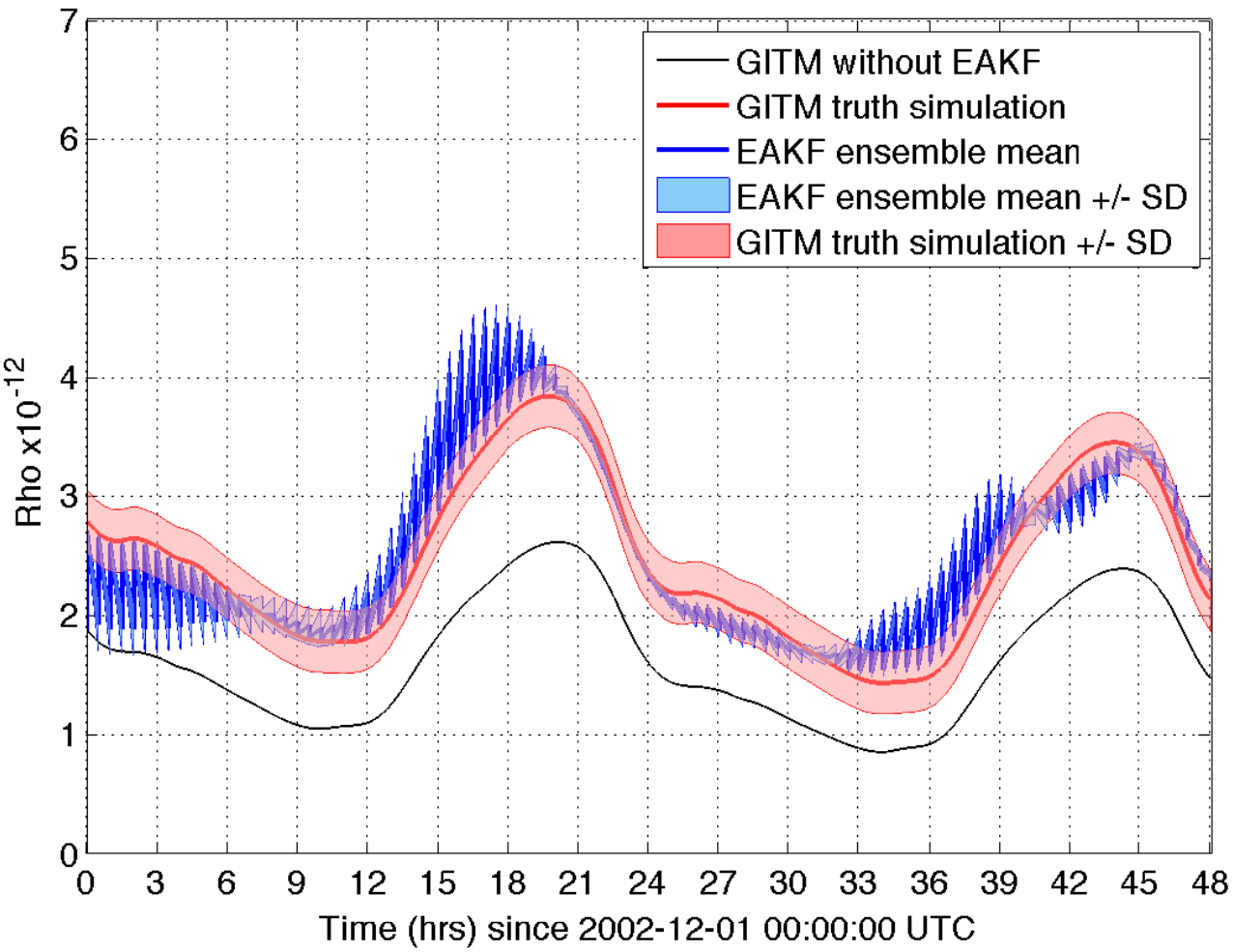

EAKF estimates of ρ are brought within the uncertainty bounds of GITM truth simulation.

Localization

- The effect of measurement assimilation can be restricted to a region to avoid updating uncorrelated states.[11]

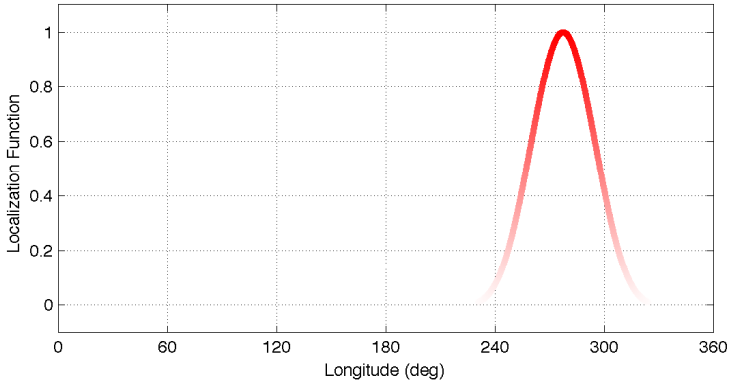

Correlation function with horizontal cutoff of 30° is shown to the right and below, and vertical cutoff of $100km$ is shown bottom right.

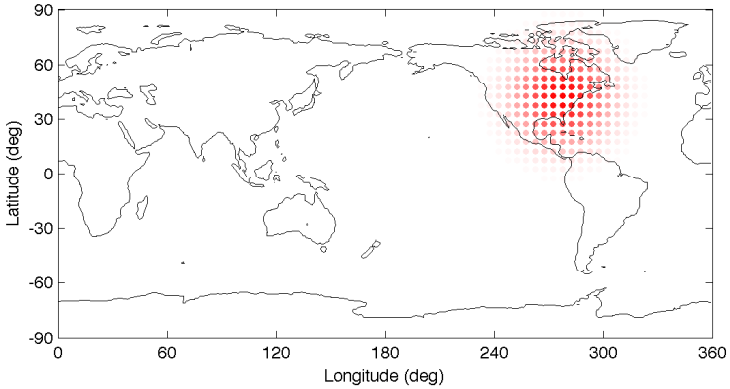

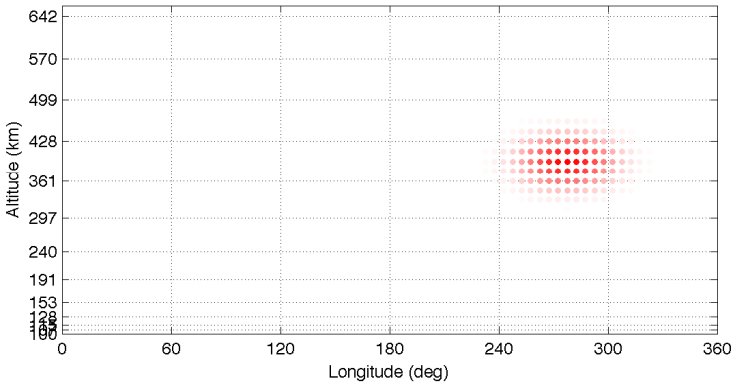

[11] Gaspari, G., and S. E. Cohn. "Construction of correlation functions in two and

ρ at subsolar point

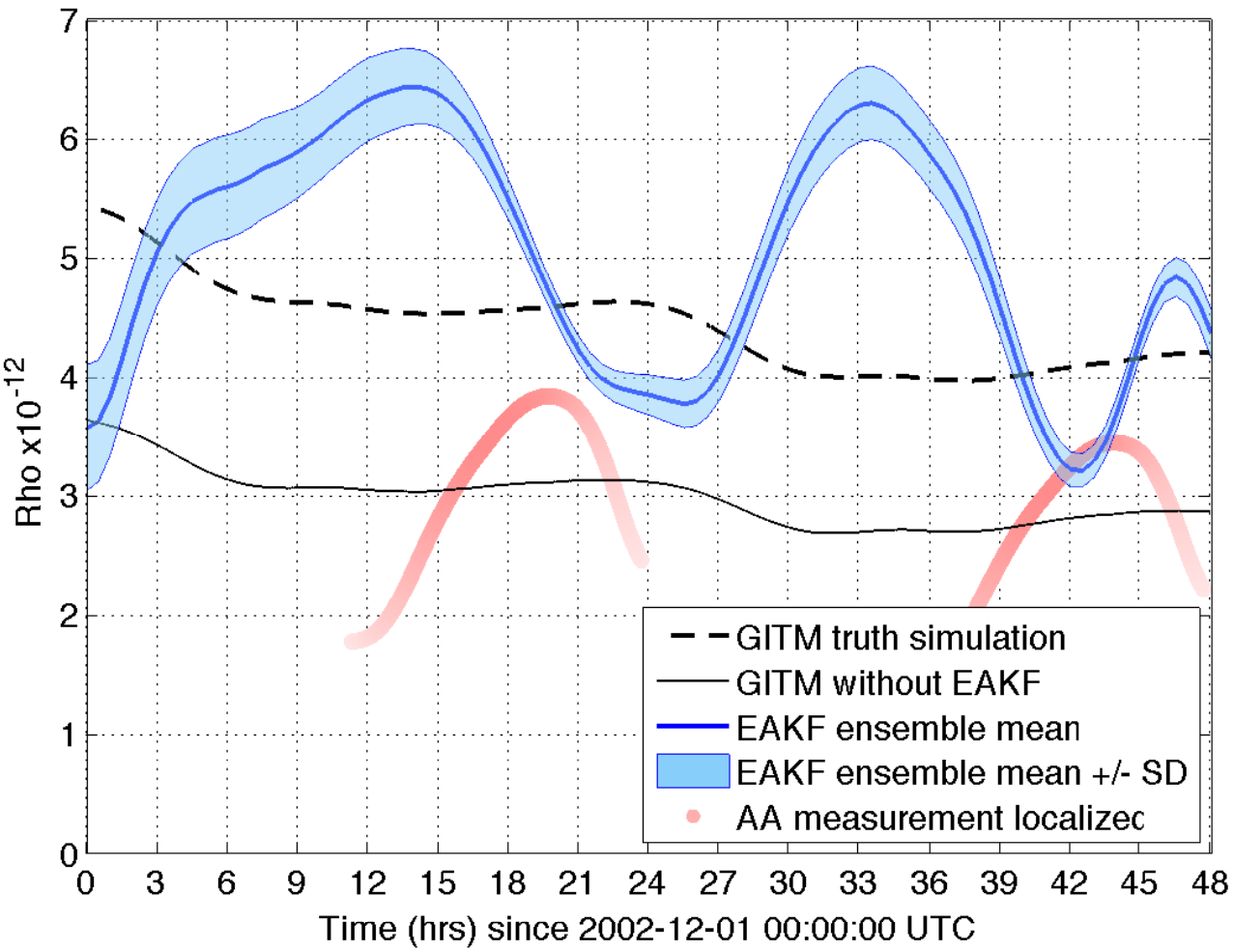

Note, ρ at subsolar point does not vary too much since $F_{10.7}$ is relatively constant. The localized AA measurement is tripled in intensity.

ρ at CHAMP location

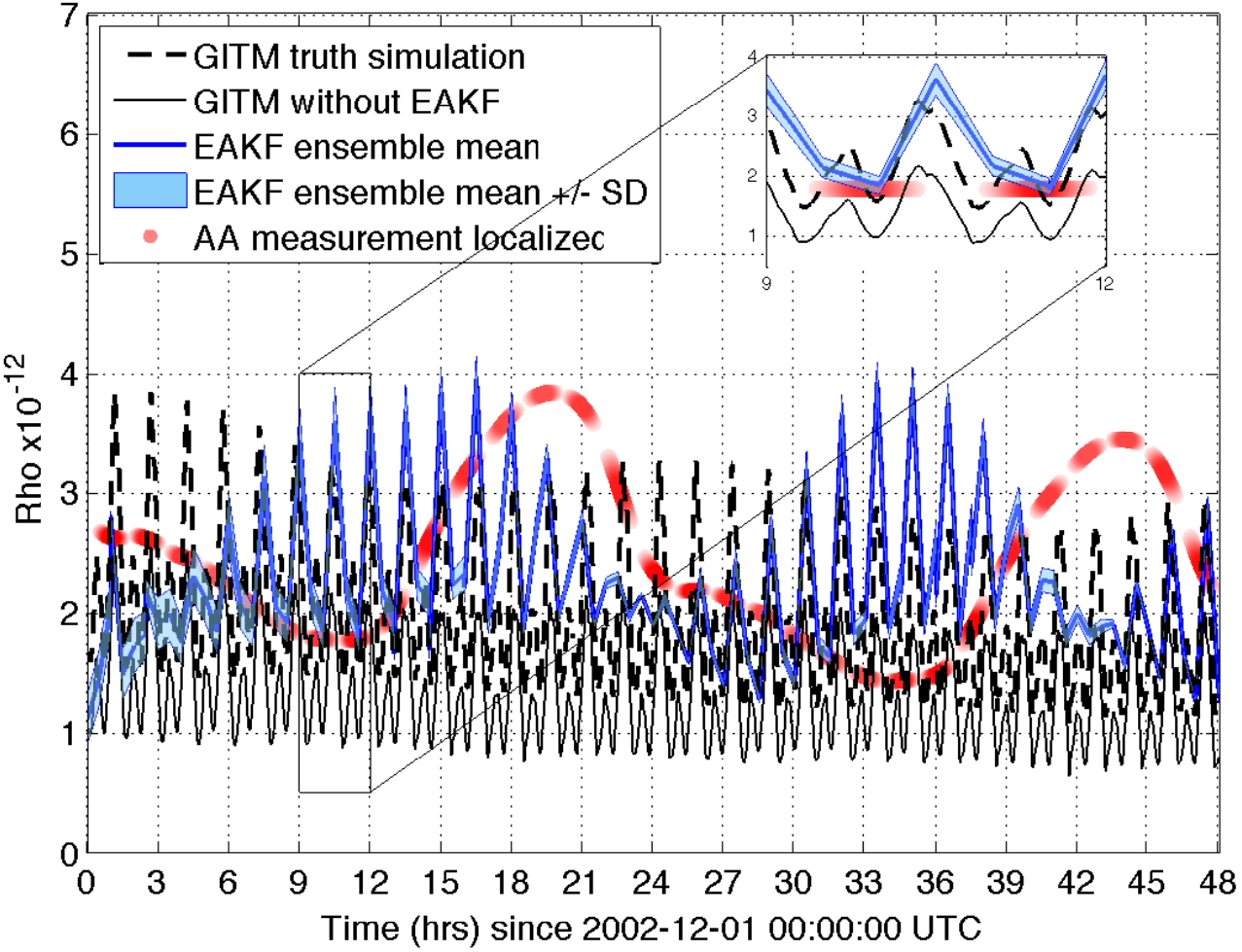

The localized AA measurement is tripled in intensity.

ρ at CHAMP location RMSPE

- We define RMS percentage error $\mathrm{RMSPE} \triangleq \frac{\sqrt{\overline{(\rho-\hat{\rho})^2}}}{\sqrt{\overline{\rho^2}}}$

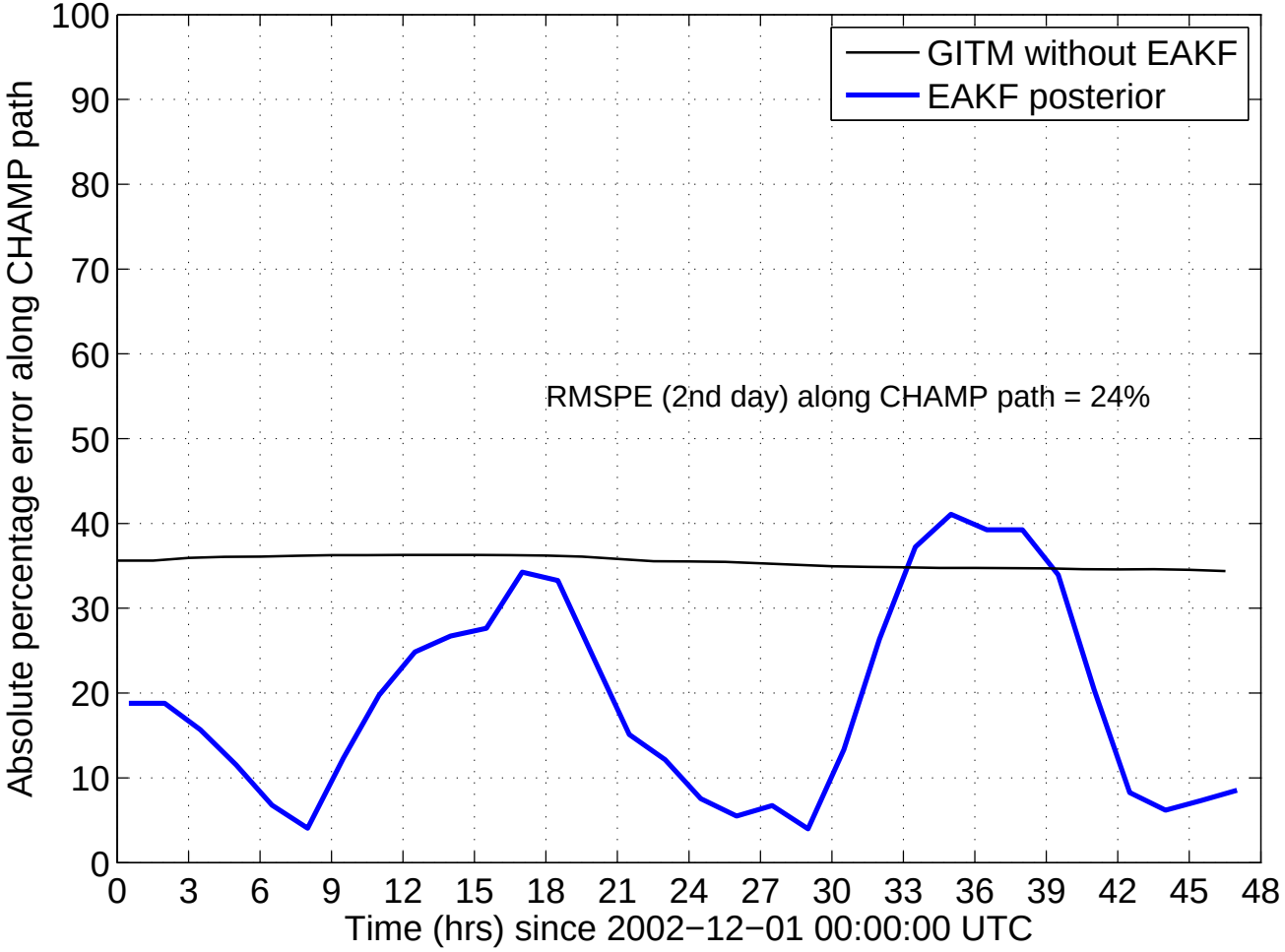

Simulated measurement above Ann Arbor Summary

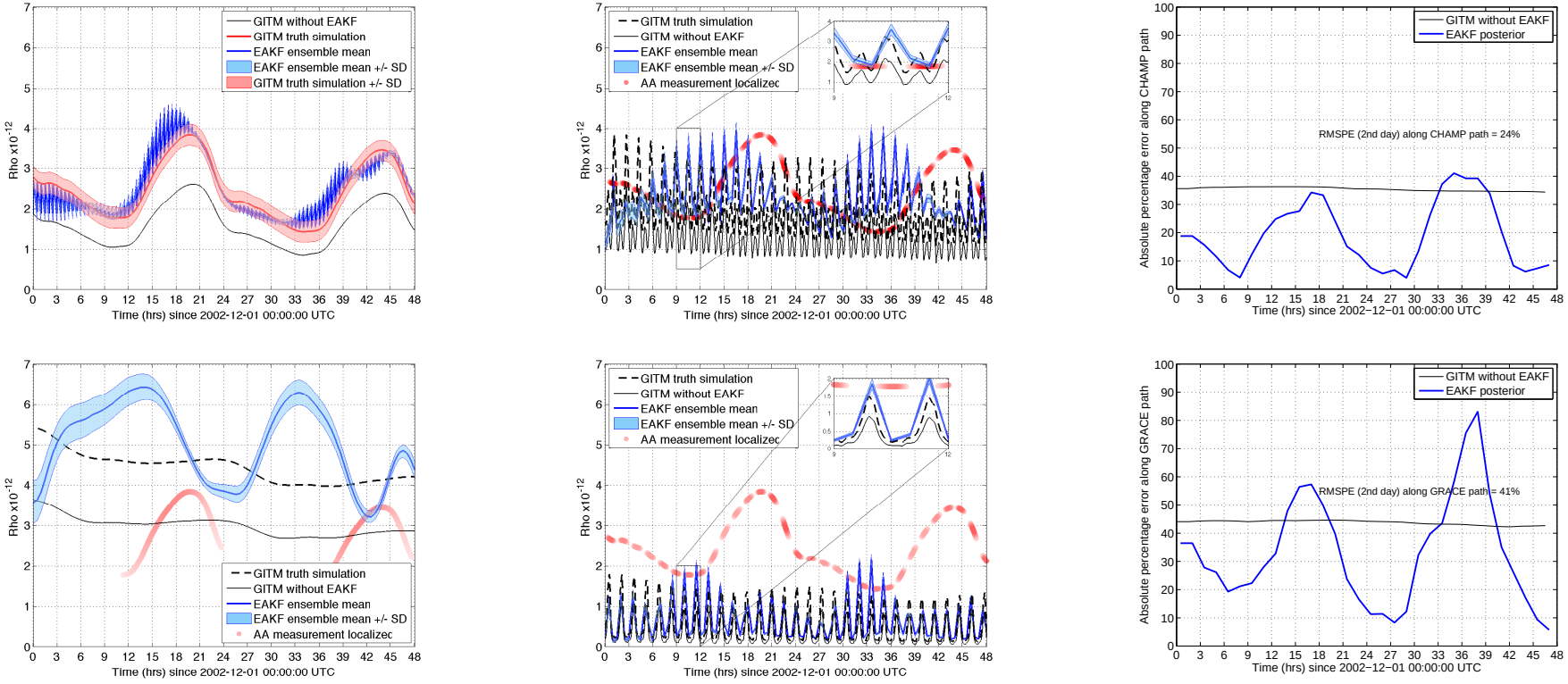

$F_{10.7}$ estimate AA

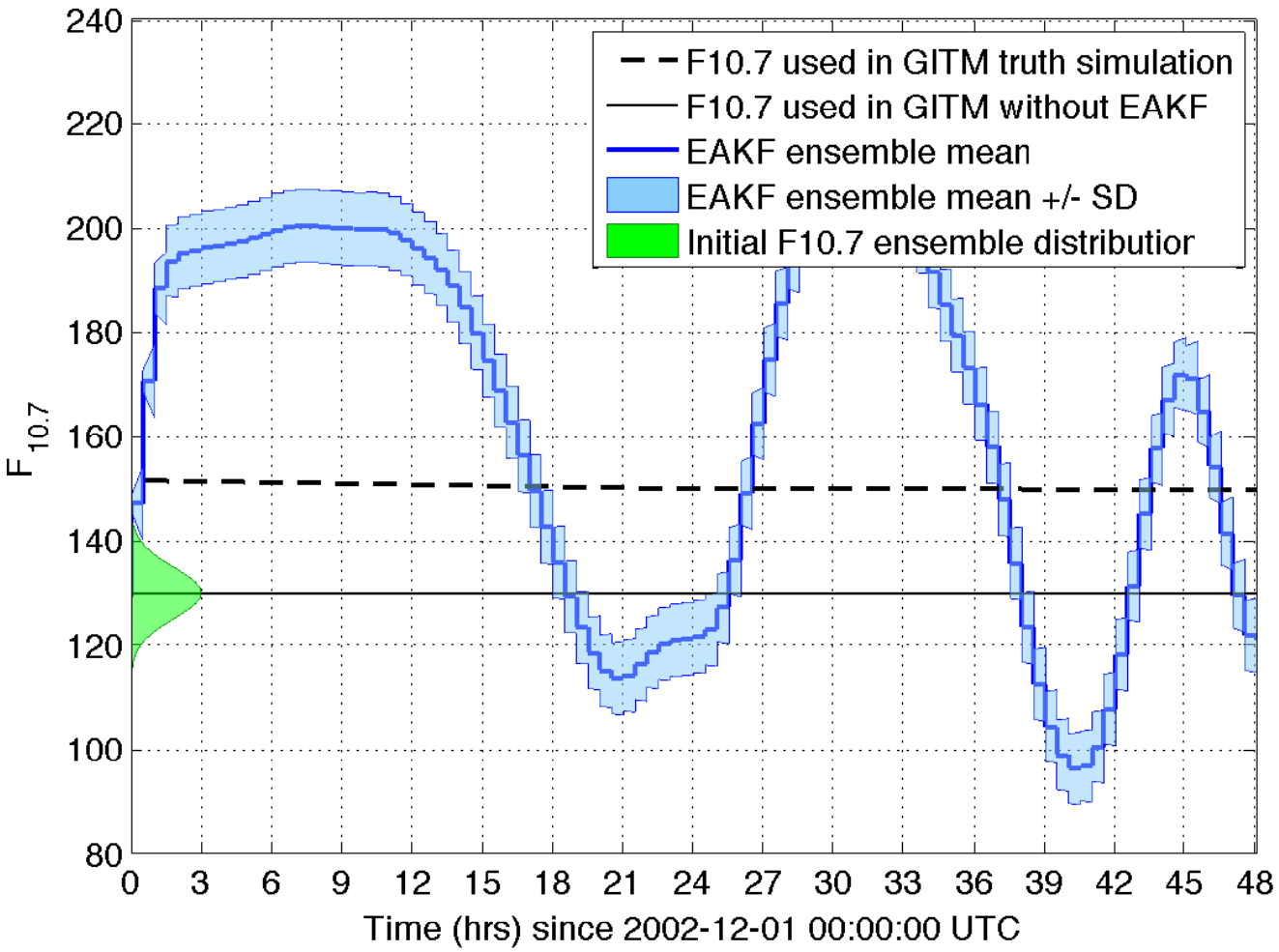

So what we learned is that it is hard to get a good estimate of $F_{10.7}$ based on measurement that is fixed in longitude.

Simulated measurement at Subsolar Point

- **Measurement source:** ρ at *subsolar point* is recorded with associated uncertainty (R) of $2.6 \times 10^{-12} kg/m3$.

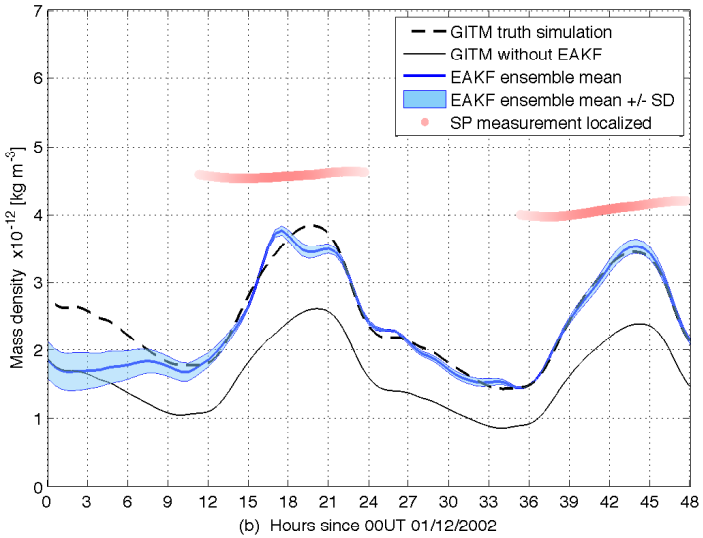

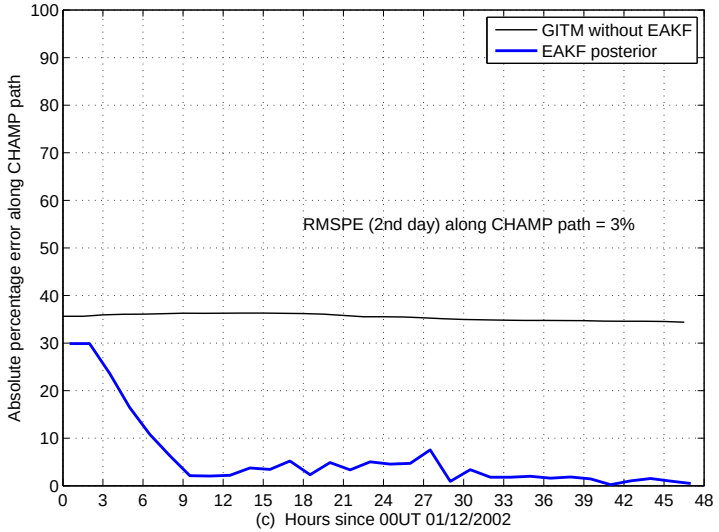

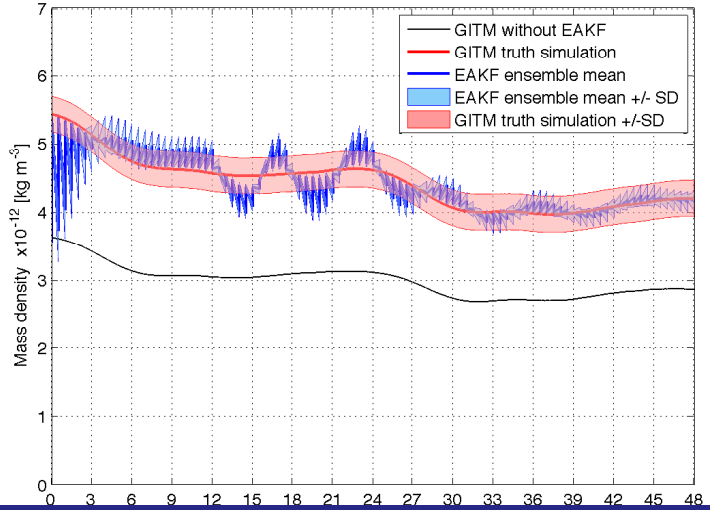

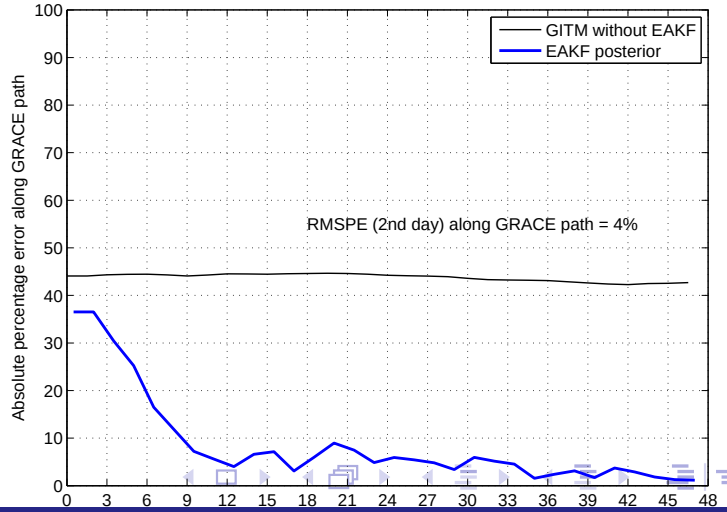

$F_{10.7}$ estimate SP

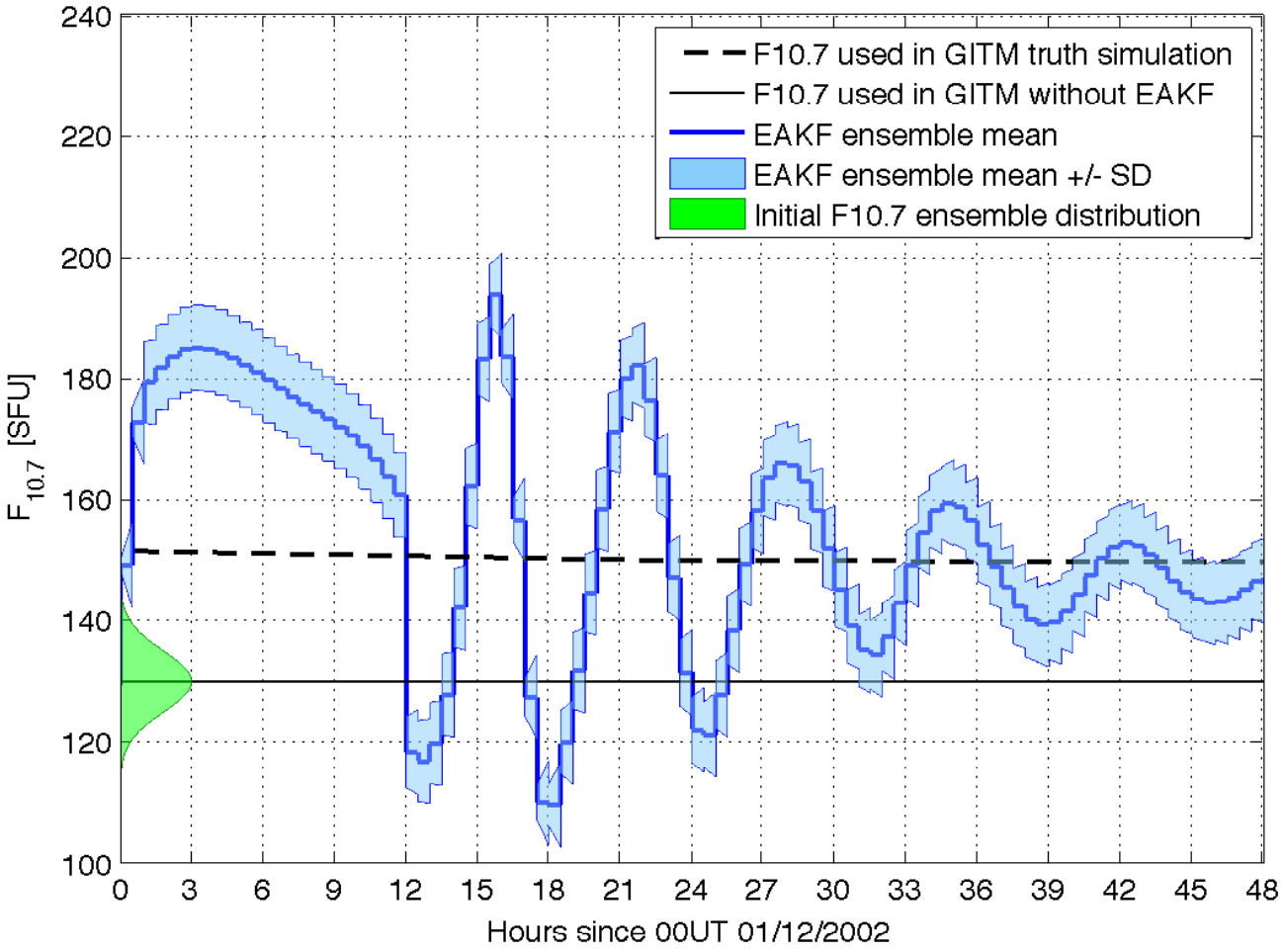

Conclusion here is that ρ at subsolar point is more closely related to $F_{10.7}$ than ρ at any point fixed in longitude (for example, Ann Arbor).

Simulated measurement at CHAMP location

- **Measurement source:** ρ at *CHAMP location* is recorded with associated uncertainty (R) of $2.6 \times 10^{-12} kg/m3$.

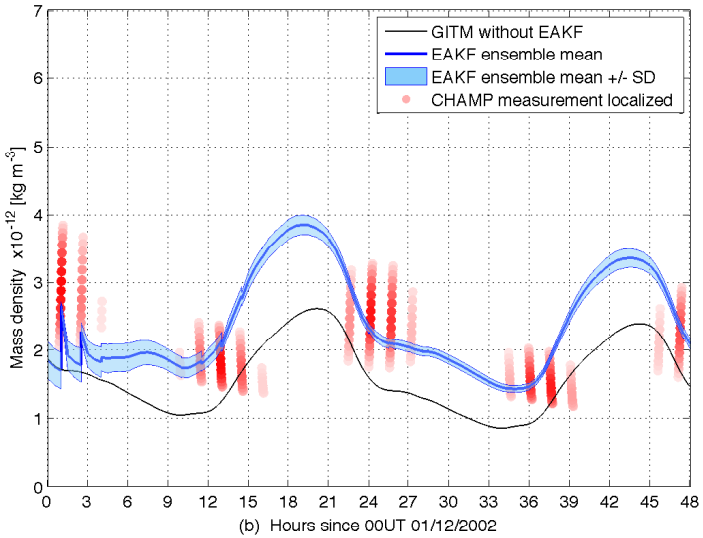

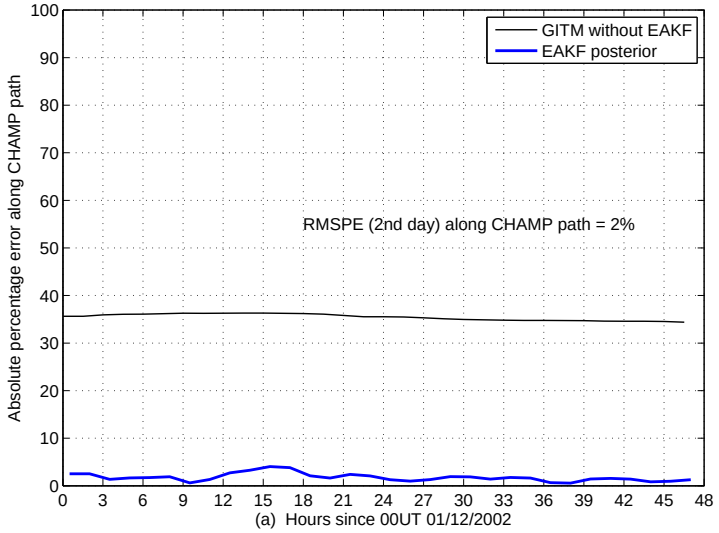

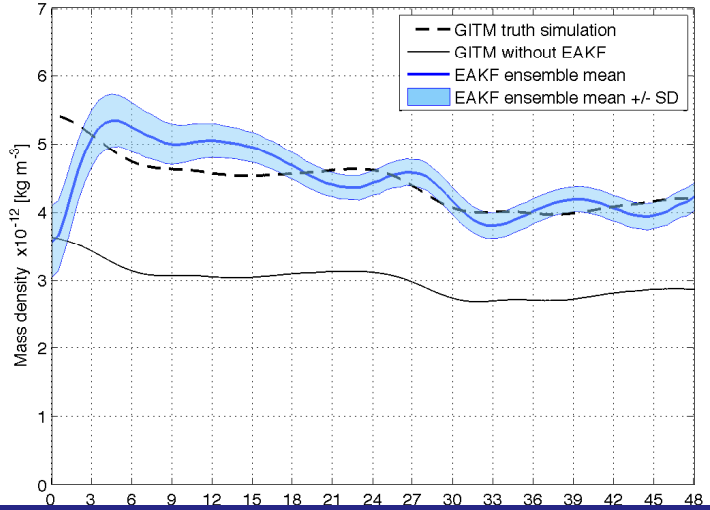

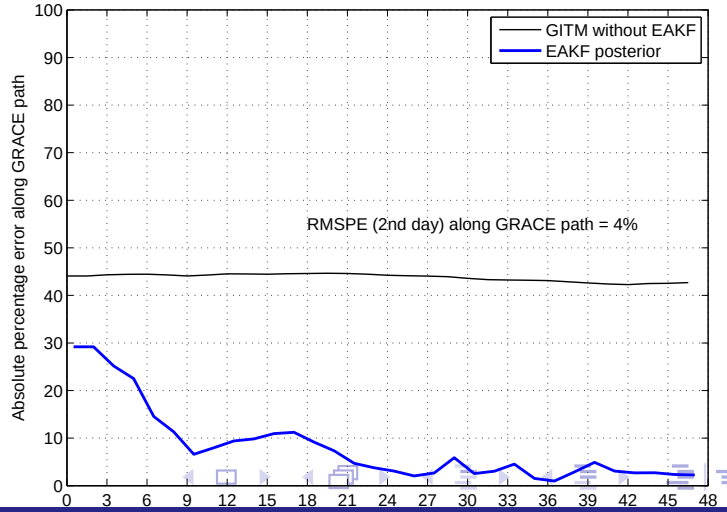

$F_{10.7}$ estimate CL

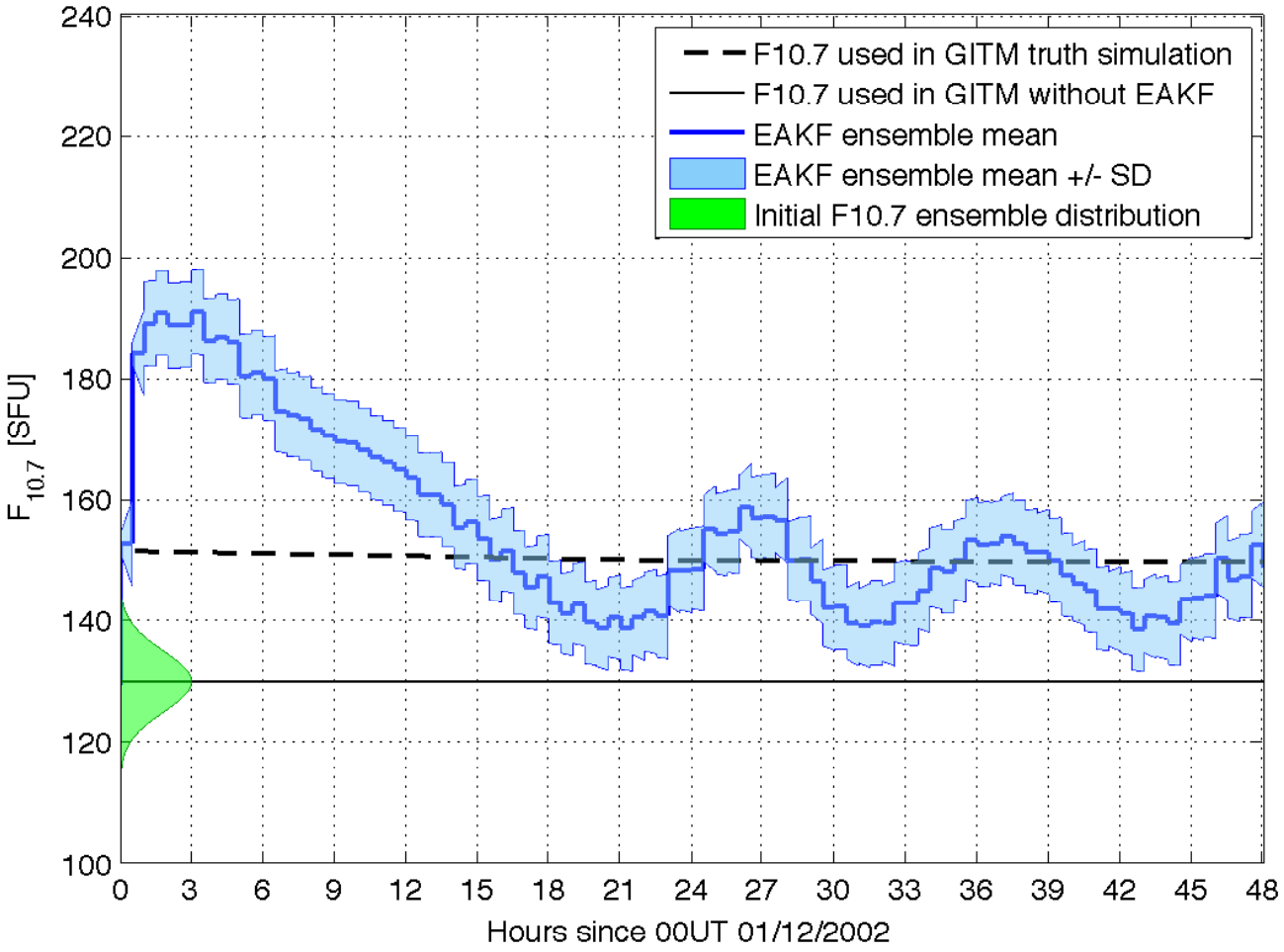

We conclude that this case is better conditioned than AA or SP ones.

Real measurement from CHAMP

- **Measurement source:** ρ from *real CHAMP* has associated uncertainty (R_k) that varies, but has a mean of $2.6 \times 10^{-12} kg/m3$.

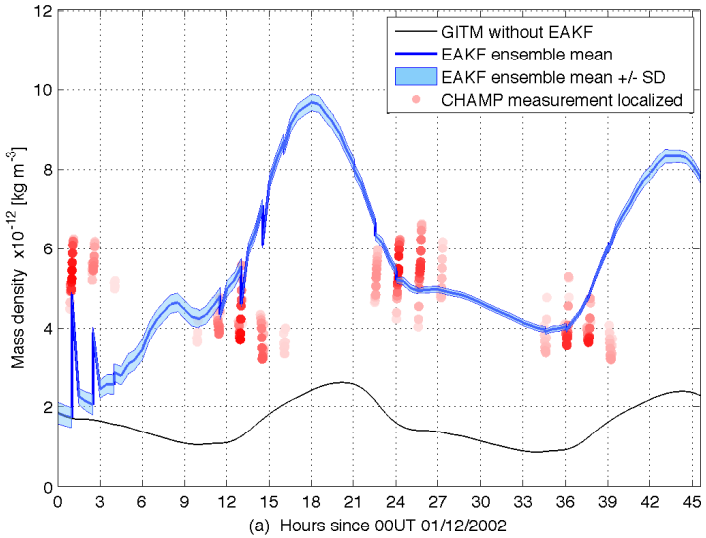

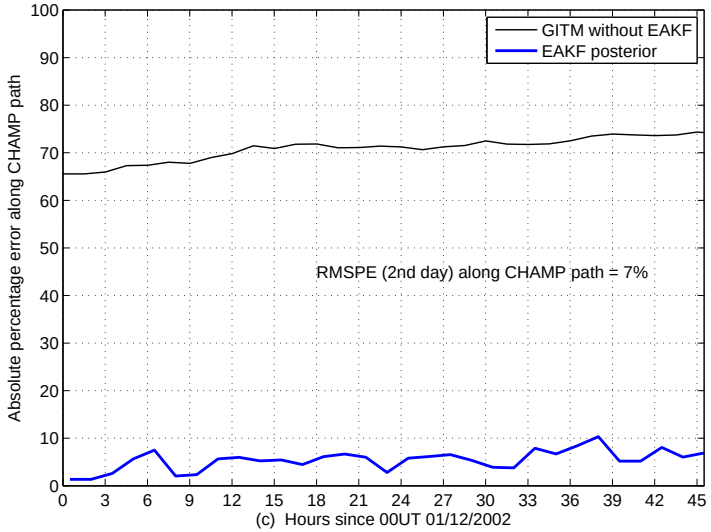

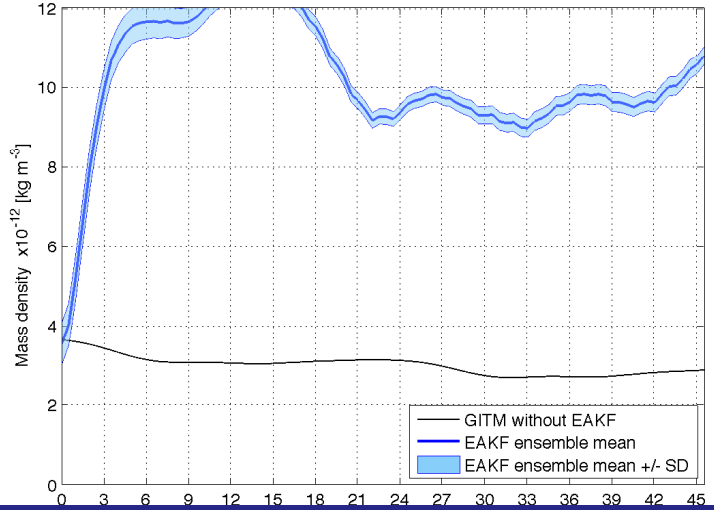

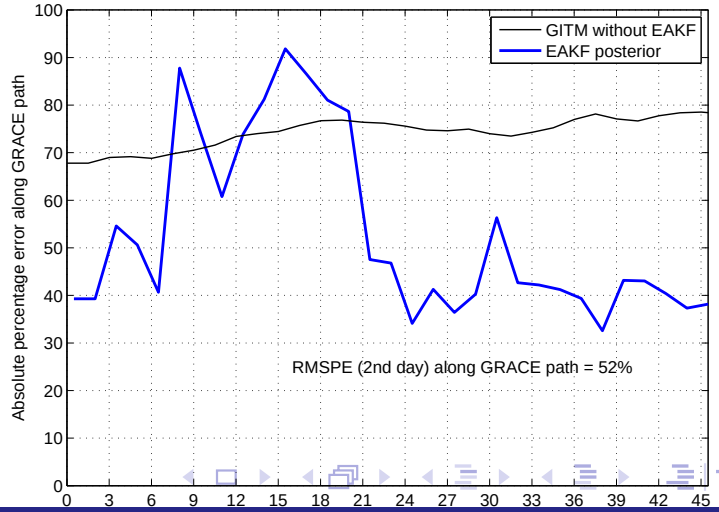

$F_{10.7}$ estimate CR

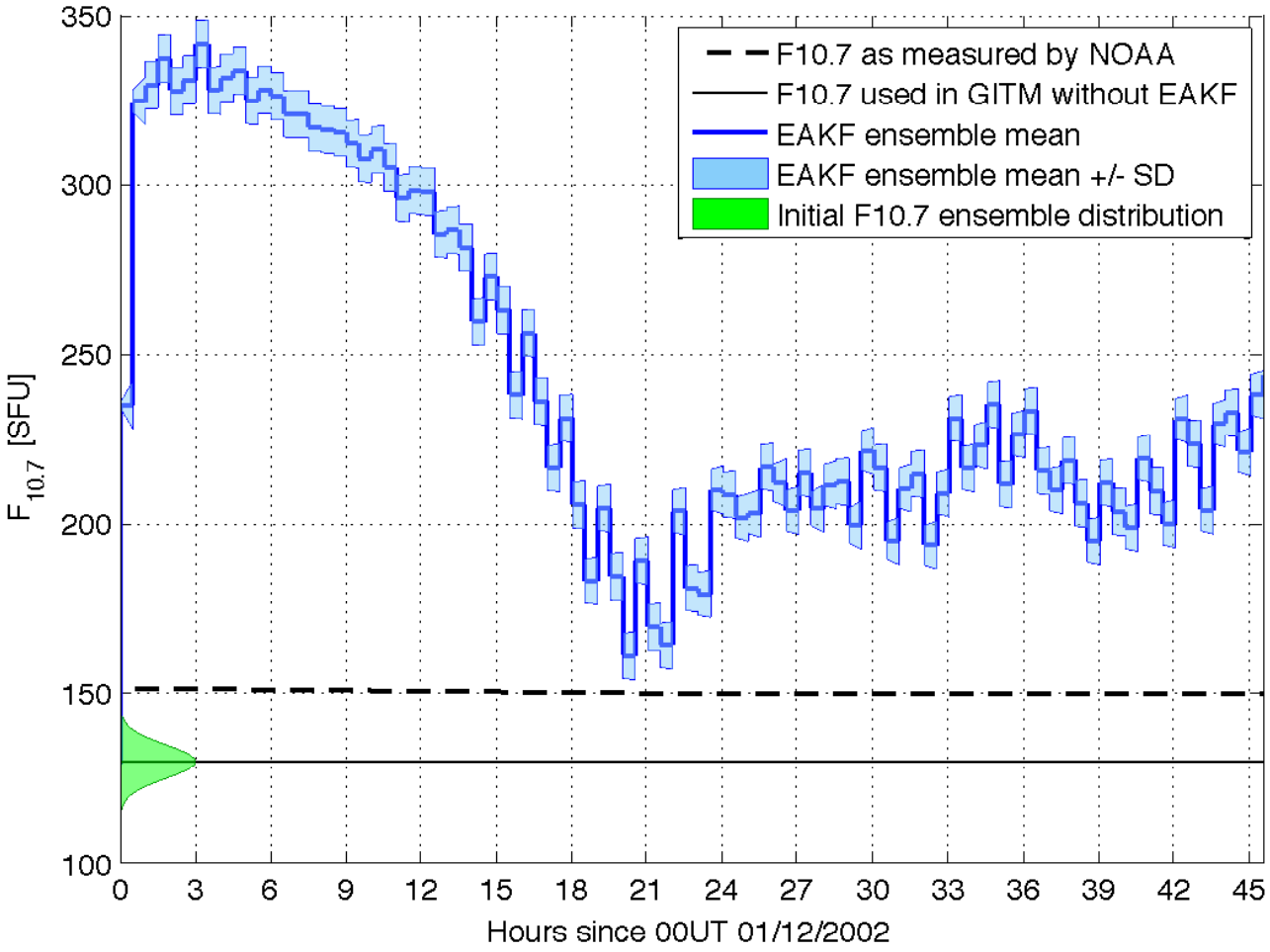

We conclude that EAKF $F_{10.7}$ estimate did not converge to the commonly accepted value in order to compensate for model bias.

Real measurement from CHAMP with IMF and HPI

- **Measurement source:** ρ from *real CHAMP* has associated uncertainty (R_k) that varies, but has a mean of $2.6 \times 10^{-12} kg/m3$.

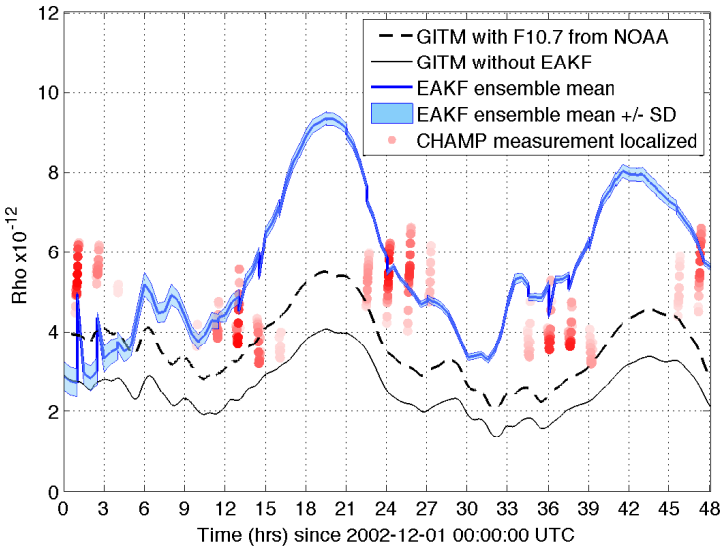

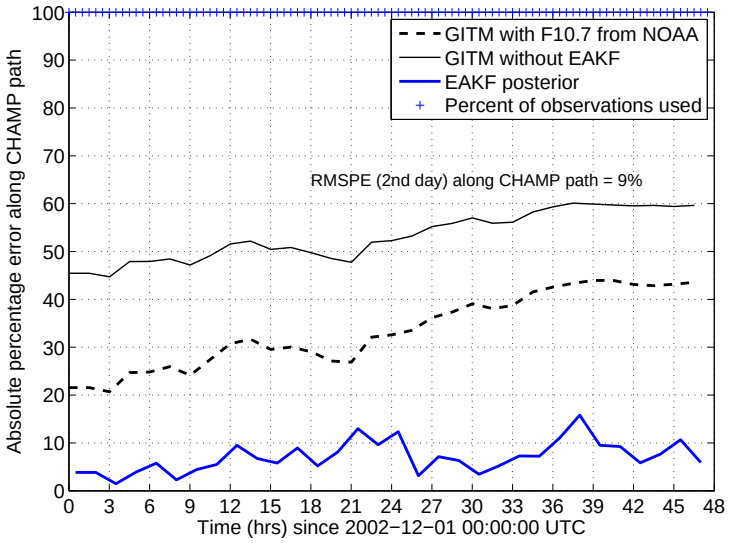

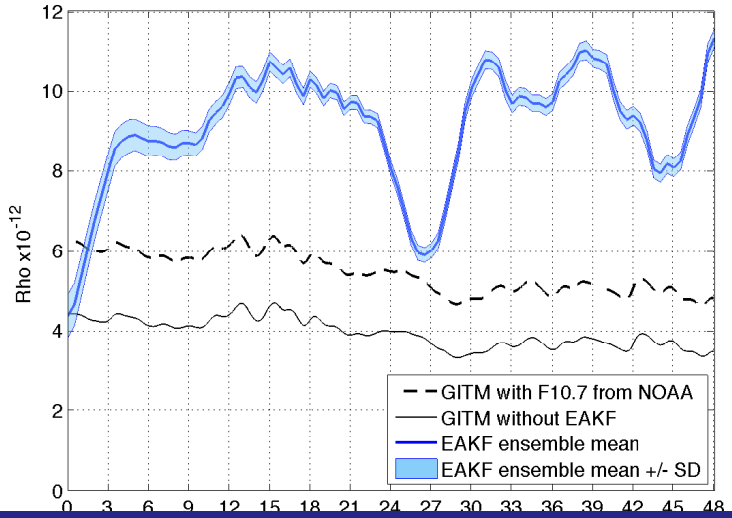

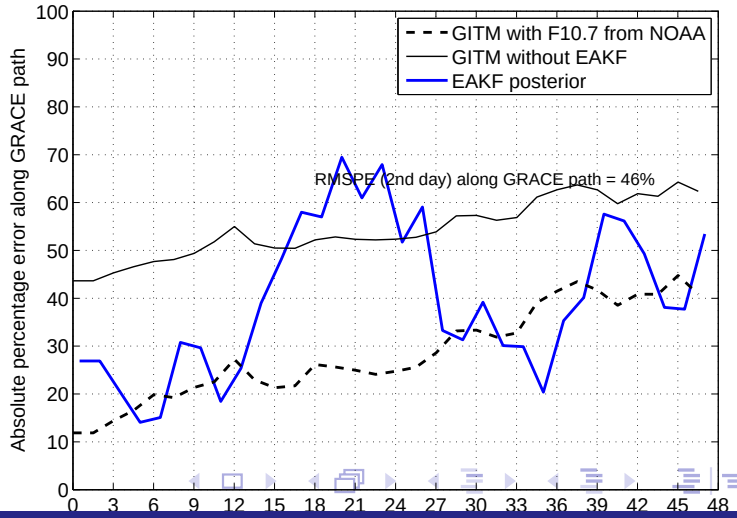

$F_{10.7}$ estimate CR

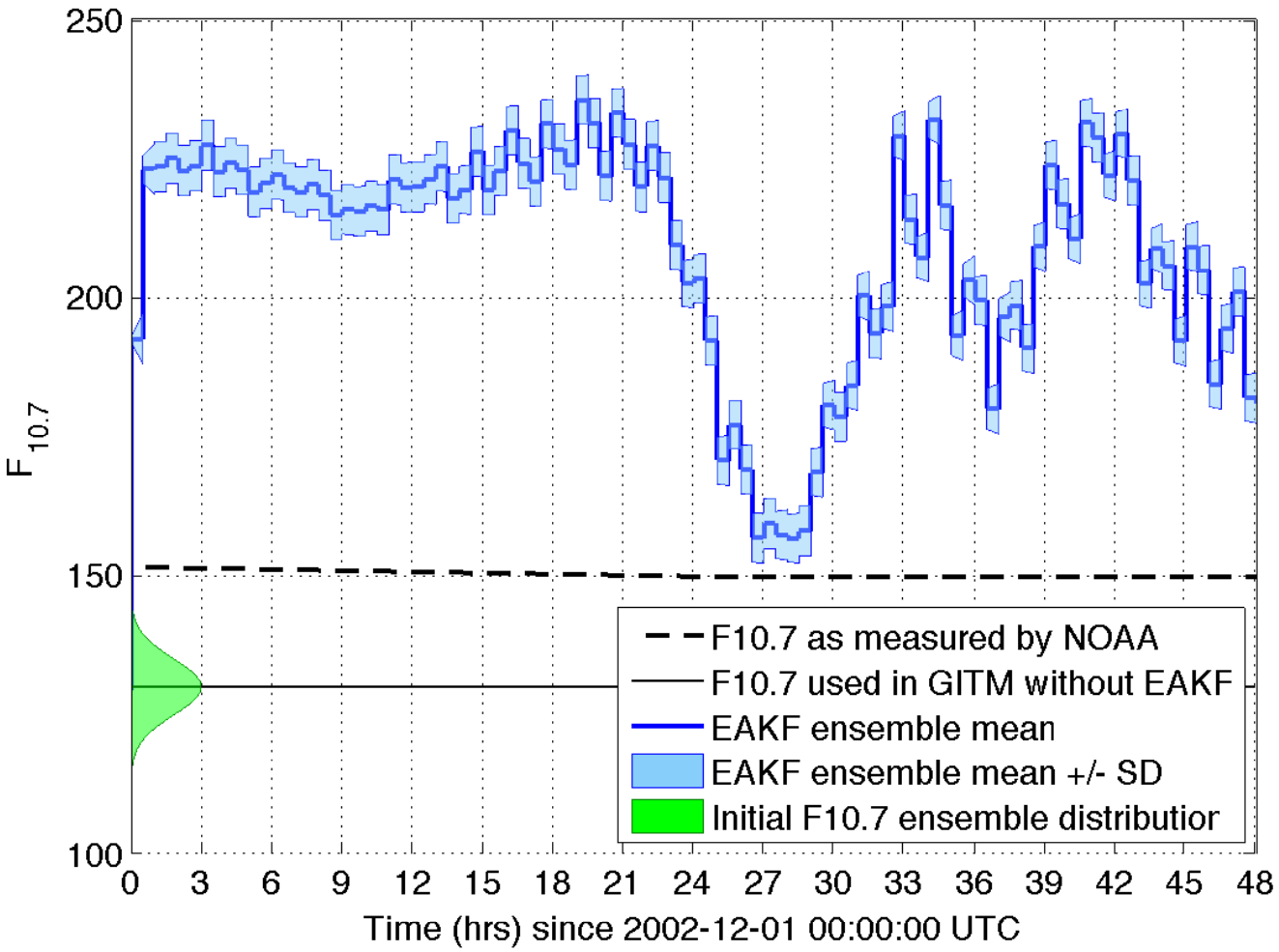

We conclude that EAKF $F_{10.7}$ estimate did not converge to the commonly accepted value in order to compensate for model bias, even more advanced IMF and HPI models are used.